DEVELOPMENT OF A NONDESTRUCTIVE VIBRATION TECHNIQUE FOR BOND ASSESSMENT OF SPACE SHUTTLE TILES

FINAL REPORT

Prepared for the
National Aeronautics and Space Administration
John F. Kennedy Space Center
Under Grant # NAG 10-0117

Principal Investigator

Dr. Faissal A. Moslehy, P.E.

Professor

Department of Mechanical and Aerospace Engineering
University of Central Florida
Orlando Florida, 32816

February 1994

DEVELOPMENT OF A NONDESTRUCTIVE VIBRATION TECHNIQUE FOR BOND ASSESSMENT OF SPACE SHUTTLE TILES

(NASA Grant # NAG 10-0117)

FINAL REPORT

February 1994

Principal Investigator

Dr. Faissal A. Moslehy, P.E.
Professor
Department of Mechanical and Aerospace Engineering
University of Central Florida
(407) 823-2416

ABSTRACT

This final report describes the achievements of the above titled project. The project is funded by the National Aeronautics and Space Administration - John F. Kennedy Space Center (Grant No. NAG 10-0117) for the period of January 1 to December 31, 1993. The purpose of this project was to develop a nondestructive, noncontact technique based on "vibration signature" of tile systems to quantify the bond conditions of the thermal protection system (TPS) tiles of Space Shuttle orbiters. the technique uses a laser rapid scan system, modal measurements, and finite element modeling.

Finite element models were developed for tiles bonded to both clamped and deformable integrated skin-stringer orbiter mid-fuselage. results showed that the size and location of a disbonded tile can be determined from frequency and mode shape information. Moreover, a frequency response survey was used to quickly identify the disbonded tiles. The finite element results were compared with experimentally determined frequency responses of a 17-tile test panel, where a rapidscan laser system was employed. An excellent degree of correlation between the mathematical simulation and experimental results was realized. An inverse solution for single-tile assemblies was also derived and is being implemented into a computer program that can interact with the modal testing software. The output of the program displays the size and location of disbond. This program has been tested with simulated input (i.e., finite element data), and excellent agreement between predicted and simulated disbonds was shown. Finally, laser vibration imaging and acoustic emission techniques were shown to be well suited for detecting and monitoring the progressive damage in Graphite/Epoxy composite materials.

Future work on the project will include validating the technique by testing additional tile panels and the Space Shuttle orbiter.

TABLE OF CONTENTS

1 INTRODUCTION

Since reentry temperatures can reach 2700 F°, a thermal protection system (TPS) for the Space Shuttle orbiter consisting of over 24,000 fiber-composite tiles [1] is essential (see Figure 1-1). The large thermal strains in the tiles require that the tiles be isolated from the Orbiter by flexible strain isolation pads (SIP). An RTV silicone elastomer is used to bond the SIP to both the tile and Orbiter skin. A typical tile assembly is shown in Figure 1-2.

Bond condition may be affected by fabrication and installation errors (e.g., physical interference) as well as repeated flights. Therefore, evaluation of the bond condition of these TPS tiles during installation and after each flight is necessary. The current method to verify the bond condition of these tiles is "*pull and wiggling*" test. This test is slow and requires contacting the tiles, and thus could affect the bond conditions and damage tiles. Thus, a reliable, efficient, nondestructive, and non-contact technique is essential.

The principal investigator and his co-workers [2-5] successfully demonstrated that vibration signature of tiles is a feasible technique to determine the bond condition and showed that the dynamic characteristics of tiles are sensitive to changes in bond conditions. This technique is most suitable for the bond verification due to the unique nature of tiles and SIP materials. The technique is based on extracting the modal information of tiles in a non-intrusive, non-contacting way. A baseline is established on modal information of a specific tile or an array of similar tiles. This baseline, which is obtained either mathematically or experimentally, serves as a standard for comparison of subsequently acquired testing data to determine if changes in the bond have occurred.

The report describes the finite element modeling of tile assemblies, including excitation of the vibrations, determination of natural frequencies, mode shapes, and forced response of tiles. It also describes experimental procedures and presents results of test panels and reports on a proposed inverse solution for tile bond assessment [6]. Finally, laser vibration imaging and acoustic emission techniques were applied to Graphite/Epoxy composite material and shown to be well suited for detecting and monitoring the progressive delamination.

The technical approach followed/recommended in this project was:

1. Develop mathematical finite element models to compute the dynamic characteristics of tile/structure assemblies.
2. Conduct vibration testing using rapidscan laser system on multi-tile panels with controlled bond conditions.
3. Correlate experimental and mathematical model results.
4. Develop an inverse solution for direct of bond conditions.
5. Validate the technique by testing tiles on the Space Shuttle orbiter.
6. Conduct feasibility studies on using laser vibration imaging and acoustic emission to detect delamination and other defects in composite materials.

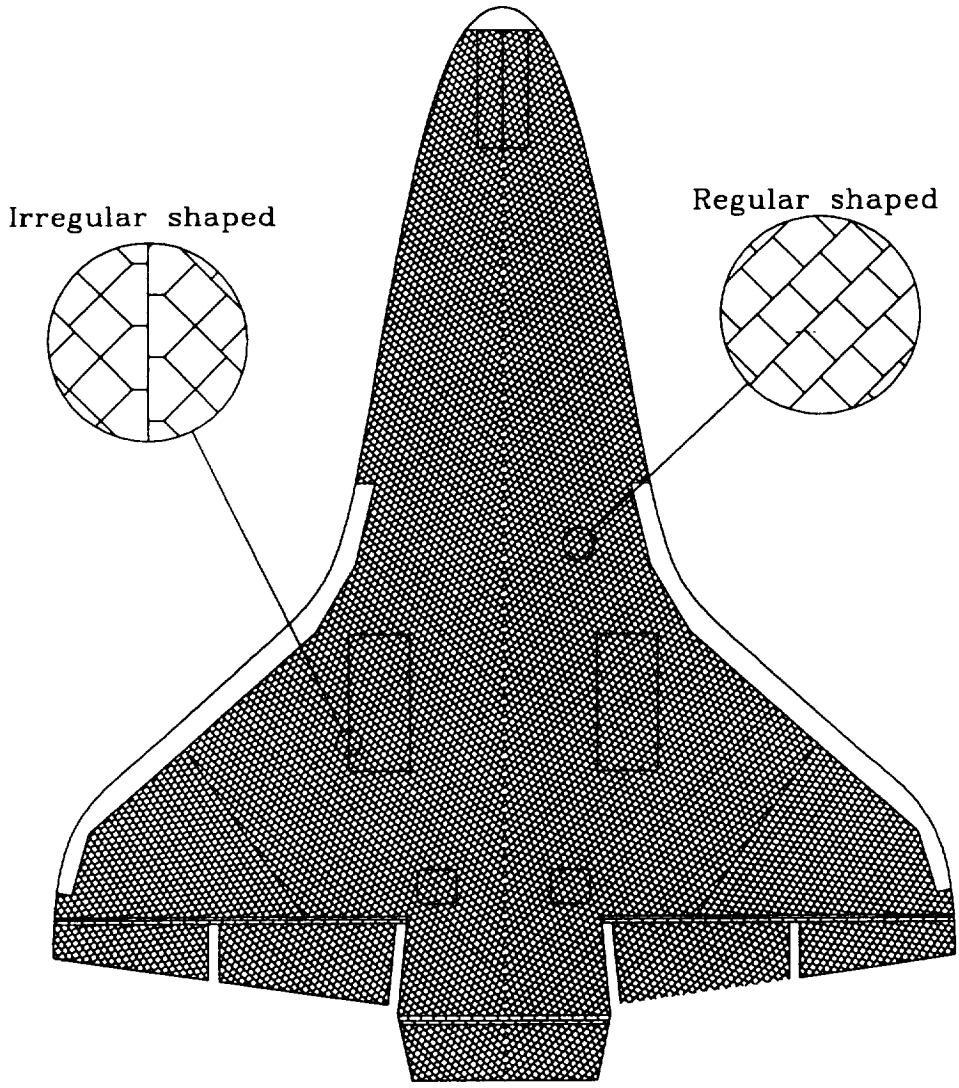

Figure 1-1 ORBITER

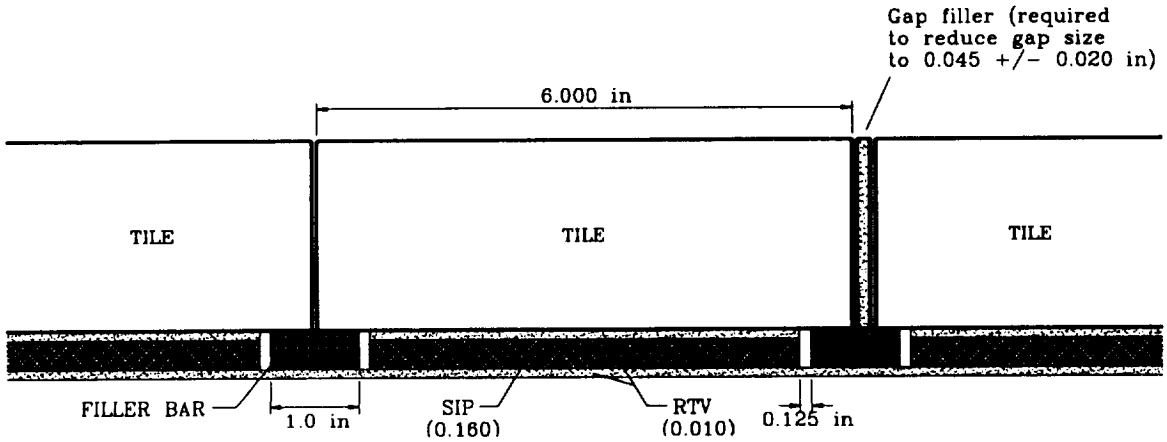

Figure 1-2 BONDED MULTI-TILE ASSEMBLY

2 FINITE ELEMENT MODELING AND ANALYSIS

2.1 SINGLE TILE MODEL

The NISA finite element computer code [20] is used on a 50 MHz 486 personal computer to analyze the finite element models developed for different TPS tile assemblies. In the analysis, the actual material properties of TPS components are used (Table 2.1-1). All tile assembly components are modeled by 8-node isoparametric brick elements with orthotropic material properties, and, if employed, the skin structure is comprised of 4-node plate elements. The model assumes rigid structure, all nodes at the RTV/aluminum interface are fixed. However, in order to simulate the different disbond cases, an appropriate number of double nodes are added between the SIP and lower RTV.

Since disbond size is the most important parameter to be investigated in tile modeling, 100%, 80%, and 60% bonded tiles (with disbonded regions located along the edge) are considered in this study. Finite element models are developed for tile number 191025-299 of space shuttle Columbia with filler bar mounted on a clamped structure. This tile is selected because it was used in modal testing on the Orbiter. Its dimensions are 6.0x6.0x2.066 inches and the SIP thickness is 16 inch. The finite element model is comprised of 528 elements and has 2640 degrees of freedom for the 100% bond case.

The above eigenvalue analyses provide the undamped natural frequencies and mode shapes of tiles. This information is used to study the effects of the size and location of the disbond. Ensuing analyses of models of interest involve frequency response calculations to simulate the response of tiles to acoustic energy, applied as pressure, to its upper surface. A dynamic pressure of 2 N/m^2 (equivalent to 100 dB) is applied at frequencies swept from 100 to 2500 Hz, and a damping factor of 1% is used in the computation. Displacement, velocity, and acceleration results are extracted for nodes at the center and corners of tiles of interest.

Table 2.1-2 and Figure 2.1-1 show the first ten modes for 100%, 80%, and 60% bonded single tiles (with disbonded regions located along the edge). It is noted that natural frequencies for all modes decrease with increased disbond. Thus, knowledge of these values would enable the test engineer to accurately quantify the amount of bond for this particular tile from modal test data. In addition, the disbond location can be determined from the rigid-body out-of-plane mode shapes of the tile. Figure 2.1-2 shows the rocking mode for the 100% bond case, and Figure 2.1-3 shows the same mode for the 80% bond case. Note that the rocking motion for the 100% bond case is symmetric about the centroidal axis of the tile, while in the 80% bond case, the rocking axis is shifted away from the disbonded area.

Figure 2.1-4 shows the computed frequency response for the center point on the upper surface of a 100% bonded tile. In this figure, the dominant response is indicated by a single peak at 1020 Hz, which corresponds to the piston mode. Only the piston mode

Property		Tile (LI-900)	Tile (FRCI-12)	Tile (LI-2200)	SIP (0.16)	SIP (0.09)	RTV (560)
Young's Modulus (lb/in^2)	E_x	25,000	50,000	80,000	180	410	450
	E_y	25,000	50,000	80,000	600	600	450
	E_z	7,000	10,000	27,000	180	410	450
Poisson's Ratio	ν_{xy}	0.18	0.18	0.18	0.15°	0.34°	0.48
	ν_{xz}	0.16	0.16	0.16	0.4	0.4	0.48
	ν_{yz}	0.16	0.16	0.16	0.0	0.0	0.48
Shear Modulus (lb/in^2)	G_{xy}	10,500	13,500□	33,000	50	18	152
	G_{xz}	3,000	4,500	11,000	50	18	152
	G_{yz}	3,000	4,500	11,000	50	18	152
Mass Density ($lb*s^2/in^4$)	ρ	$13.5x10^{-6}$	$18.0x10^{-6}$	$33.0x10^{-6}$	$7.8x10^{-6}$	$11.1x10^{-6}$	$126x10^{-6}$

Legend

° Based on ν_{yx}=0.5

□ Estimate; Actual Value Not Available

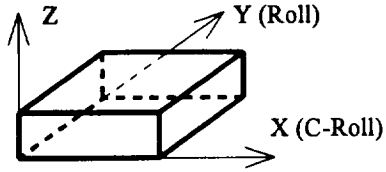

Table 2.1-1. TPS MATERIAL PROPERTIES (AVERAGE VALUES)

Mode Number	Natural Frequencies (Hz)			Mode Shape Description
	100% Bond	80% Bond	60% Bond	
1	480	449	409	Translation in X
2	487	450	416	Translation in Y
3	525	505	495	Rotation about Z
4	1,016	850	728	Rocking about Y (RY)
5	1,020 (P)	969	905	Rocking about X (RX)
6	1,025 (RX)	1,013	1,001	Piston in Z (P)
7	1,489	1,439	1,423	Tile flexing
8	1,898	1,865	1,847	Tile flexing
9	2,031	2,009	1,981	Tile flexing
10	2,371	2,350	2,341	Tile flexing

Table 2.1-2 FINITE ELEMENT RESULTS OF NATURAL FREQUENCIES OF TILE #299

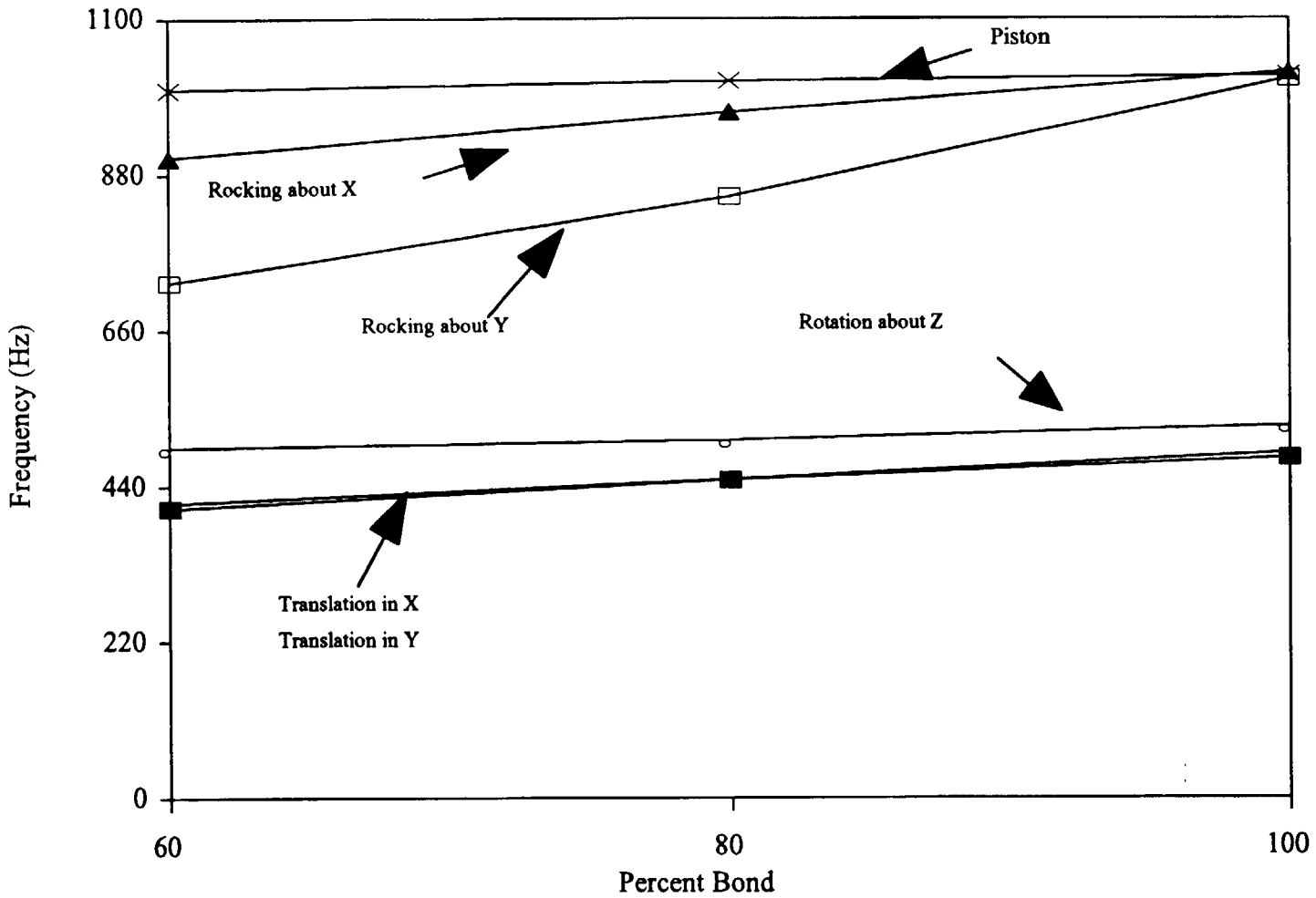

Figure 2.1-1 FREQUENCY VS. PERCENT BOND FOR SINGLE TILE

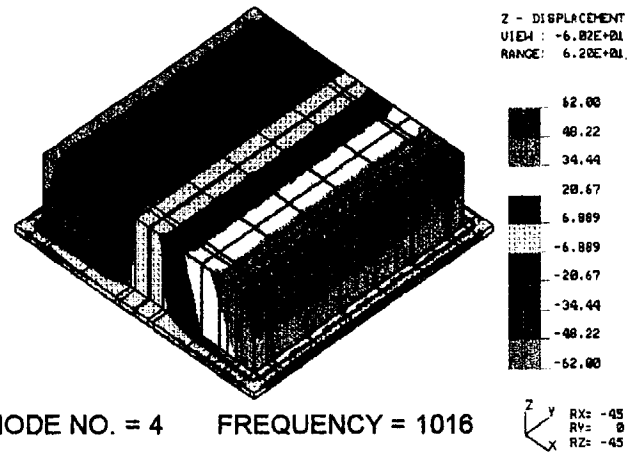

MODE NO. = 4 FREQUENCY = 1016

Figure 2.1-2 ROCKING MODE OF 100% BONDED TILE

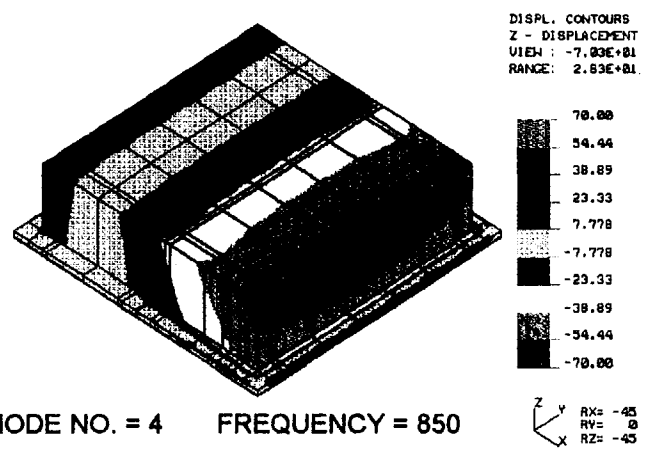

MODE NO. = 4 FREQUENCY = 850

Figure 2.1-3 ROCKING MODE OF 80% BONDED TILE

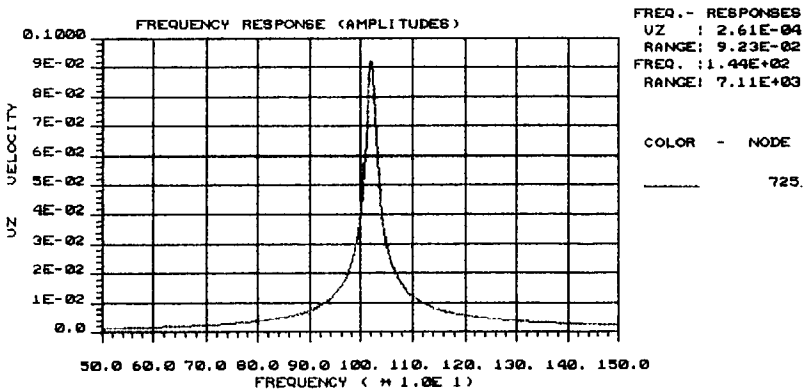

Figure 2.1-4 FREQUENCY RESPONSE OF 100% BONDED TILE (CENTER POINT)

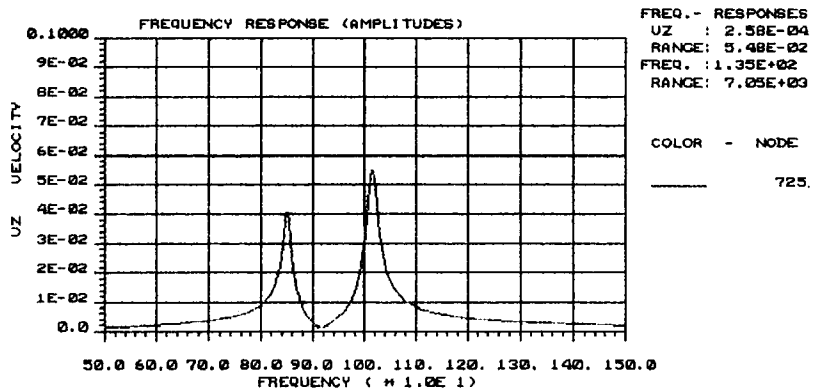

Figure 2.1-5 FREQUENCY RESPONSE OF 80% BONDED TILE (CENTER POINT)

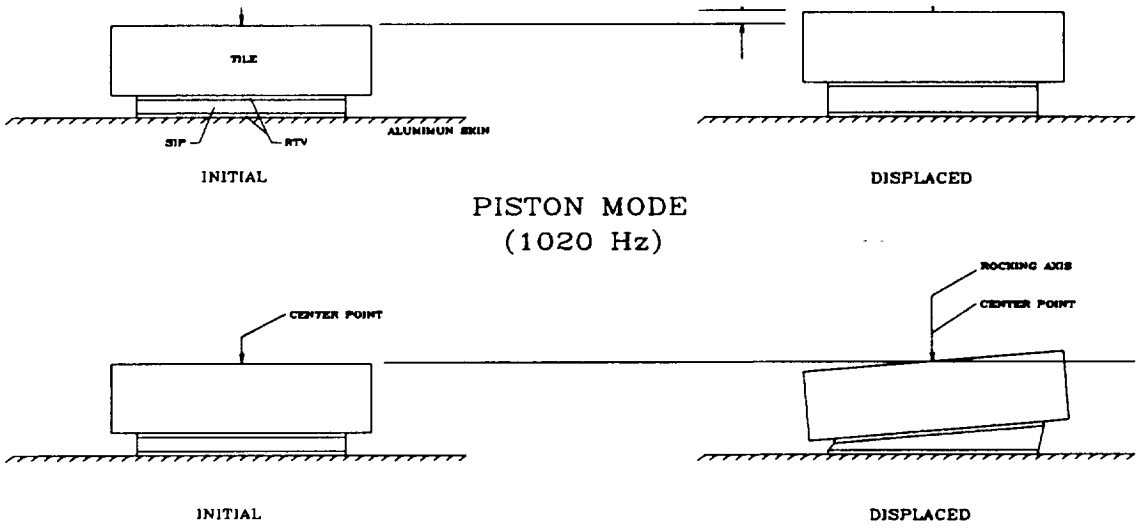

Figure 2.1-6 SINGLE TILE 100% BOND

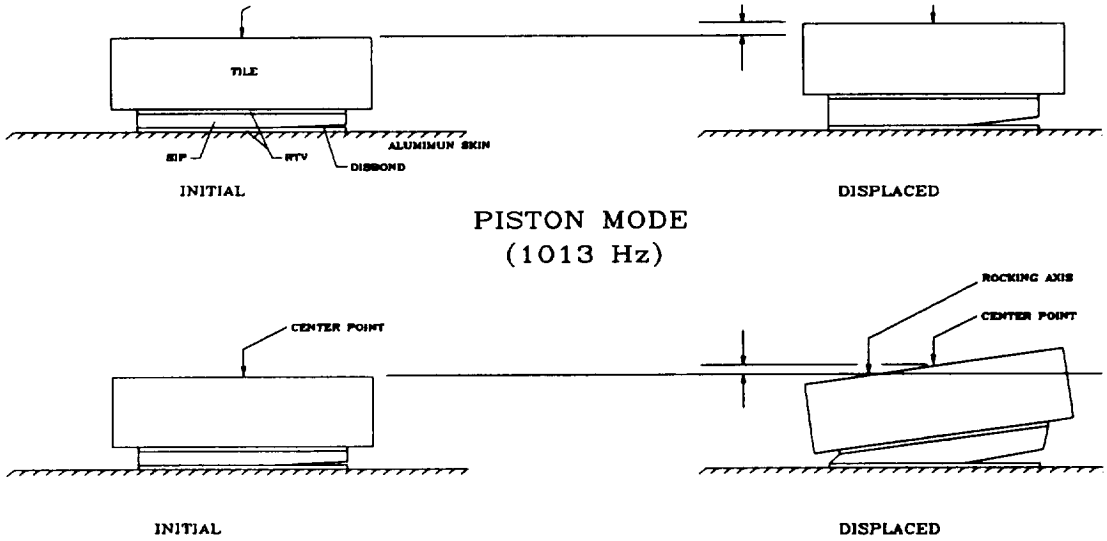

Figure 2.1-7 SINGLE TILE 80% BOND

responds to this type of excitation because a uniform pressure is applied to the tile, and thus the rocking modes are not excited. On the other hand, Figure 2.1-5 shows the frequency response at the same point for an 80% bond case (the edge disbond is in the y-direction). Here, two distinct peaks are present; one at 1013 Hz, corresponding to the piston mode, and the other at 850 Hz, corresponding to the rocking mode about an axis parallel to the y axis and shifted away from the area of disbond. A schematic explanation is depicted in figures 2.1-6 and 2.1-7. This information can be successfully utilized to quickly identify "*good*" and "*bad*" tiles. That is to say, a fully-bonded tile will exhibit single peak, while a tile with a disbond will exhibit multiple peaks in the frequency response plot.

It should be noted, however, that tiles containing disbond will not always exhibit multiple peaks in the frequency response plot. For example, a tile with center disbond will exhibit only one peak corresponding to the piston mode. Clearly, its natural frequency is lower than that of a 100% bonded tile. It is possible to excite the rocking modes for non-symmetric disbond cases by applying the pressure to only a portion of the tile. This is accomplished in the finite element model by applying the pressure, for example, to one quarter of the tile face.

Another point of interest is the amplitude of displacement of the excited tile. This is obtained by the frequency response analysis and is roughly 23 micro-inch for the 100% bonded tile subjected to 100 dB sound pressure. This value is well within the sensitivity range of the commercially available laser vibrometers.

2.2 SEVENTEEN TILE TEST PANEL

A seventeen tile test panel was received for testing (see Fig. 2.2-1). A finite element analysis of this panel was required. An initial step was to determine whether the modal characteristics of each tile where dependent on the other tiles of the panel. A finite element model was created of the entire panel with all the tiles 100% bonded and rigidly supported. Eigenvalue and frequency response analyses were performed. The results of this analysis showed that the natural frequencies of the tiles are not significantly affected by the other tiles on the panel. Tiles completely surrounded by other tiles had modeshapes very close to a single tile model, however tiles on the outer boundary of the panel displayed significant changes in modeshape from a single tile model.

Since the natural frequencies of the tiles of the seventeen tile panel can be found from a single tile model, each of the 7 different bond cases of the 17 tile panel were modeled as a single tile and eigenvalue analysis was performed (see Figure 2.2-2).

2.3 MULTI-TILE MODEL INCLUDING ORBITER VEHICLE SKIN STRUCTURE (45°)

A finite element model was created of a section of the aluminum skin - stringer structure with a pattern of seven tiles attached. This was done in order to study the effects of the multi-tile / structure interaction of the system. Three different cases were analyzed, where the center tile is 100% bonded , 80% bonded (20% edge disbond), and 60%

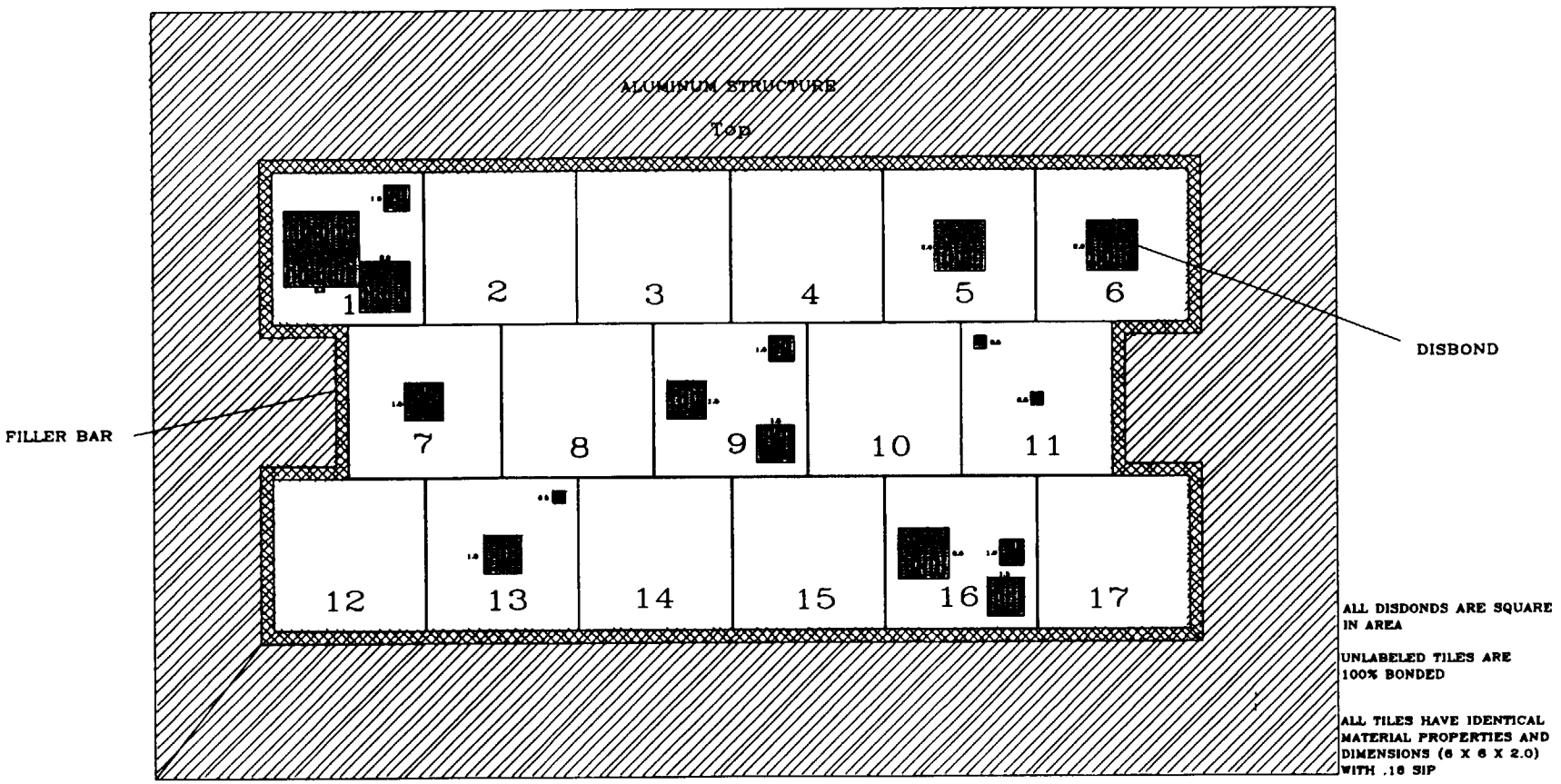

Figure 2.2-1 17-TILE TEST PANEL DISBOND LOCATIONS

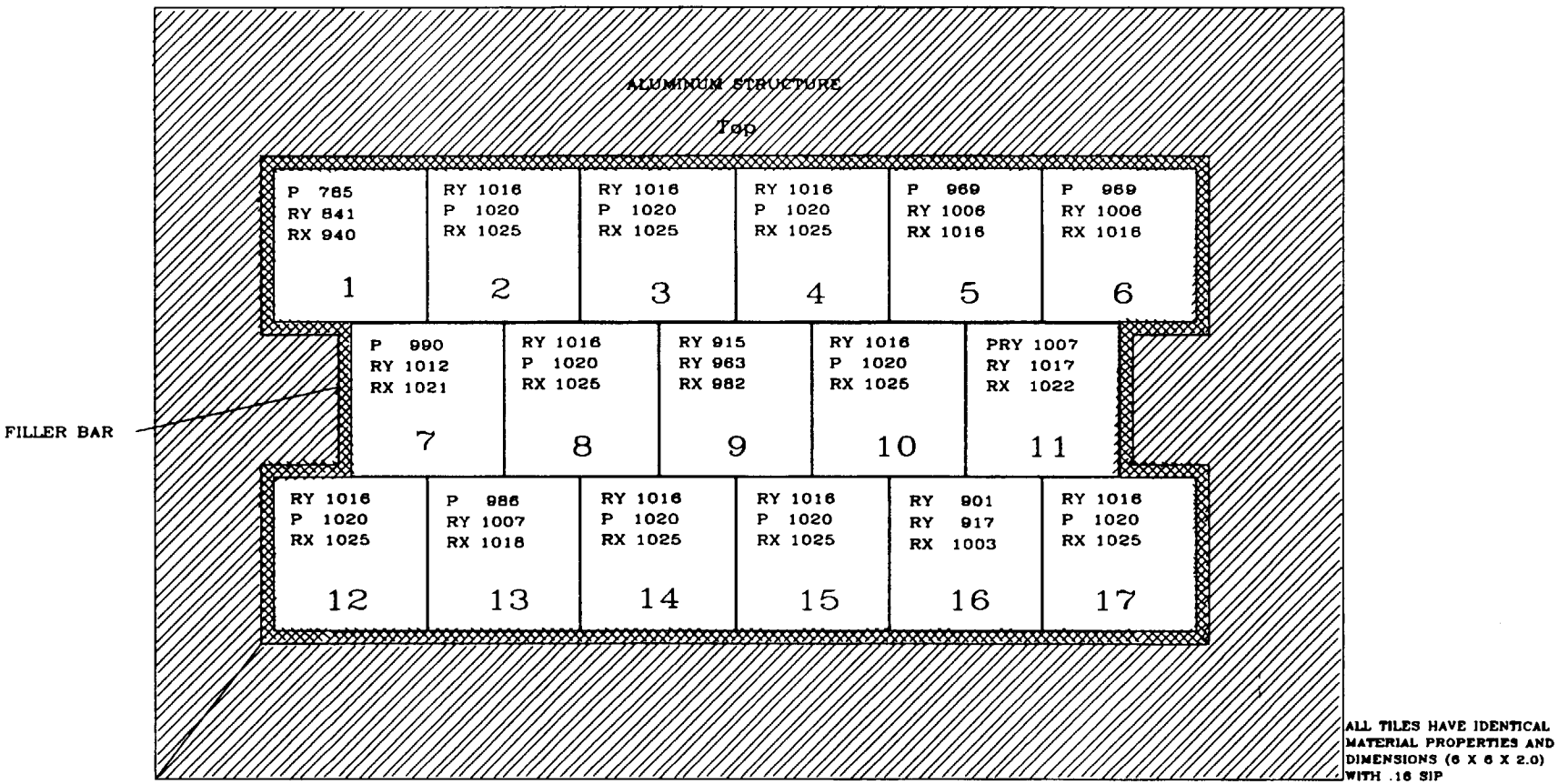

Figure 2.1-2 17-TILE TEST PANEL FINITE ELEMENT RESULTS

bonded (40% edge disbond). The surrounding tiles are 100% bonded for all cases. Eigenvalue and frequency response analyses were performed. In addition a "peak" calculation was performed for 5 points on the tile in question, where the squares of the magnitude of each point is summed together (see Figures. 2.3-1 to 2.3-3)

In order to have the model a feasible size to run on the PC, the sip and RTV layers were combined into a single layer with equivalent properties. Also the size of the aluminum structure is limited by the feasibility of the size of the model. The maximum size was used in order to satisfy the maximum wavefront requirement.

It must also be observed that some of the elements of the model have "bad" aspect ratios due to the complicated geometry and limitations of the size of the model. The results may not be exact, however general characteristics can be observed. The overall stiffness of the structure seems to be sufficient for nearly independent tile modes. When compared to the single tile models, the local stiffness characteristics due to the stringer orientation affect the natural frequencies slightly and the mode shapes greatly. Before any solid conclusion can be made about the structure type modeled here, experimental testing should be done.

Table 2.3-1 displays the "tile modes" for the center tile of the panel modeled for each case. The tile modes where determined from the frequency response of the system when pressure was applied only to the tile in question. Modeshapes for these modes are shown in Figures 2.3-4 to 2.3-6.

Percent Bond (Center Tile)	Natural Frequency (Hz)	Mode Shape
100%	887	P
	1,076	RXY
80%	875	P
	1,011	RXY
60%	835	PRY
	948	RY
	987	RXY

Table 2.3-1 FINITE ELEMENT RESULTS FOR MULTI-TILE ON EXTENDED STRUCTURE

2.4 SENSITIVITY ANALYSIS TO VARIATION OF PHYSICAL PARAMETERS

2.4.1 Single Tile with Two Voids

To study the effect of voids in a tile, a finite element model of a single tile was constructed so that the tile contained three horizontal layers. The center layer was made to be 1/2 inch thick and two 1 inch x 1 inch elements were arbitrarily deleted from the center layer. The eigenvalue analysis results show a increase in natural frequencies for the rigid body modes from the original model (see Table 2.4-1). This is consistent with predicted increase in frequency due to a decrease in mass.

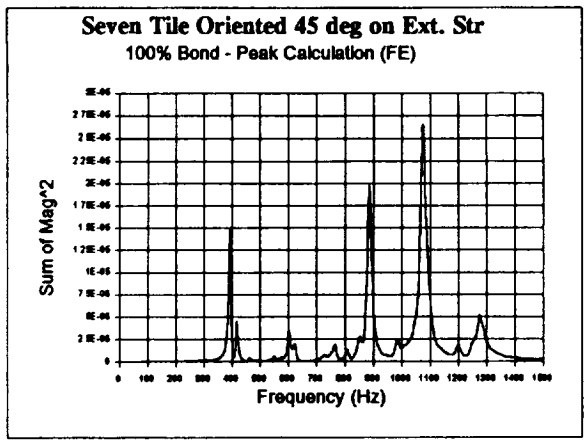

Figure 2.3-1 FREQUENCY RESPONSE FOR SEVEN TILE ORIENTED AT 45° ON EXTENDED STRUCTURE 100% BOND

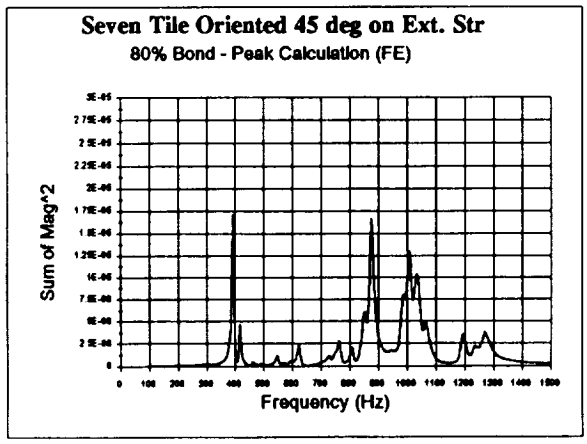

Figure 2.3-2 FREQUENCY RESPONSE FOR SEVEN TILE ORIENTED AT 45° ON EXTENDED STRUCTURE 80% BOND

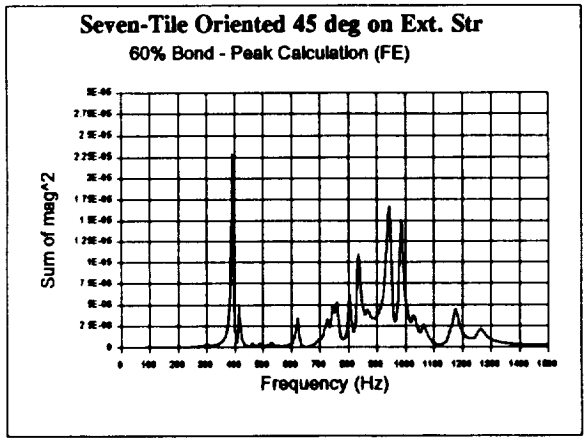

Figure 2.3-3 FREQUENCY RESPONSE FOR SEVEN TILE ORIENTED AT 45° ON EXTENDED STRUCTURE 60% BOND

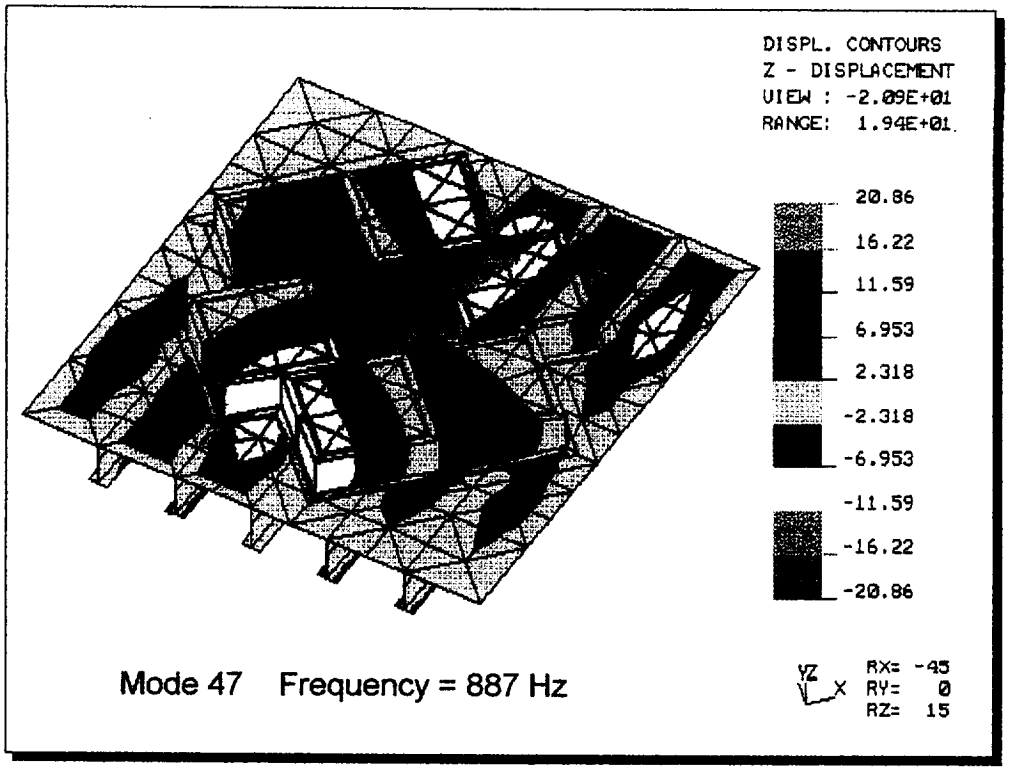

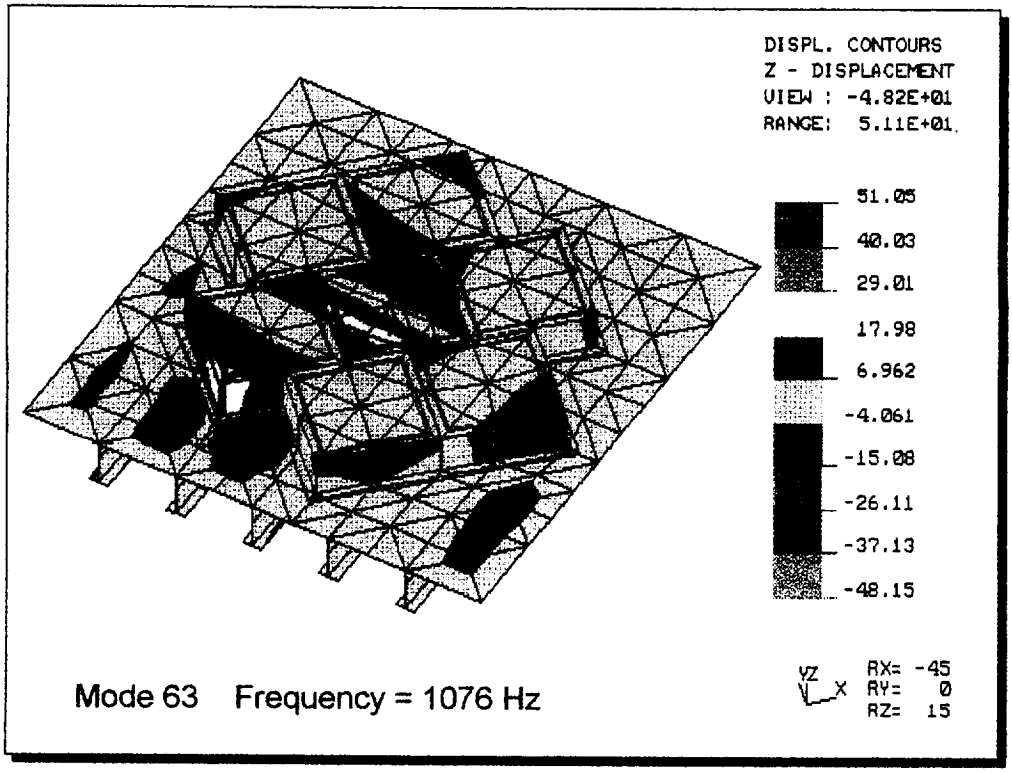

Figure 2.3-4 MODESHAPES FOR SEVEN TILE ORIENTED AT 45° ON EXTENDED STRUCTURE 100% BOND

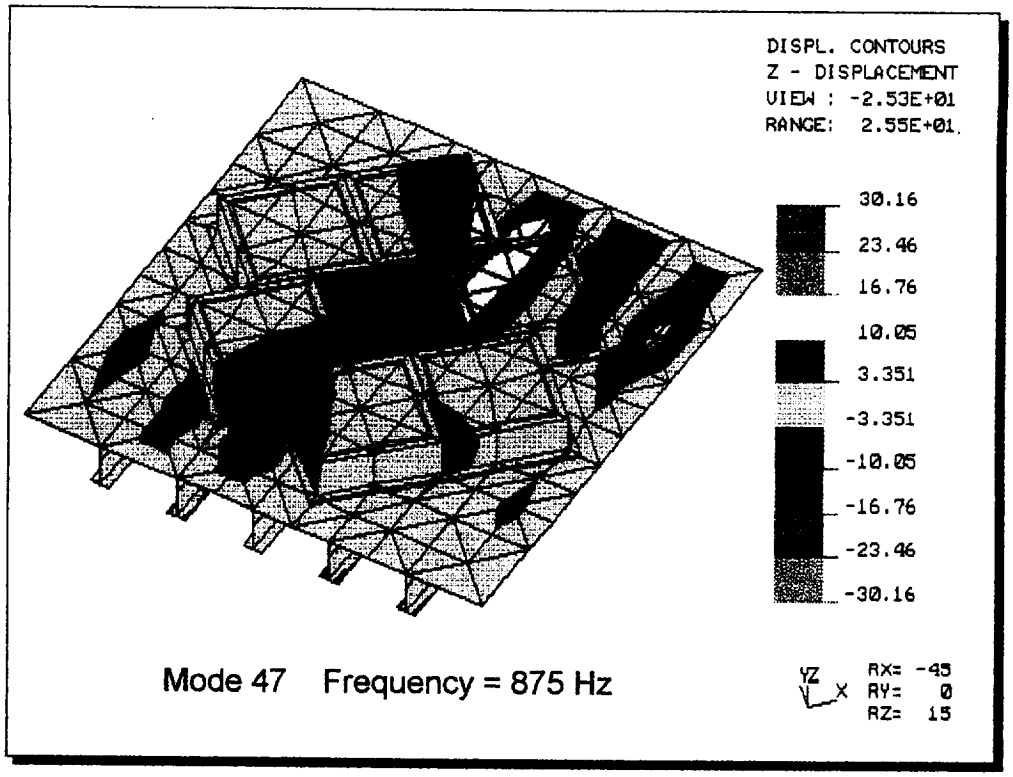

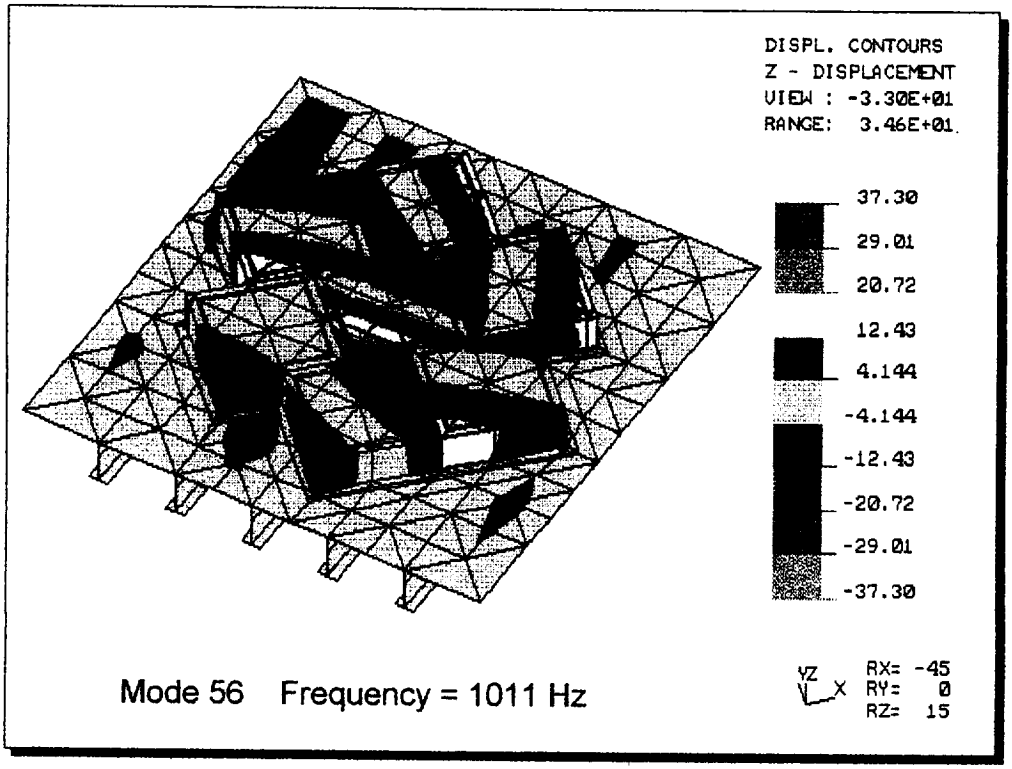

Figure 2.3-5 MODESHAPES FOR SEVEN TILE ORIENTED AT 45° ON EXTENDED STRUCTURE 80% BOND

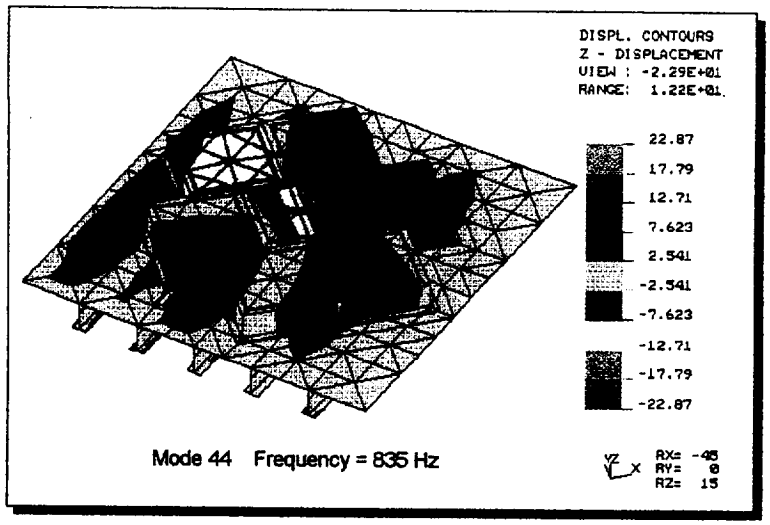

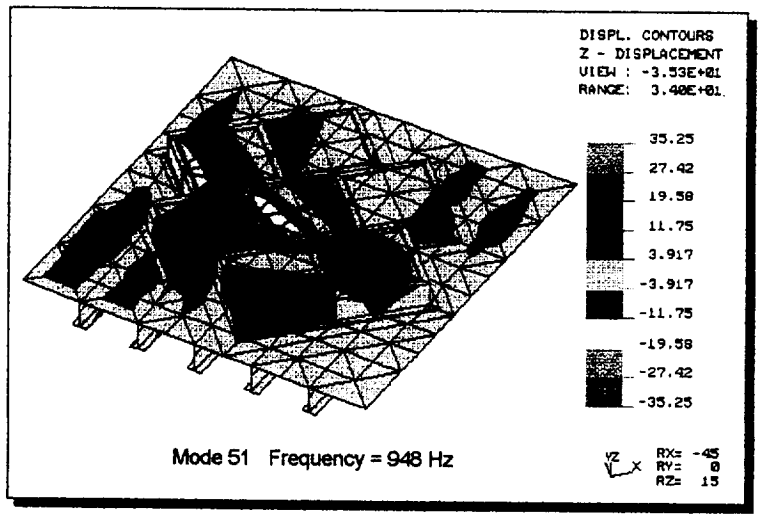

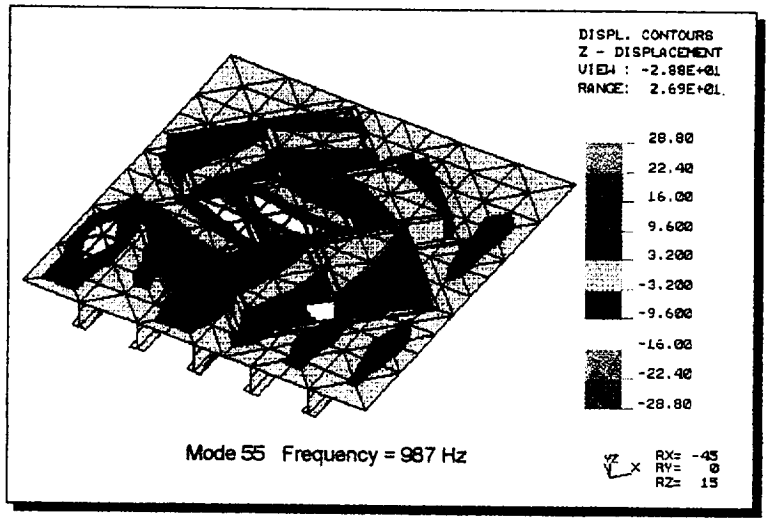

Figure 2.3-6 MODESHAPES FOR SEVEN TILE ORIENTED AT 45° ON EXTENDED STRUCTURE 60% BOND

Mode Number	Frequency					
	100% Bond		80% Bond		60% Bond	
1	481	TX	450	TY	409	TY
2	487	TY	451	TX	417	TX
3	521	ROT	502	ROT	492	ROT
4	1,006	RY	850	RY	729	RY
5	1,016	RX	962	RX	899	RX
6	1,016	P	1,005	P(RY)	993	P(RY)
7	1,474	F	1,426	F	1,409	F
8	1,875	F	1,842	F	1,824	F
9	2,014	F	1,993	F	1,967	F
10	2,331	F	2,308	F	2,297	F

Table 2.4.1-1 FINITE ELEMENT RESULTS FOR SINGLE TILE WITH TWO VOIDS

2.4.2 Single Tile with Water Proofing

To study the effect of variations in density, such as caused by a waterproofing the tile. The finite element model of the single tile that contained the three horizontal layers was used as a basis for this analysis. No information was known at this point about the process of water proofing other than some substance is injected into the tile at several points. As an initial estimate elements of the center layer 1 inch x 1 inch were selected in a checker pattern and the density was increased to twice the original value. As expected the natural frequencies of the rigid body modes were decreased from the original model. The eigenvalue results are shown in table 2.4.2-1.

Mode Number	Frequency					
	100% Bond		80% Bond		60% Bond	
1	459	TX	430	TX	391	TY
2	465	TY	431	TY	398	TX
3	504	ROT	485	ROT	475	ROT
4	968	P	818	RY	700	RY
5	976	RY	933	RX	872	RX
6	984	RX	967	P(RY)	957	P(RY)
7	1,436	F	1,390	F	1,374	F
8	1,839	F	1,808	F	1,792	F
9	1,944	F	1,924	F	1,899	F
10	2,279	F	2,261	F	2,252	F

Table 2.4.2-1 FINITE ELEMENT RESULTS FOR SINGLE TILE WITH WATER PROOFING

2.5 DISBOND SENSITIVITY - EDGE, CORNER, CENTER

Finite element models were created for a single tile with 16% edge, center and corner disbonds (see Figure 2.5-1). Eigenvalue and frequency response analyses were

performed for each case (see Figure 2.5-2). The results showed that the natural frequencies and mode shapes are dependent on the location of the disbond.

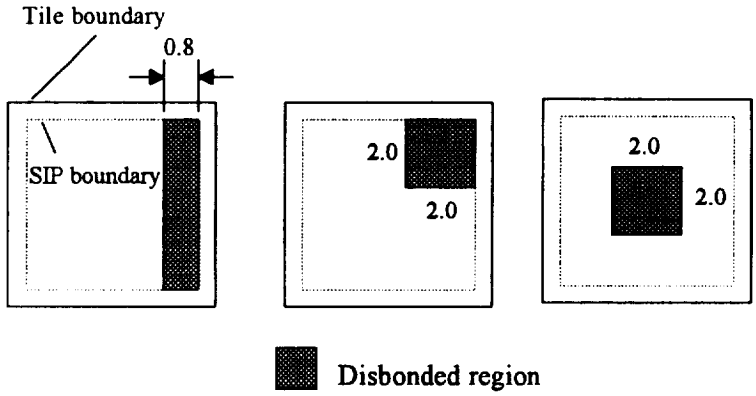

Figure 2.5-1 DISBOND LOCATIONS

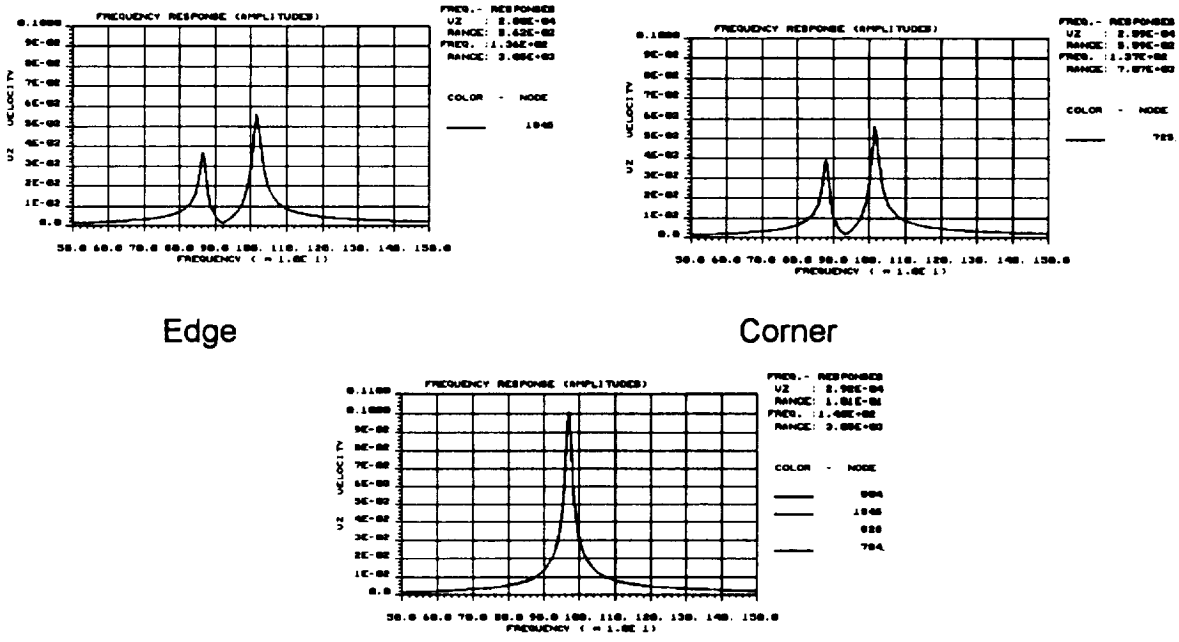

Figure 2.5-2 FREQUENCY RESPONSE OF TILES

2.6 PRESSURE ON 1/4 TILE

The driving force is usually applied the tile in the form of sound energy over the entire face of the tile. For a case of double symmetry, i.e. symmetric about the x and y axes of the bonded area of the sip, only the piston mode responds to this type of excitation. Since an even pressure is applied to the face of the tile and the tile behaves essentially as a rigid body, it is equivalent to a single force applied at the center of pressure which

in this corresponds to the center of the tile. For this case the center point of the tile is stationary for the rocking modes and these modes will not respond for this type of excitation.

On the other hand, the frequency response at the same point for a bond case that is symmetric about only one axis such as the edge disbond case will exhibit two distinct peaks. Using the same argument as above the rocking mode about the symmetry axis will not respond to this type of excitation since the center point of the tile is stationary for this mode. The other two out of plane modes exhibit motion of the center point of the tile due to the piston components of each and therefore show as peaks on the frequency response plot.

Following this same logic, the frequency response of a tile with a non-symetric bond, such that none of the three out of plane modes has a rocking axis that passes through the center of pressure, will have three peaks corresponding to all the three out of plane modes.
It is possible to excite the rocking modes for a symmetric disbond case by applying the pressure to only a portion of the tile. By applying the center of pressure at a point other than the center of flexure or rocking axis, the rocking modes can be exited. This is accomplished in the finite element model by applying the pressure for example to one quarter of the tile face. Experimentally this is accomplished with the use of an acoustical cone in conjunction with the speaker such that the opening of the cone is a fraction of the size of the tile face and placing it off center.

Frequency response analysis was performed on finite element models that contained some sort of symmetry in order to excite all the out of plane modes. Figure 2.6-1 displays frequency response plots for 100% bond, edge disbond, and center disbonds with pressure applied to the entire face of the tile. Notice that only one peak is present for the 100% bond and center disbond tiles. Two peaks are present for the edge disbond case. Figure 2.6-2. displays the frequency response for the same tiles with pressure applied to only one quater of the tile face (off center). Notice that all three out of plane modes are exited.

2.7 GAP FILLER BONDED TO TWO TILES

To address the condition that a gap filler may be used to fill the gap between two adjacent tiles, a finite element model was created to study the inter tile effects. A ten tile panel was used with the center two tiles connected with gap filler. To model the gap filler, the tiles were connected together with brick elements with the RTV material properties. Two models were run, one case in which the center two tiles are 100% bonded (the surrounding tiles are also 100% bonded) (see Figure 2.7-1) and another case in which one is 60% bonded and the other is 100% bonded (see Figure 2.7-2). Eigenvalue analysis was performed.

Full Pressure

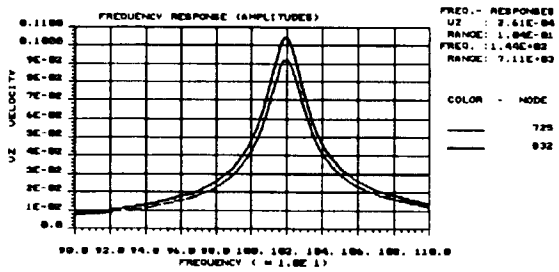

100% Bond

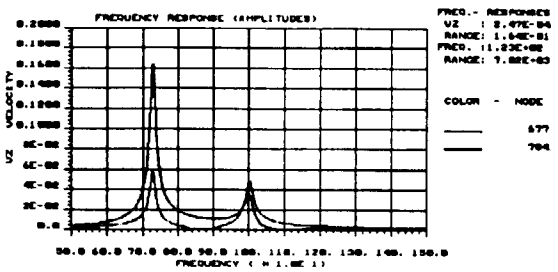

Edge disbond

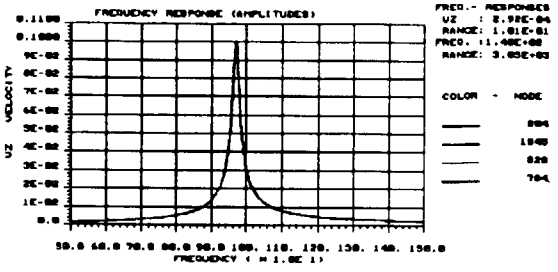

Center disbond

Figure 2.6-1 FREQUENCY RESPONSE OF TILES WITH PRESSURE APPLIED TO ENTIRE FACE OF THE TILE.

Quarter Pressure

(Off center)

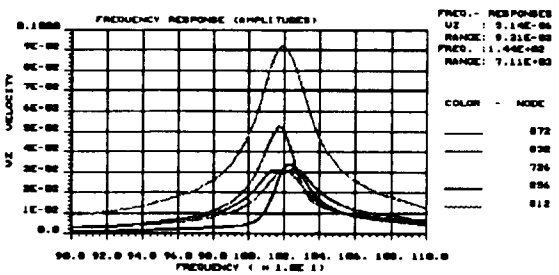

100% Bond

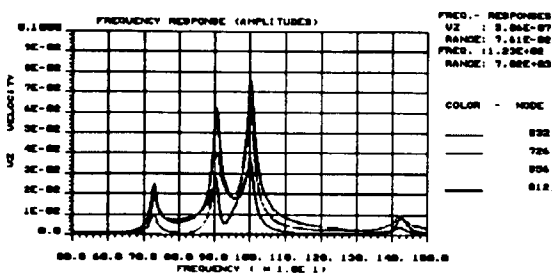

Edge disbond

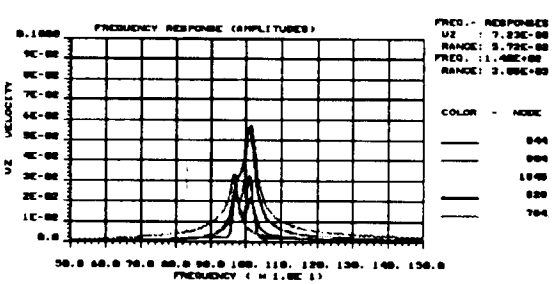

Center disbond

Figure 2.6-2 FREQUENCY RESPONSE OF TILES WITH PRESSURE APPLIED TO ONE QUATER OF THE FACE OF THE TILE.

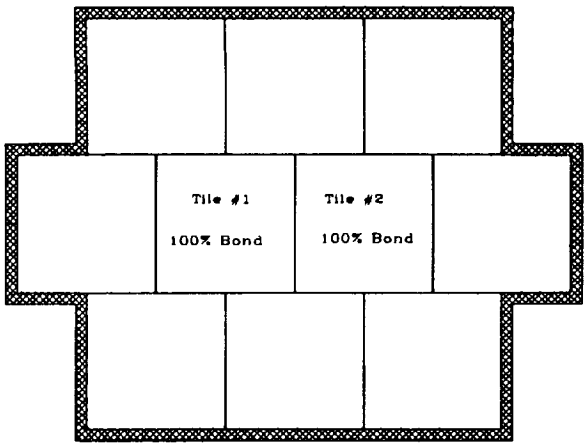

Figure 2.7-1 CASE #1
BOTH TILES 100% BOND

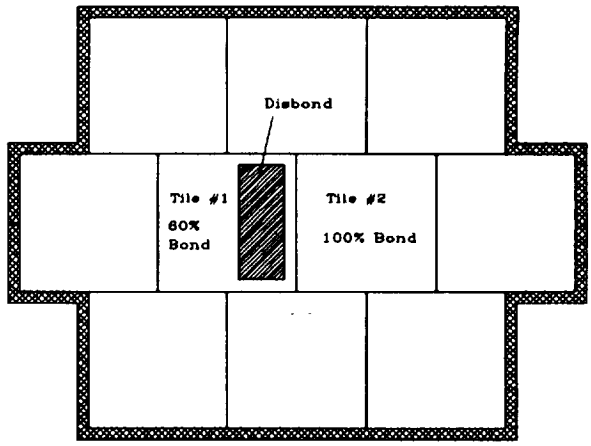

Figure 2.7-2 CASE #2
TILE #1 - 60% BOND, TILE #2 - 100% BOND

Frequency response analysis was done for the pressure applied to each of the center two tiles individually. The results for both tiles 100% bond, show equal results for the pressure applied to either tile, i.e. the response of tiles 1 and 2 when the pressure is applied to tile #1 is the same as the response of tiles 2 and 1 respectively when the pressure is applied to tile #2, as is expected (see Figure 2.7-3). For the case of tile #1 60% bond and tile #2 100% bond, two peaks result (see Figure 2.7-4). When the pressure is applied to tile #1 (the 60% bonded tile), the lower frequency peak has a greater amplitude. When the pressure is applied to tile #2 (the 100% bonded tile), the higher frequency peak has a greater amplitude. Contour plots of the eigenvalue mode shapes corresponding to the peaks in the frequency response are also included (see Figures 2.7-5 and 2.7-6).

Results show that with this type of gap filler, the modal response of the two tiles are very much coupled. This may present a problem in the assumption of the single tile model. However in the actual case, ideally, the gap filler is not directly attached to the tiles themselves but only at the bottom to the underlying filler bar.

2.8 FUZZ BOND MODELING

The case of the fuzz bond presents a difficulty in the finite element analysis. The nature of the fuzz bond is for the most part unknown except that it is an incomplete penetration of the RTV into the sip boundary. This obviously effects the strength of the bond, but how it effects the stiffness of the assembly is unknown at this point. It is assumed that the fuzz bond reduces the stiffness of the RTV/SIP assembly in that region but to what degree is unknown. Also the degree of the fuzz bond may vary. A sensitivity analysis was performed for a 64% bonded tile, or a 36% (3 x 3) center fuzz bond. The fuzz bond was modeled as a reduced stiffness of the lower RTV in the fuzz bonded region. The elastic modulus was reduced to a percentage of the original value, and a sensitivity analysis was performed on this parameter. Since a center fuzz bond was chosen for the

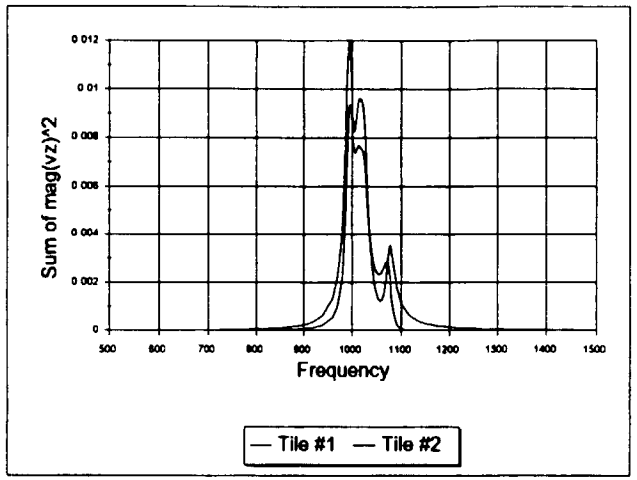

Pressure on Tile #1

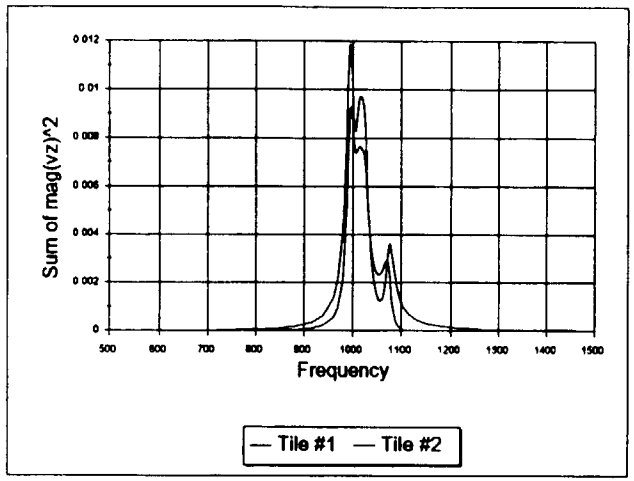

Pressure on Tile #2

Figure 2.7-3 FREQUENCY RESPONSE OF THE TILES, BOTH TILES 100% BOND

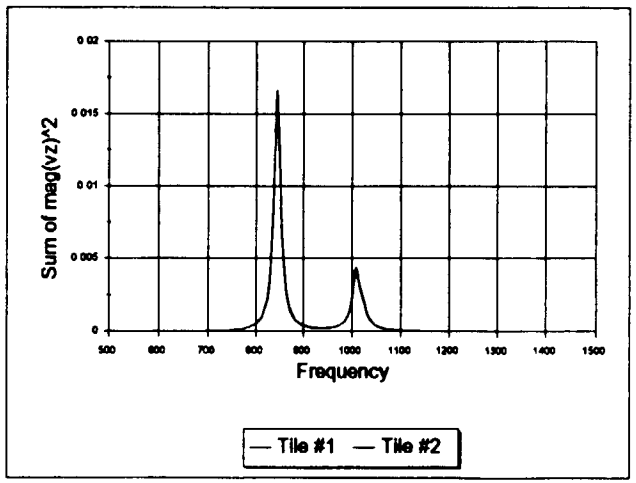

Pressure on Tile #1

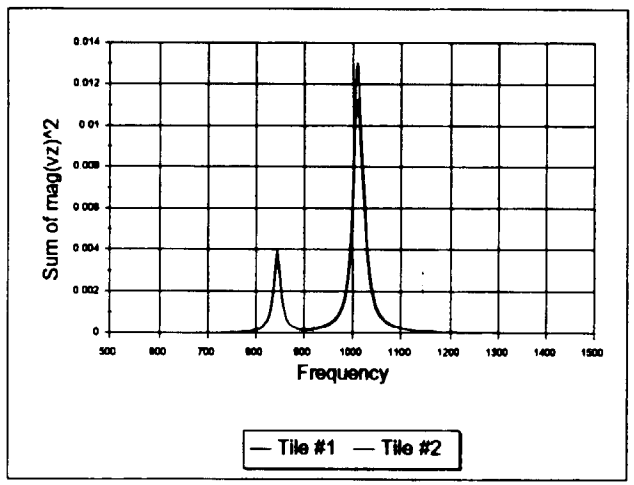

Pressure on Tile #2

Figure 2.7-4 FREQUENCY RESPONSE OF THE TILES, TILE #1 - 60% BOND, TILE #2 - 100% BOND

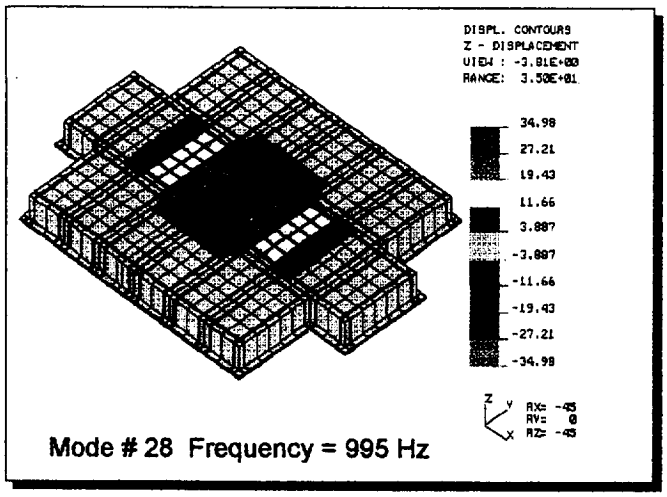

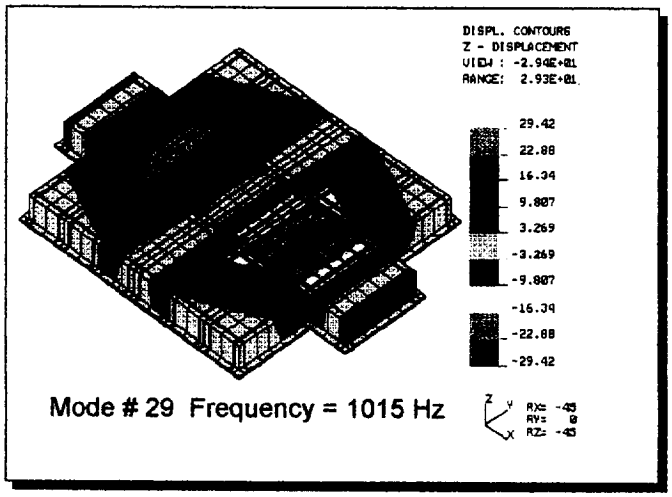

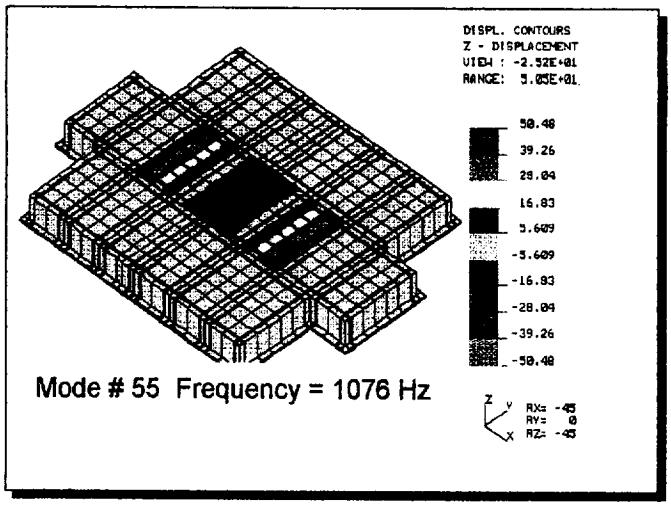

Figure 2.7-5 MODE SHAPES FOR TEN TILE PANEL, GAP FILLER BETWEEN CENTER TWO TILES
TILES #1 & #2 100% BOND

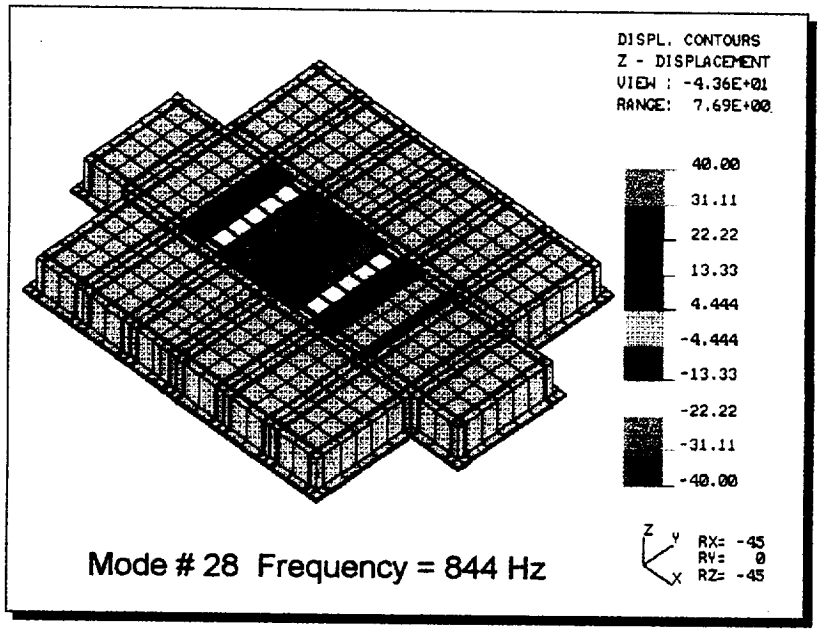

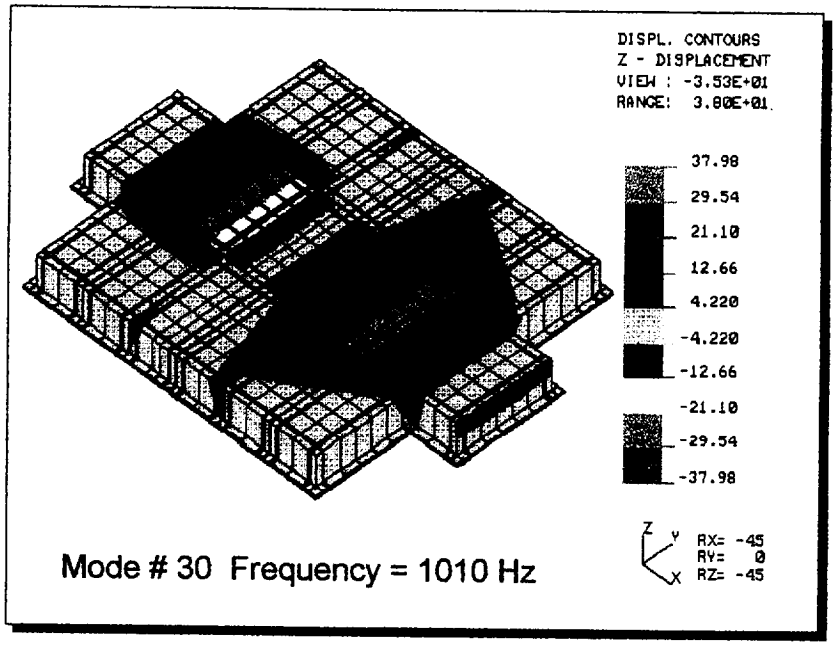

Figure 2.7-6 MODE SHAPES FOR TEN TILE PANEL, GAP FILLER BETWEEN CENTER TWO TILES
TILE #1 - 60% BOND, TILE #2 - 100% BOND

analysis, the mode shapes will remain constant so that frequencies can be directly compared. A model for each of the nine cases below was created and eigenvalue and frequency response analysis was performed for each. The frequencies for the piston, and rocking modes of the tile are shown in Table 2.8-1. A plot of frequency vs. %E is shown in figure 2.8-1 for the three out of plane modes. The frequency response plots for each case is shown in figure 2.8-2.

Another attempt to model this fuzz bond was done by attaching only every other node in the fuzz bonded region. Here a 3x3 center fuzzbond is modeled. Table 2.8-2 displays the eigenvalue results for a 0.75 inch mesh and a 0.375 inch mesh.

A sensitivity analysis was performed for a 60% bonded tile, or a 40% edge fuzz bond. The fuzz bond was modeled as a reduced stiffness of the lower RTV in the fuzz bonded region. The elastic modulus was reduced to a percentage of the original value, and a sensitivity analysis was performed on this parameter (see Table 2.8-2).

% Ez in lower RTV in Fuzz Bond region	P (Hz)	RY (Hz)	RX (Hz)
100%	1,021.4	1,021.2	1,028.2
75%	1,021.3	1,021	1,028
50%	1,021	1,020.7	1,027.7
25%	1,020.3	1,019.8	1,026.8
15%	1,019.3	1,018.7	1,025.9
10%	1,018.1	1,017.5	1,024.8
5%	1,014.7	1,014.6	1,022.2
1%	993.2	1,003.9	1,012.9
0%	987.6	986.1	996.5

Table 2.8-1 EIGENVALUE RESULTS FOR 3X3 CENTER FUZZBOND

Mesh Size	P (Hz)	RY (Hz)	RX (Hz)
0.75 inch mesh	919.6	993.1	1,004.1
0.375 inch mesh	895.6	997.5	1,004

Table 2.8-2 EIGENVALUE RESULTS FOR 3X3 CENTER FUZZBOND

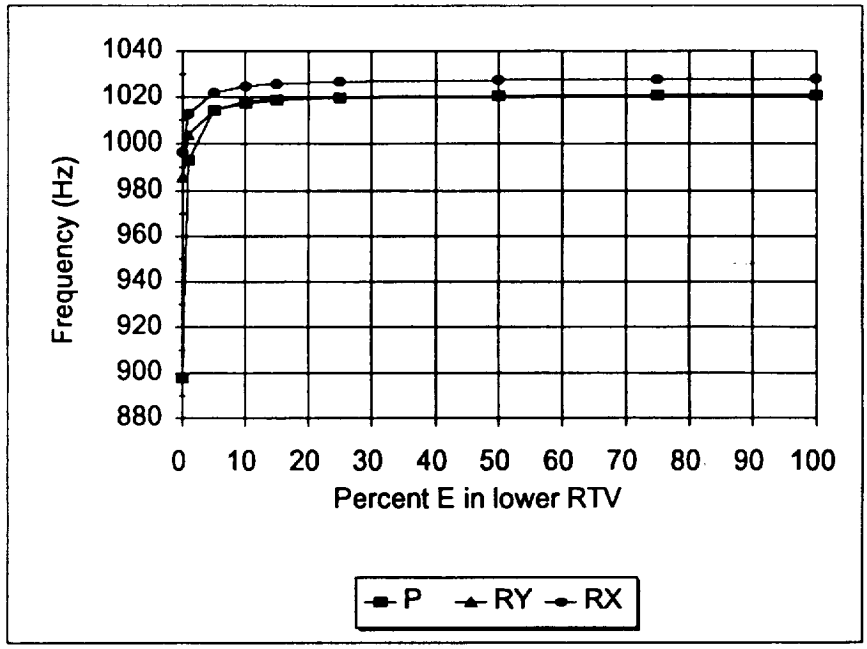

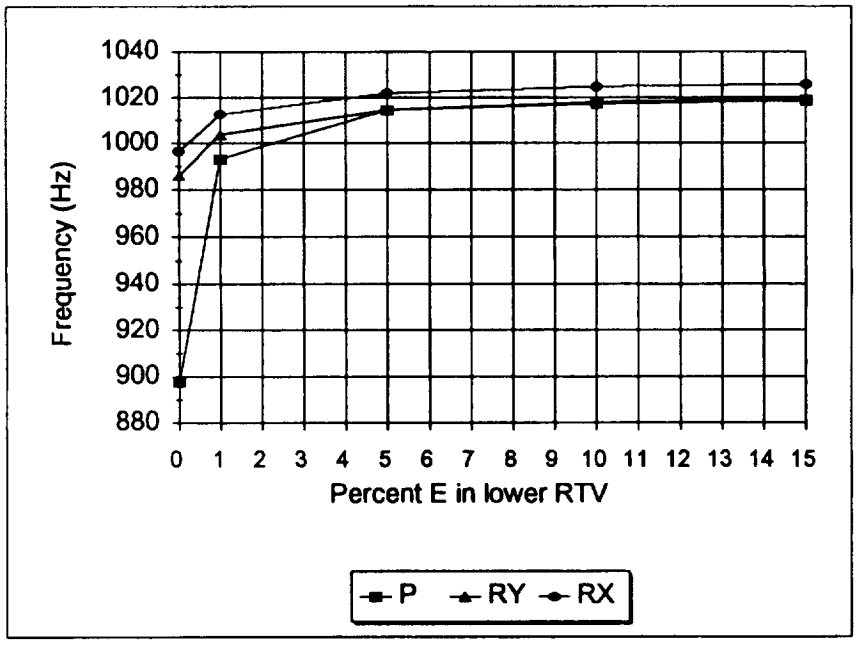

Figure 2.8-1 FREQUENCY VS. DEGREE OF FUZZ BOND FOR 3X3 CENTER FUZZ BOND

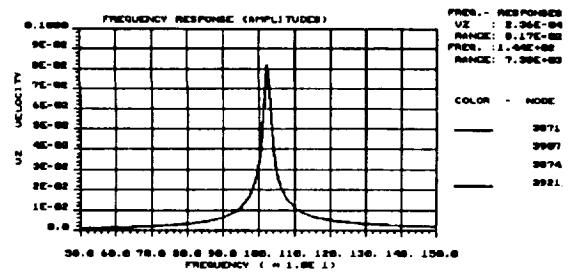

E of lower RTV - 100%

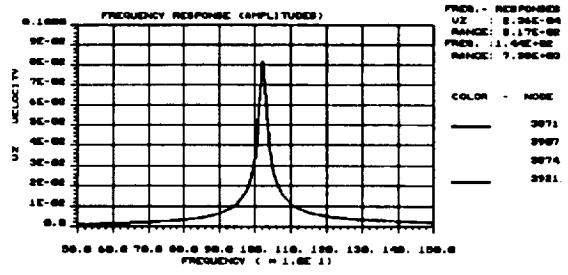

E of lower RTV - 75%

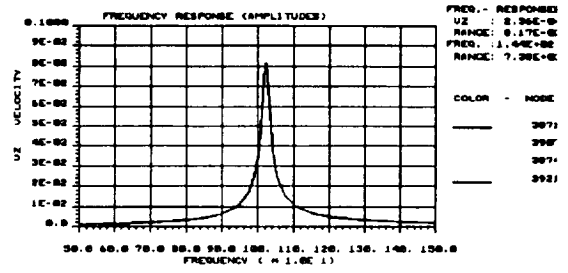

E of lower RTV - 50%

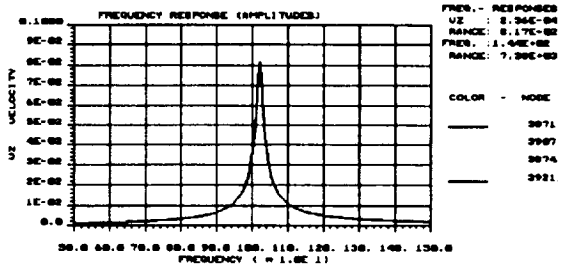

E of lower RTV - 25%

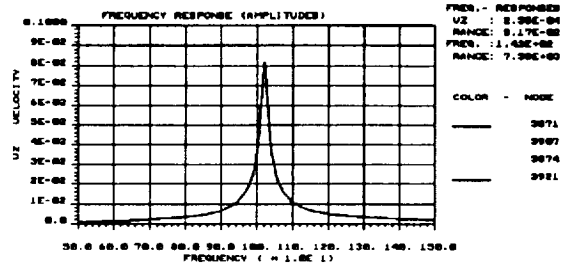

E of lower RTV - 15%

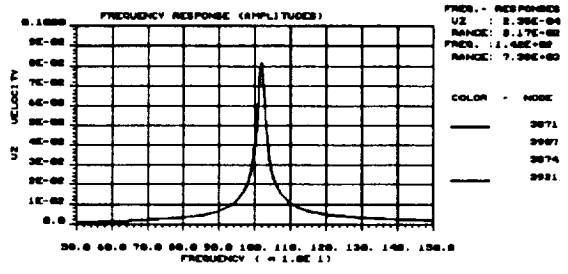

E of lower RTV - 10%

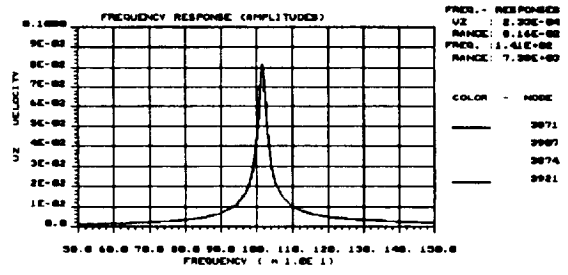

E of lower RTV - 5%

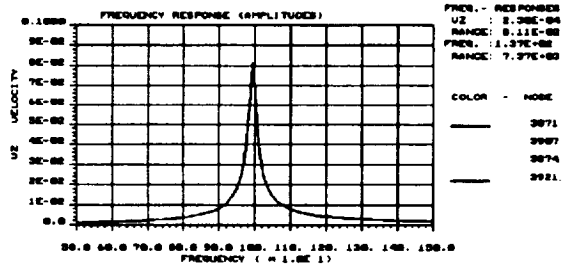

E of lower RTV - 1%

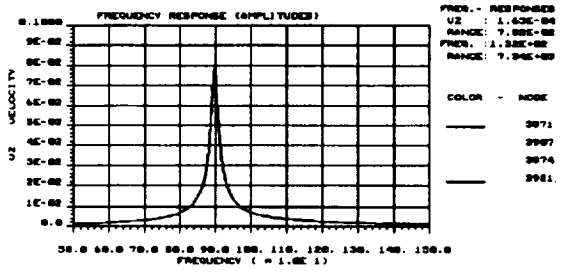

E of lower RTV - 0%

Figure 2.8-2 SENSITIVITY OF FREQUENCY RESPONSE FOR 3X3 CENTER FUZZ BOND

% Ez in lower RTV in Fuzz Bond region	RY(P) (Hz)	P(RY) (Hz)	RX (Hz)
100%	1,016	1,020	1,025
75%	1,015	1,019	1,025
50%	1,011	1,018	1,023
25%	1,002	1,017	1,021
15%	990	1,017	1,017
5%	946	1,016	1,006
0%	728	905	1,001

Table 2.8-3 EIGENVALUE RESULTS FOR 60% BOND OR 40% EDGE FUZZ BONDED AREA

2.9 STRUCTURE TILE INTERACTION, SUPPRESSION OF STRUCTURAL MODES

The presence of structural modes in the modal analysis of a tile on a deformable structure makes the interpretation of the results difficult. The evaluation of the frequency response of a single point on the tile may be insufficient in determining the bond condition for this case. The structure has many modes within the range of the tile modes. It is feasible that the response of the structural modes could have close to the same response as the center point of the tile in a tile mode and therefore the tile mode would be indistinguishable if the center point were used. To identify tile modes from the structural modes, the peaks corresponding to the tile modes must protrude from the rest. To accomplish this, the point on the tile having the maximum response at a particular tile mode must be plotted. For example, the rocking mode of an edge disbond case will have a much lower response at the center point of the tile than the maximum response occurring at one of the four corner points (see Figure 2.9-1). The point on the tile which has the maximum response at any frequency will always be one of the four corner points. Since the corner point having the maximum response is unknown and can vary from one tile mode to another, the frequency response for all four corner points of the tile need to be plotted together.

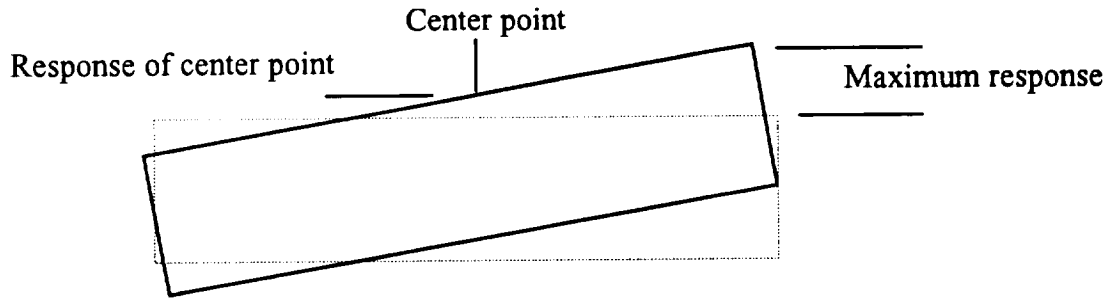

Figure 2.9-1 EDGE DISBOND CASE

3 INVERSE SOLUTION

3.1 EQUATION DEVELOPMENT

The inverse approach is an alternative to comparing experimental data to an established database through finite element modeling to assess the bond conditions of tiles. This approach has the advantage of not requiring the extensive data base of finite element models for every possible disbond condition for every tile configuration case. Thus the inverse approach provides a more direct mathematical solution that requires the least number of measurements to determine the size and location of disbonds.

In this approach, we assume the tile to behave essentially as a rigid body in the six degrees of freedom characteristic to a rigid body, while allowing the SIP material to flex. This assumption has been verified both mathematically and experimentally for tiles at least 2-inch thick with a SIP thickness of 0.16 inches. The eigenvalue problem for the vibrating system is represented by Eq. (1).

$$-\lambda[M]\{\phi\} + [K]\{\phi\} = 0 \qquad (1)$$

For this model, the degrees of freedom of the system are limited to the degrees of freedom of the rigid body tile. The coordinate system is chosen such that there are three in-plane degrees of freedom: translation in x, translation in y, and rotation about z; and three out-of-plane degrees of freedom: translation in z, rotation about x, and rotation about y (see Figure 3.1-1). For a tile having uniform thickness and uniform SIP that is small compared to its other dimensions the in-plane degrees of freedom become essentially uncoupled from the out-of-plane degrees of freedom. Therefore only the three out-of-plane degrees of freedom need be considered. These degrees of freedom are expressed as the out of plane displacement of the center of mass of the tile (z_o) and the angles between the x and y axis of the tile and the horizontal (α_o and β_o).

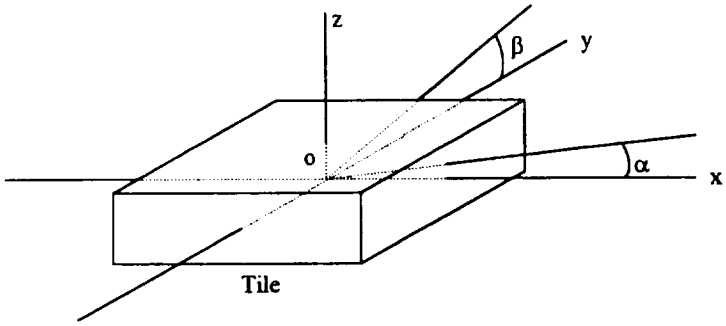

Figure. 3.1-1 COORDINATE SYSTEM

To solve the inverse problem the mass matrix is assumed not to change and therefore is known. The inverse problem is solved for the stiffness. To relate the stiffness matrix

to the physical system the stiffness matrix is derived in terms of physical parameters. The stiffness matrix only consists of terms related to the stiffness of the sip over its volume. The stiffness can be found from finite element theory

$$[K] = \int_{vol} [E]^T [B][E] dV \qquad (2)$$

where $[B] = [L][N]$

$[N]$ is the shape function describing the displacement of any point in the domain in terms of the nodal displacements ($\{u\} = [N]\{\phi\}$).

$[L]$ is a matrix of differential operators that relate the strain to displacements in the domain ($\{\varepsilon\} = [L]\{u\}$).

$[E]$ is the matrix of modulus of elasticity relating stress to strain ($\{\sigma\} = [E][\varepsilon]$).

A single shape function was derived for the entire volume of the SIP. The entire sip (and filler bar) can be modeled as a single element containing two nodes. Each node has three degrees of freedom: an out of plane displacement z, a rotation about the y axis α, and a rotation about the x axis β. Since the stiffness of the tile and the aluminum structure in the plane are much higher than that of the sip material and the thickness of the sip is small to its other dimensions, the in plane strain and the in plane components of the displacement field are assumed to be zero for small angle approximations.

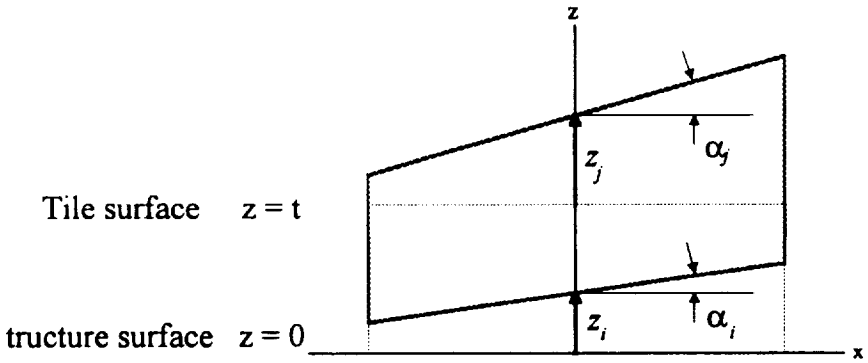

(Similar for β_i and β_j)

Figure 3.1-2 SHAPE FUNCTION

In terms of the nodal displacements, the displacement field in the domain of the sip can be written as

$$u_x = 0$$

$$u_y = 0$$

$$u_z = (z_i + \alpha_i x + \beta_i y) + \tfrac{z}{t}[(z_j + \alpha_j x + \beta_j y) - (z_i + \alpha_i x + \beta_i y))]$$

or

$$u_z = \tfrac{(t-z)}{t}(z_i + \alpha_i x + \beta_i y) + \tfrac{z}{t}(z_j + \alpha_j x + \beta_j y)$$

In matrix form

$$\{u\} = \begin{Bmatrix} u_x \\ u_y \\ u_z \end{Bmatrix} = \tfrac{1}{t}\begin{bmatrix} 0 & 0 & 0 & 0 & 0 & 0 \\ 0 & 0 & 0 & 0 & 0 & 0 \\ (t-z) & (t-z)x & (t-z)y & z & zx & zy \end{bmatrix}\begin{Bmatrix} z_i \\ \alpha_i \\ \beta_i \\ z_j \\ \alpha_j \\ \beta_j \end{Bmatrix} \tag{3}$$

It can now be seen that the shape function $[N]$ is equal to

$$[N] = \tfrac{1}{t}\begin{bmatrix} 0 & 0 & 0 & 0 & 0 & 0 \\ 0 & 0 & 0 & 0 & 0 & 0 \\ (t-z) & (t-z)x & (t-z)y & z & zx & zy \end{bmatrix} \tag{4}$$

The strain displacement relation is given by

It can now be seen that the differential matrix is equal to

$$\{\varepsilon\} = \begin{Bmatrix} \varepsilon_x \\ \varepsilon_y \\ \varepsilon_z \\ \varepsilon_{xy} \\ \varepsilon_{yz} \\ \varepsilon_{xz} \end{Bmatrix} = \begin{bmatrix} \frac{d}{dx} & 0 & 0 \\ 0 & \frac{d}{dy} & 0 \\ 0 & 0 & \frac{d}{dz} \\ \frac{d}{dy} & \frac{d}{dx} & 0 \\ 0 & \frac{d}{dz} & \frac{d}{dy} \\ \frac{d}{dz} & 0 & \frac{d}{dx} \end{bmatrix}\begin{Bmatrix} u_x \\ u_y \\ u_z \end{Bmatrix}, \quad \text{therfore } [L] = \begin{bmatrix} \frac{d}{dx} & 0 & 0 \\ 0 & \frac{d}{dy} & 0 \\ 0 & 0 & \frac{d}{dz} \\ \frac{d}{dy} & \frac{d}{dx} & 0 \\ 0 & \frac{d}{dz} & \frac{d}{dy} \\ \frac{d}{dz} & 0 & \frac{d}{dx} \end{bmatrix} \tag{5}$$

The matrix $[B]$ can now be found

$$[B] = \frac{1}{t}\begin{bmatrix} 0 & 0 & 0 & 0 & 0 & 0 \\ 0 & 0 & 0 & 0 & 0 & 0 \\ -1 & -x & -y & 1 & x & y \\ 0 & 0 & 0 & 0 & 0 & 0 \\ 0 & 0 & (t-z) & 0 & 0 & z \\ 0 & (t-z) & 0 & 0 & z & 0 \end{bmatrix} \tag{6}$$

The modulus of elasticity matrix is given by

$$[E] = \begin{bmatrix} E_{11} & E_{12} & E_{13} & 0 & 0 & 0 \\ E_{21} & E_{22} & E_{23} & 0 & 0 & 0 \\ E_{31} & E_{32} & E_{33} & 0 & 0 & 0 \\ 0 & 0 & 0 & E_{44} & 0 & 0 \\ 0 & 0 & 0 & 0 & E_{55} & 0 \\ 0 & 0 & 0 & 0 & 0 & E_{66} \end{bmatrix} = \begin{bmatrix} \frac{1}{E_x} & \frac{-\nu_{xy}}{E_x} & \frac{-\nu_{xz}}{E_x} & 0 & 0 & 0 \\ \frac{-\nu_{xy}}{E_y} & \frac{1}{E_y} & \frac{-\nu_{yz}}{E_y} & 0 & 0 & 0 \\ \frac{-\nu_{xz}}{E_z} & \frac{-\nu_{yz}}{E_z} & \frac{1}{E_z} & 0 & 0 & 0 \\ 0 & 0 & 0 & \frac{1}{2G_{xy}} & 0 & 0 \\ 0 & 0 & 0 & 0 & \frac{1}{2G_{yz}} & 0 \\ 0 & 0 & 0 & 0 & 0 & \frac{1}{2G_{xz}} \end{bmatrix}^{-1} \tag{7}$$

Now the integrand of the equation for the stiffness matrix can be found

$$[B]^T[E][B] = \frac{1}{t^2}\begin{bmatrix} E_{33} & E_{33}x & E_{33}y & -E_{33} & -E_{33}x & -E_{33}y \\ E_{33}x & E_{33}x^2 + E_{66}(t-z)^2 & E_{33}xy & -E_{33}x & -E_{33}x^2 + E_{66}z(t-z) & -E_{33}xy \\ E_{33}y & E_{33}xy & E_{33}y^2 + E_{55}(t-z)^2 & -E_{33}y & -E_{33}xy & -E_{33}y^2 + E_{55}z(t-z) \\ -E_{33} & -E_{33}x & -E_{33}y & E_{33} & E_{33}x & E_{33}y \\ -E_{33}x & -E_{33}x^2 + E_{66}z(t-z) & -E_{33}xy & E_{33}x & E_{33}x^2 + E_{66}z^2 & E_{33}xy \\ -E_{33}y & -E_{33}xy & -E_{33}y^2 + E_{55}z(t-z) & E_{33}y & E_{33}xy & E_{33}y^2 + E_{55}z^2 \end{bmatrix} \tag{8}$$

Now integrating over the volume of the domain gives the stiffness matrix.

$$[K] = \int_{\text{vol}} [E]^T[B][E]dV \tag{9}$$

The following integral definitions can be substituted

$$\begin{aligned} &\int dA = A && \int x^2\, dA = I^A_{oyy} \\ &\int x\, dA = A\bar{x} && \int y^2\, dA = I^A_{oxx} \\ &\int y\, dA = A\bar{y} && \int xy\, dA = I^A_{oxy} \end{aligned} \tag{10}$$

The stiffness matrix becomes

$$[K] = \frac{E_{33}}{t}\begin{bmatrix} A & A\bar{x} & A\bar{y} & -A & -A\bar{x} & -A\bar{y} \\ A\bar{x} & I^A_{oyy}+\frac{1}{3}A\frac{E_{66}}{E_{33}}t^2 & I^A_{oxy} & -A\bar{x} & -I^A_{oyy}+\frac{1}{6}A\frac{E_{66}}{E_{33}}t^2 & -I^A_{oxy} \\ A\bar{y} & I^A_{oxy} & I^A_{oxx}+\frac{1}{3}A\frac{E_{55}}{E_{33}}t^2 & -A\bar{y} & -I^A_{oxy} & -I^A_{oxx}+\frac{1}{6}A\frac{E_{55}}{E_{33}}t^2 \\ -A & -A\bar{x} & -A\bar{y} & A & A\bar{x} & A\bar{y} \\ -A\bar{x} & -I^A_{oyy}+\frac{1}{6}A\frac{E_{66}}{E_{33}}t^2 & -I^A_{oxy} & A\bar{x} & I^A_{oyy}+\frac{1}{3}A\frac{E_{66}}{E_{33}}t^2 & I^A_{oxy} \\ -A\bar{y} & -I^A_{oxy} & -I^A_{oxx}+\frac{1}{6}A\frac{E_{55}}{E_{33}}t^2 & A\bar{y} & I^A_{oxy} & I^A_{oxx}+\frac{1}{3}A\frac{E_{55}}{E_{33}}t^2 \end{bmatrix} \quad (11)$$

Now it can be shown that the $\frac{1}{3}\frac{E_{66}}{E_{33}}t^2$ terms are very small compared to the I^A_{oyy} and I^A_{oxx} terms for an area with length and width dimensions large compared to the thickness. Consider the case

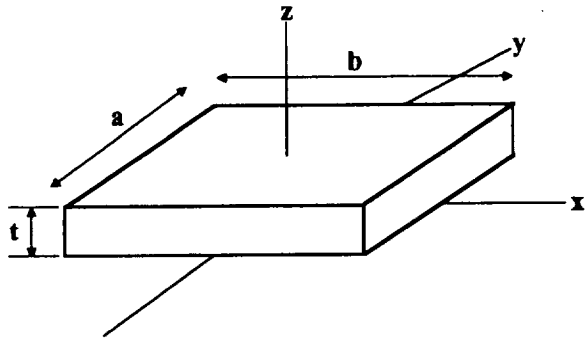

Figure 3.1-3 SIP DIMENSIONS.

$$I^A_{oxx} = \frac{1}{12}a^3 b \qquad I^A_{oyy} = \frac{1}{12}ab^3 \qquad A = ab \qquad (12\text{-}14)$$

$$(E_{33} > E_{66})$$

t much less than a and b

t^2 insignificant to a^2 and b^2

$$t^2 << a^2$$

$$4\frac{E_{66}}{E_{33}}t^2 << a^2$$

$$\frac{1}{3}\frac{E_{66}}{E_{33}}abt^2 << \frac{1}{12}a^3 b$$

Therefore $\frac{1}{3}\frac{E_{66}}{E_{33}}At^2 << I^A_{oxx}$ and can be dropped.

Similar for I^A_{oyy}

Now the stiffness matrix is simplified to

$$[K] = \frac{E_{33}}{t}\begin{bmatrix} A & A\bar{x} & A\bar{y} & -A & -A\bar{x} & -A\bar{y} \\ A\bar{x} & I^A_{oyy} & I^A_{oxy} & -A\bar{x} & -I^A_{oyy} & -I^A_{oxy} \\ A\bar{y} & I^A_{oxy} & I^A_{oxx} & -A\bar{y} & -I^A_{oxy} & -I^A_{oxx} \\ -A & -A\bar{x} & -A\bar{y} & A & A\bar{x} & A\bar{y} \\ -A\bar{x} & -I^A_{oyy} & -I^A_{oxy} & A\bar{x} & I^A_{oyy} & I^A_{oxy} \\ -A\bar{y} & -I^A_{oxy} & -I^A_{oxx} & A\bar{y} & I^A_{oxy} & I^A_{oxx} \end{bmatrix} \tag{15}$$

Mass Matrix

The mass matrix can be found with the use of Lagrange's equations

$$\frac{d}{dt}\left(\frac{dL}{d\dot{q}_i}\right) - \frac{dL}{dq_i} = Q_i \quad \text{where} \quad L = T - V \tag{16}$$

The term $\frac{d}{dt}\left(\frac{dL}{d\dot{q}_i}\right)$ contains the necessary components of the mass matrix. The tile is assumed to have a mass of m and mass moment of inertia's I_y and I_x about the center of mass. The kinetic energy is given by

$$T = \tfrac{1}{2}m\dot{z}^2 + \tfrac{1}{2}I_y\dot{\alpha}^2 + \tfrac{1}{2}I_x\dot{\beta}^2 \tag{17}$$

The potential energy V is assumed to contain no derivatives of the displacements so that

$$\frac{dL}{d\dot{q}_i} = \frac{dT}{d\dot{q}_i}$$

$$\frac{dT}{d\dot{z}} = m\dot{z} \qquad \frac{dT}{d\dot{\alpha}} = I_y\dot{\alpha} \qquad \frac{dT}{d\dot{\beta}} = I_x\dot{\beta}$$

$$\frac{d}{dt}\left(\frac{dT}{d\dot{z}}\right) = m\ddot{z} \qquad \frac{d}{dt}\left(\frac{dT}{d\dot{\alpha}}\right) = I_y\ddot{\alpha} \qquad \frac{d}{dt}\left(\frac{dT}{d\dot{\beta}}\right) = I_x\ddot{\beta} \tag{18}$$

The tile mass is wholly at the j node so the mass matrix can be written in terms of z_i, α_i, β_i, z_j, α_j, and β_j as

$$[M] = \begin{bmatrix} 0 & 0 & 0 & 0 & 0 & 0 \\ 0 & 0 & 0 & 0 & 0 & 0 \\ 0 & 0 & 0 & 0 & 0 & 0 \\ 0 & 0 & 0 & m & 0 & 0 \\ 0 & 0 & 0 & 0 & I_y & 0 \\ 0 & 0 & 0 & 0 & 0 & I_x \end{bmatrix} \tag{19}$$

Since it is very difficult to measure the strutural vibration experimentally, the stucture can be assumed to be rigid. The degrees of freedom of the system now only consists of the out of plane degrees of freedom of the tile.

The stiffness matrix $[K]$ is now

$$[K] = \frac{E_{33}}{t}\begin{bmatrix} A & A\bar{x} & A\bar{y} \\ A\bar{x} & I^A_{oyy} & I^A_{oxy} \\ A\bar{y} & I^A_{oxy} & I^A_{oxx} \end{bmatrix} \tag{20}$$

The mass matrix consists of the mass and mass moment of inertia's of the tile and sip. The mass matrix $[M]$ is now

$$[M] = \begin{bmatrix} m & 0 & 0 \\ 0 & I_y & 0 \\ 0 & 0 & I_x \end{bmatrix} \tag{21}$$

The following equation shows the final eigenvalue problem with the assumption of no structural motion.

$$\left(\frac{E_{33}}{t}\begin{bmatrix} A & A\bar{x} & A\bar{y} \\ A\bar{x} & I^A_{oyy} & I^A_{oxy} \\ A\bar{y} & I^A_{oxy} & I^A_{oxx} \end{bmatrix} - \lambda \begin{bmatrix} m & 0 & 0 \\ 0 & I_y & 0 \\ 0 & 0 & I_x \end{bmatrix} \right) \begin{Bmatrix} z_o \\ \alpha \\ \beta \end{Bmatrix} = 0 \tag{22}$$

(4)

where A is the bonded area of the sip and filler bar.

$\bar{x}$ and $\bar{y}$ are the distances from the coordinate axes to the centroid of the bonded area of the sip and filler bar.

I^A_{oyy}, I^A_{oxx}, and I^A_{oxy} are the area moment of inertia's and product of inertia's of the bonded area of the sip and filler bar.

E_{33} is an equivalent elastic modulus of the sip and filler bar in the z direction.

t is the thickness of the sip and filler bar.

Given the geometries and material properties of the tile assembly, the above equations for each natural frequency can be used to solve for the components of the stiffness matrix.

$$[K] = [M][X][\Lambda][X]^{-1} \tag{23}$$

where $[X]$ is a matrix with the eigenvectors (mode shapes) as its columns

$$[X] = \left[\{\phi\}_1 \ \{\phi\}_2 \ \{\phi\}_3 \right] \tag{24}$$

and [Λ] is a martix with the eigenvalues on the diagonal.

$$[\Lambda] = \begin{bmatrix} \lambda_1 & 0 & 0 \\ 0 & \lambda_2 & 0 \\ 0 & 0 & \lambda_3 \end{bmatrix} \tag{25}$$

Solving the stiffnes matrix for the area, centriod, and area moments of inertia of the bonded area; the percentage bond and the location and size of the disbond can be calculated.

3.2 COMPUTER PROGRAMMING

This procedure is in the process of being implemented into a C++ computer program (Bond Verification program) that will carry out this procedure in "real time". The input and output of this program are as follows.

Input

Data file containing the geometries and material properties of the tile, sip, and RTV

Data file containing either only the natural frequencies or both the natural frequencies and mode shapes of the tile assembly

Output

If only natural frequency used, an upper and lower bound of the possible percentage bond is calculated.

If both the natural frequencies and mode shapes are used,

(a) Percentage bond
(b) Area of disbond
(c) Location of disbond
(d) Aspect ratio and orientation of disbond
(e) Diagram showing the disbond and its location

The program is written in Borland C++ for Windows and runs in the Windows environment. This makes it easy to run it simultaneously with the STARS modal analysis software used in the experimental analysis since it is also a Windows based program. Data modal data from the STARS program can be outputed to a data file which then can be inputed directly into the Bond Verification Program.

3.3 COMPARISON WITH FINITE ELEMENT RESULTS

This technique will be validated with some finite element models. Finite element models will be created for specific disbond cases, and eigenvalue analysis carried out. The output (i.e., natural frequencies and mode shapes) will be used as input to the inverse solution. Preliminary results of the inverse approach have produced a nearly exact disbond as that which was originally incorporated on the finite element models. Hoever, at this point in the development of the Bond Verification program the disbonded area is represented as a single rectangular region. For multiple disbonds, the area of disbond is represented as a rectangle with its center at the centriod of the disbond. Figure 3.3-1 displays some results of the inverse method with input with finite element data. Since the results are very close to the actual case, the theory and assumptions made in the derivation of the inverse problem are proveb to be valid.

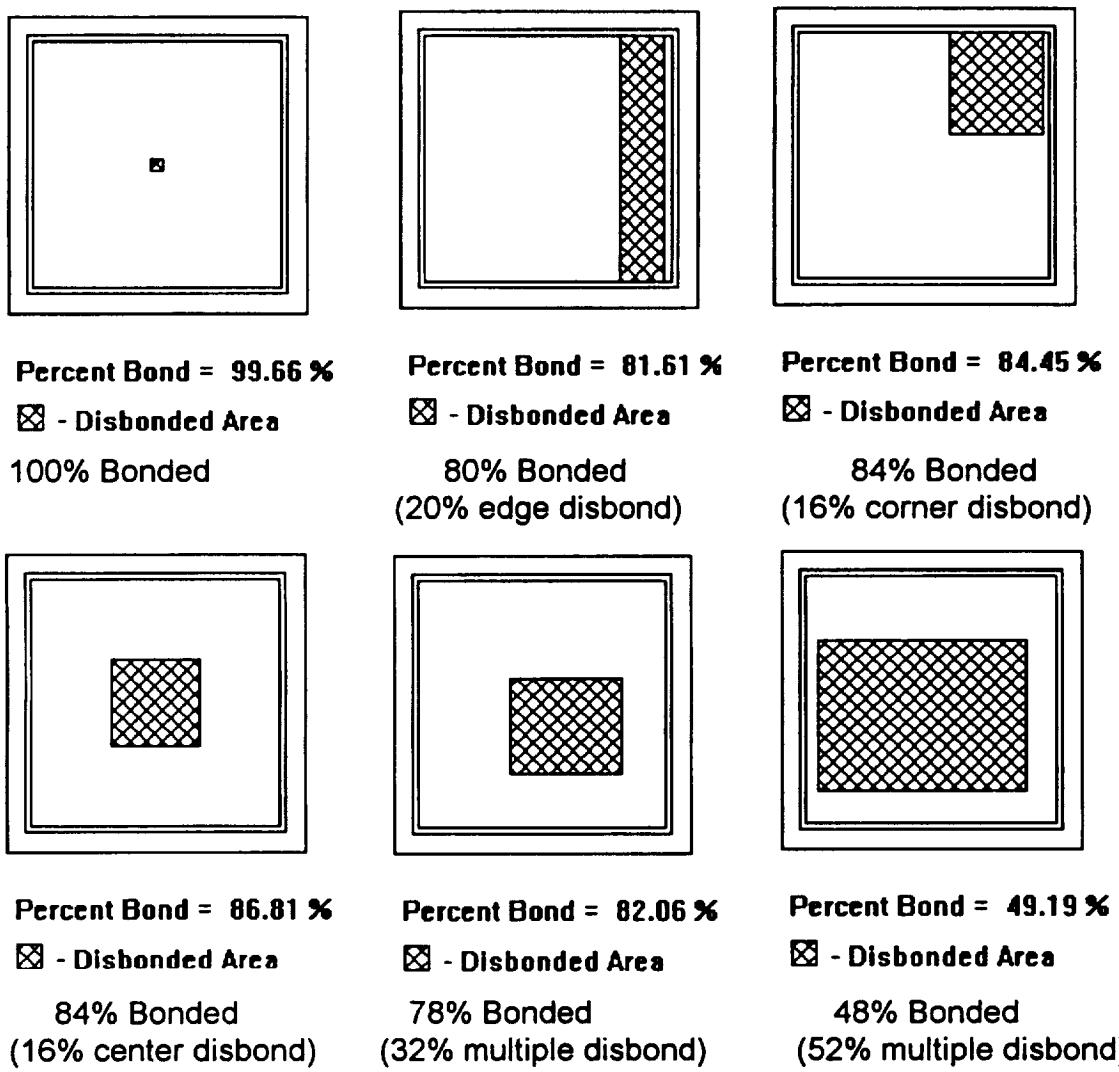

Figure 3.3-1 RESULTS OF THE INVERSE METHOD USING FINITE ELEMENT DATA AS INPUT.

3.4 COUPLING WITH EMA AND STARS PROGRAM

The inverse solution software will be compatible with the modal analysis software used in the experimental analysis. Also this inverse solution must be validated with experimental data for many types of disbond conditions as well as several types of tile geometries. Also the assumed type of disbond case needs to be considered such as singular rectangular disbonds, multiple disbonds, etc.

3.5 TESTING WITH 17-TILE TEST PANEL EMA

Some data found from experimental testing of the tiles of the the 17-tile test panel was used as input into the Bond Verification program. The results of the inverse method are shown in Figure 3.5-1.

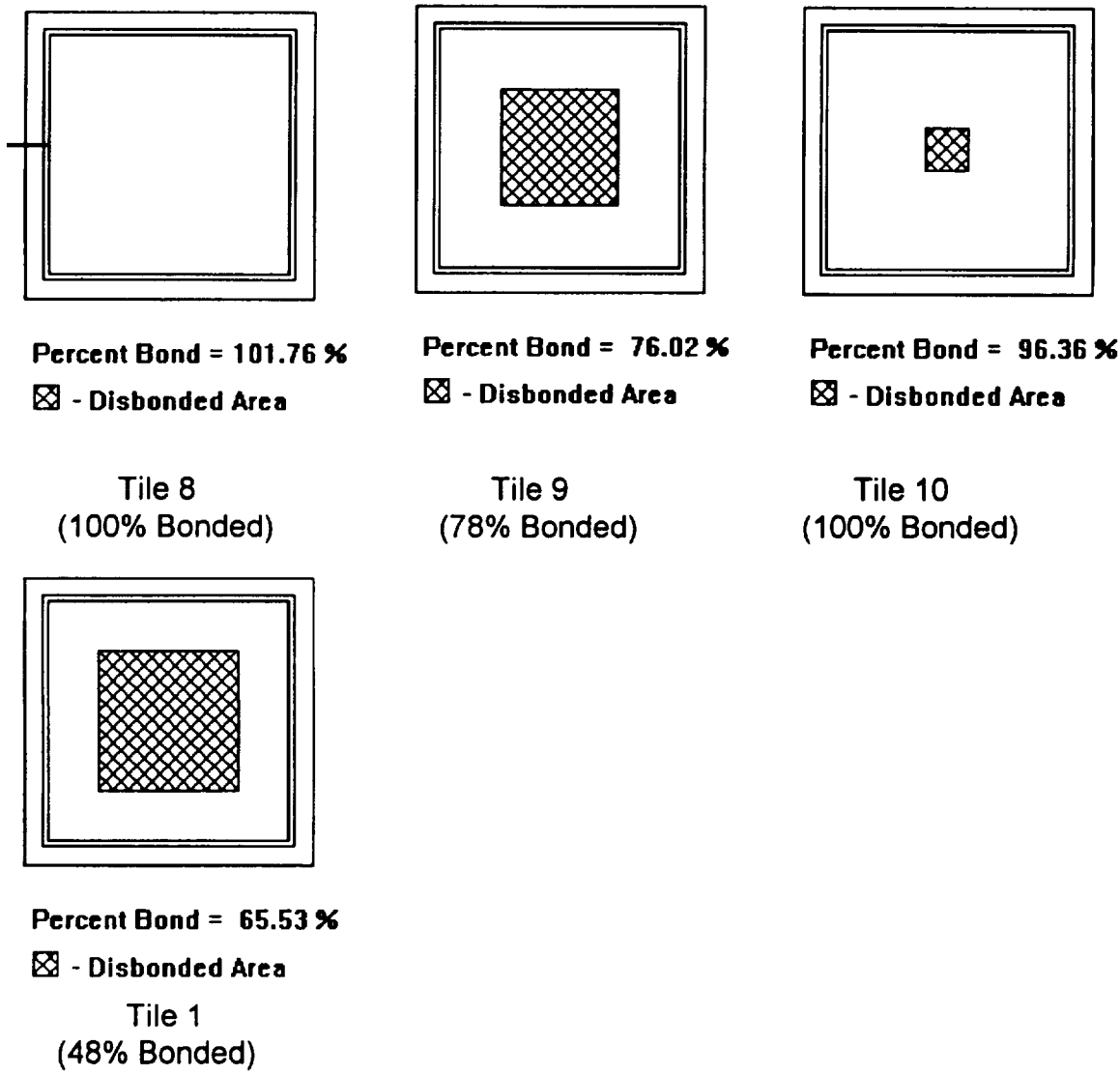

Figure 3.5-1 RESULTS OF THE INVERSE METHOD USING EMA DATA AS INPUT.

4 EXPERIMENTAL ANALYSIS

4.1 EXPERIMENTAL MODAL ANALYSIS - EXPERIMENTAL SETUP

Experimental modal analysis was conducted on multi-tile panel assemblies supplied by NASA at the UCF Experimental Mechanics Laboratory. A schematic of a typical test setup is shown in Figure 4.1-1.

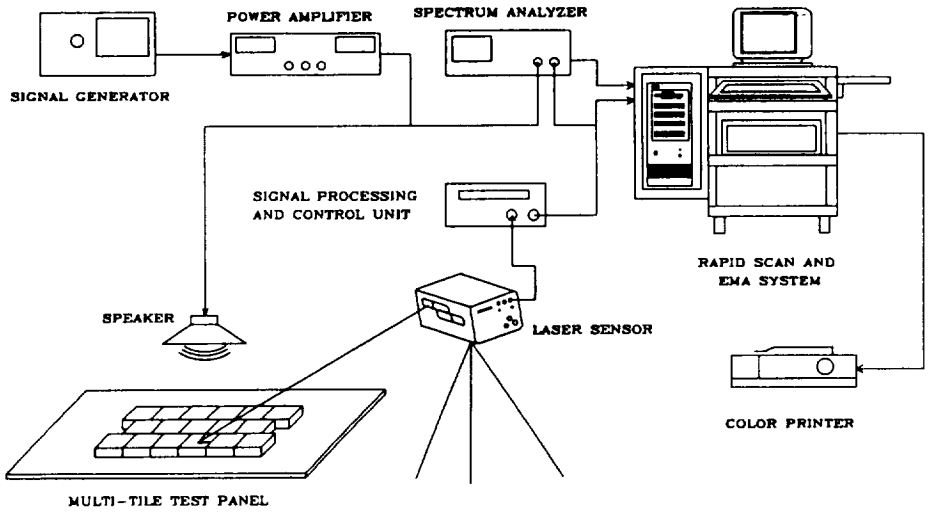

Figure 4.1-1 The Experimental Setup

As shown a speaker is used to excited an individual tile. The Ometron laser system is used to measure the induced vibration. A two-channel spectrum analyzer, modal analysis software (STAR 4.2) and other instruments are utilized to acquire and process the experimental data.

Three types of experiment were conducted on the 17-tile panel: frequency response survey of tiles, complete modal testing and vibration imaging of tiles.

4.2 FREQUENCY RESPONSE SURVEY

The frequency response survey was conducted to determine the tile's natural frequencies. In this, a specific tile was excited by a narrow band random noise between 500 and 1500 Hz at about 100 dB, and the response at some points of tile were measured by the laser system. The frequency response functions (FRF) were then computed, and the tile's natural frequencies were identified from the peaks of these functions. Also the average of FRFs was calculated, which is the summation of the magnitude square of all the interested FRFs. The natural frequencies are easier to be

identified from the average of FRFs. Figures 4.2-1 through 4.2-4 show the FRF and the average for some tiles on 17-tile panel.

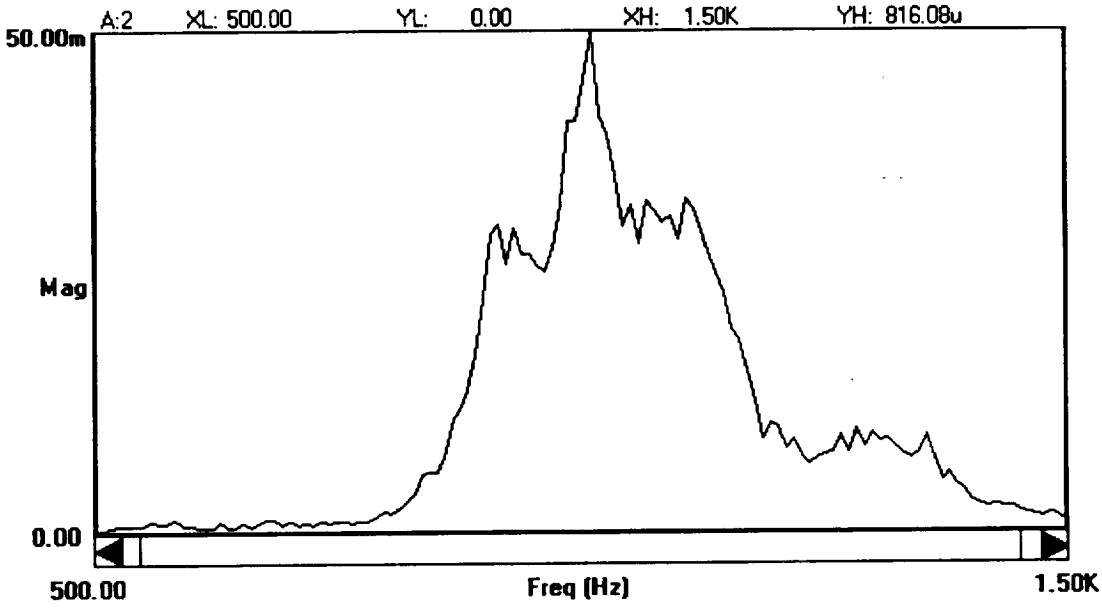

Figure 4.2-1 AVERAGE OF THE FRFs OF TILE No.14

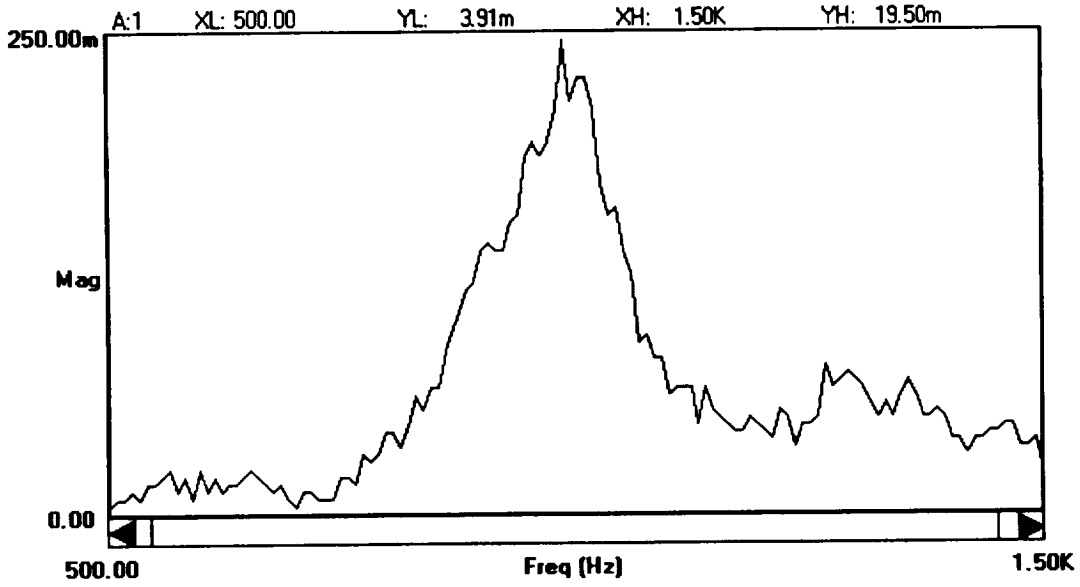

Figure 4.2-2 FRF OF 2Z/3Z OF TILE No.14

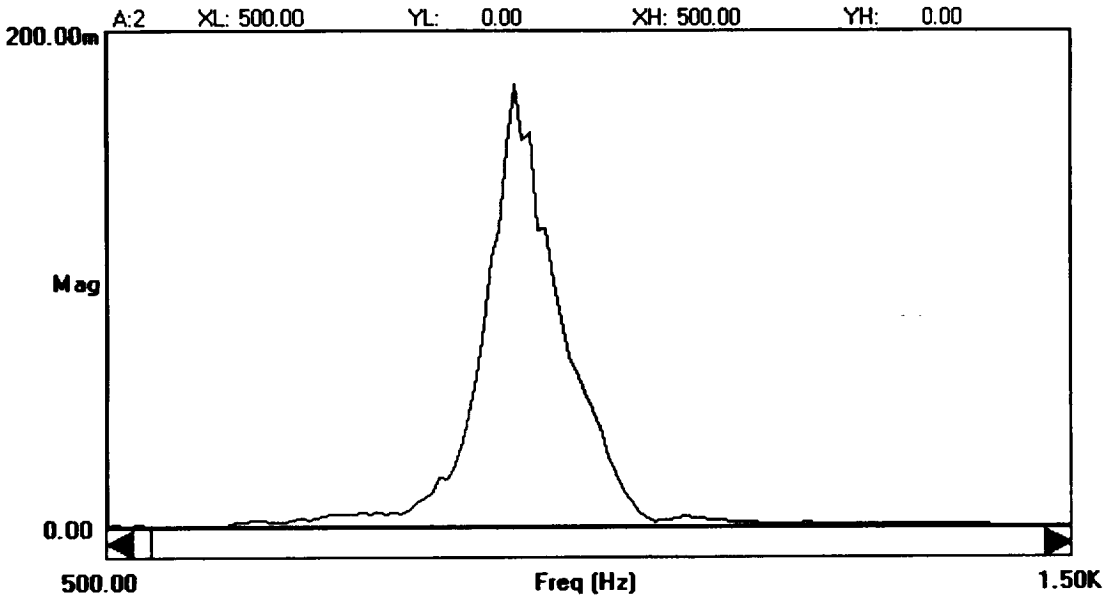

Figure 4.2-3 AVERAGE OF THE FRFs OF TILE No.9

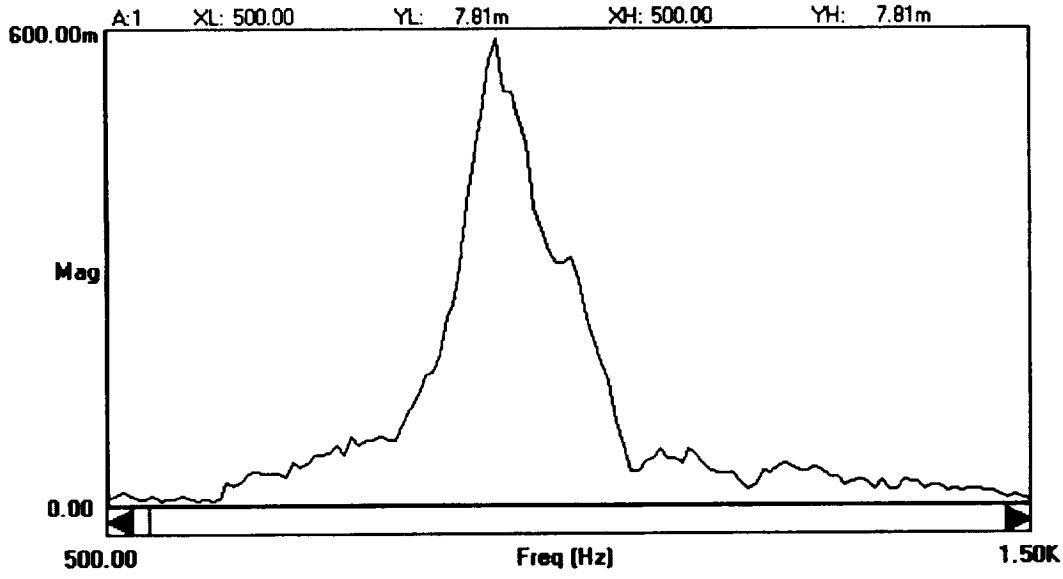

Figure 4.2-4 FRF OF 1Z/3Z OF TILE No.9

4.3 MODE SHAPES

The modal testing was performed of every tile on 17-tile test panel. This test is used to identify the tile's dynamic characteristics, e.g., natural frequencies, damping ratio and mode shapes. The number of measured points to construct mode shapes varies according to different purpose. For the inverse technique or a rough test, 5 points were used; otherwise 9 points or 25 points were used to show the detail of the mode shape. Figure 4.3-1 through Figure 4.3-3 show the mode shapes of some tiles.

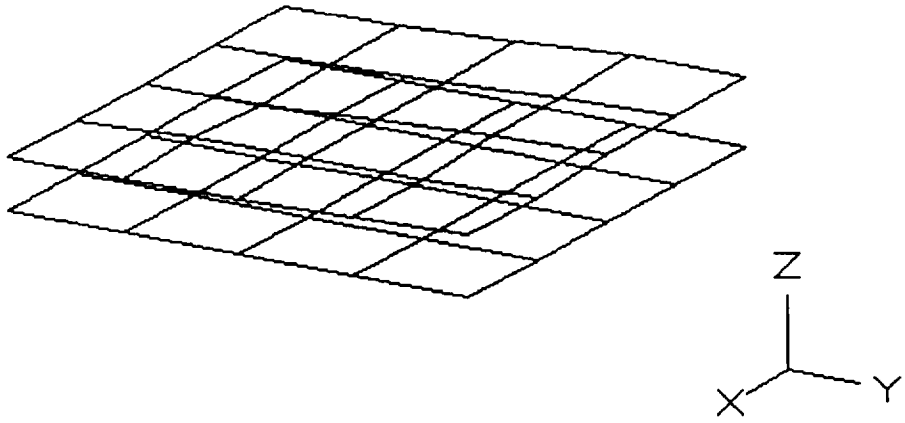

Figure 4.3-1 MODE SHAPE OF TILE No.10

(The natural frequency: 1020 Hz, Using 25 points)

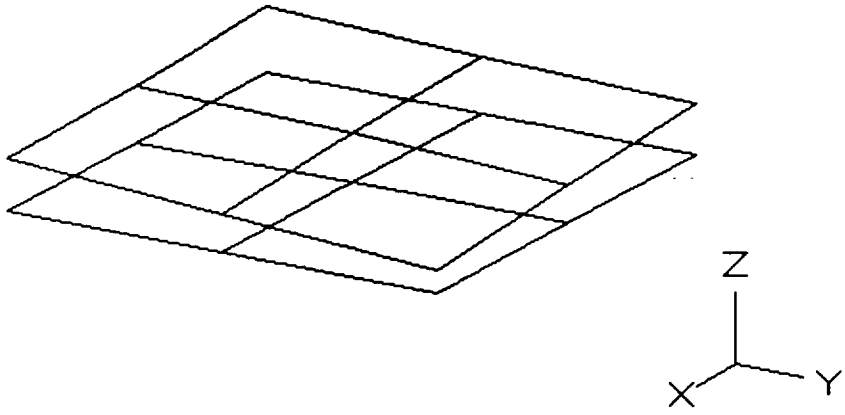

Figure 4.3-2 MODE SHAPE OF TILE No.13

(The natural frequency: 964 Hz, Using 9 points)

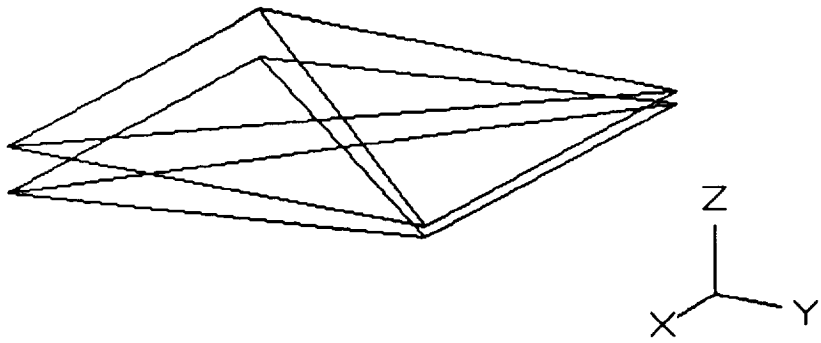

Figure 4.3-3 MODE SHAPE OF TILE No.

(The natural frequency: 924 Hz, Using 5 points)

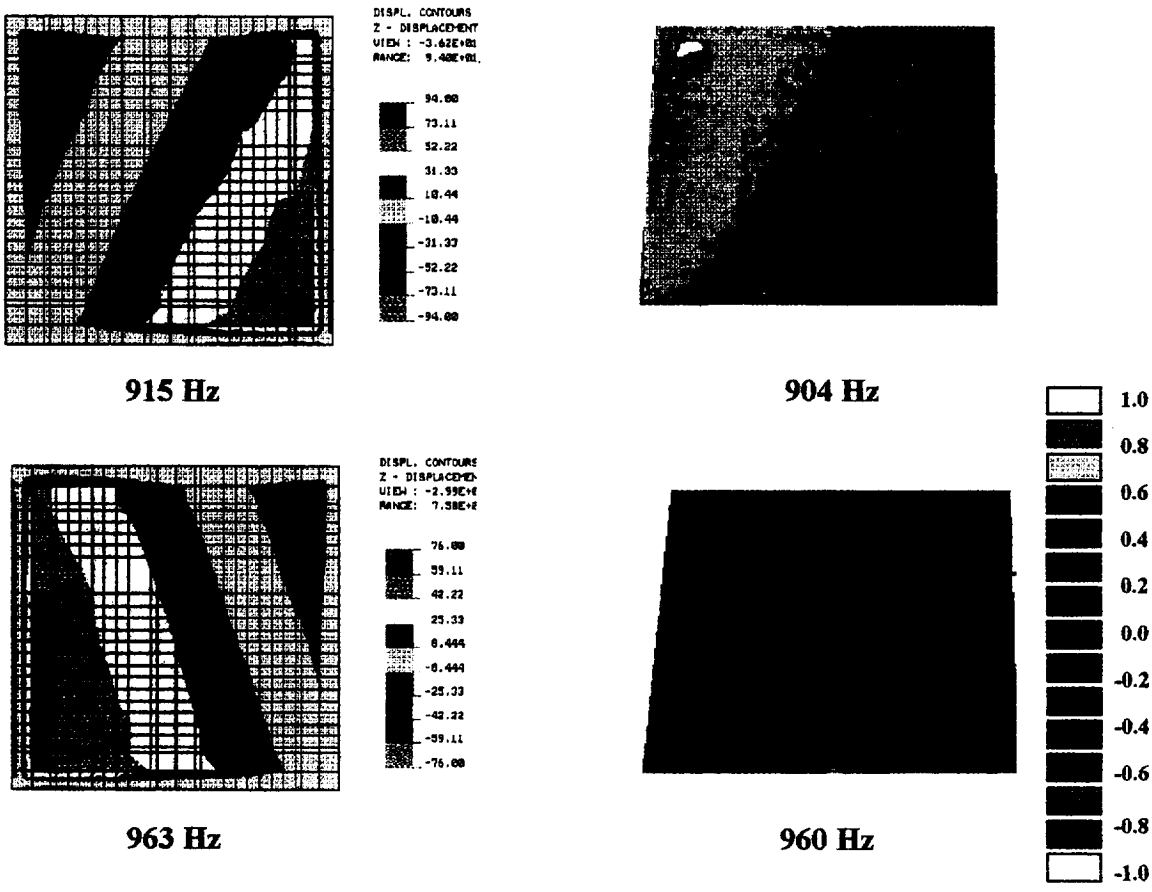

Figure 4.4-1. MODE SHAPES FOR TILE #9 OF THE 17-TILE TEST PANEL

4.4 VIBRATION IMAGE

Finally, the vibration image was performed on some tile in the panel. The testing was conducted by exciting the tile with sinusoidal signal at one of the resonant frequencies of the tile. the tile's velocity response was measured point by point, and line by line to construct the image by Ometron rapid scan laser system. This system computes the "spatial" ratio of the response divided by the input acoustic signal, while preserving the phase between the two. Thus, contour of the specific mode shape can be displayed. Figure 4.4-1 displays the vibration images and the equivalent finite element mode shape of tile No. 9 for three frequencies. Figure 4.4-2 is the same mode shape constructed by modal testing. the results by the two techniques are consistent.

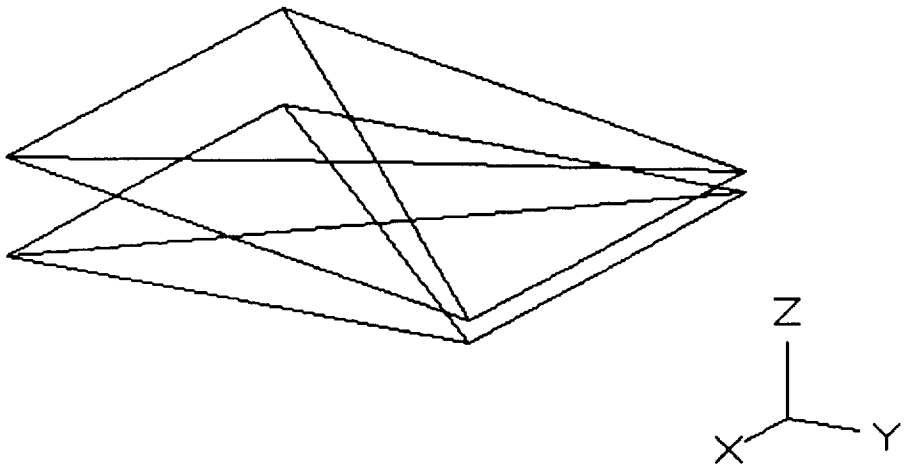

Figure 4.4-2 MODE SHAPE OF THE TILE No. 9

4.5 EXPERIMENTAL RESULTS OF SEVENTEEN TILE TEST PANEL

To show some test results for 17-tile panel, Table 4.5-1 lists the natural frequencies for each tile. In Figure 4.5-1, the natural frequencies are plotted against disbond, the figure also display the finite element values. As expected, the results indicated a consistent decrease in the natural frequency as the size of the disbond increased.

Table 4.5-1. Experimental and Finite Element Results for the 17-Tile Test Panel

Tile Number	% Bond	Frequency (Hz) EMA	FEM
2,3,4,6,10,12,14,15,17	100	1020	1020
11	98	1008	1007
7	91	1000	990
13	90	984	986
5,6	84	976	969
9	78	904	963
16	71	880	917
1	48	816	785

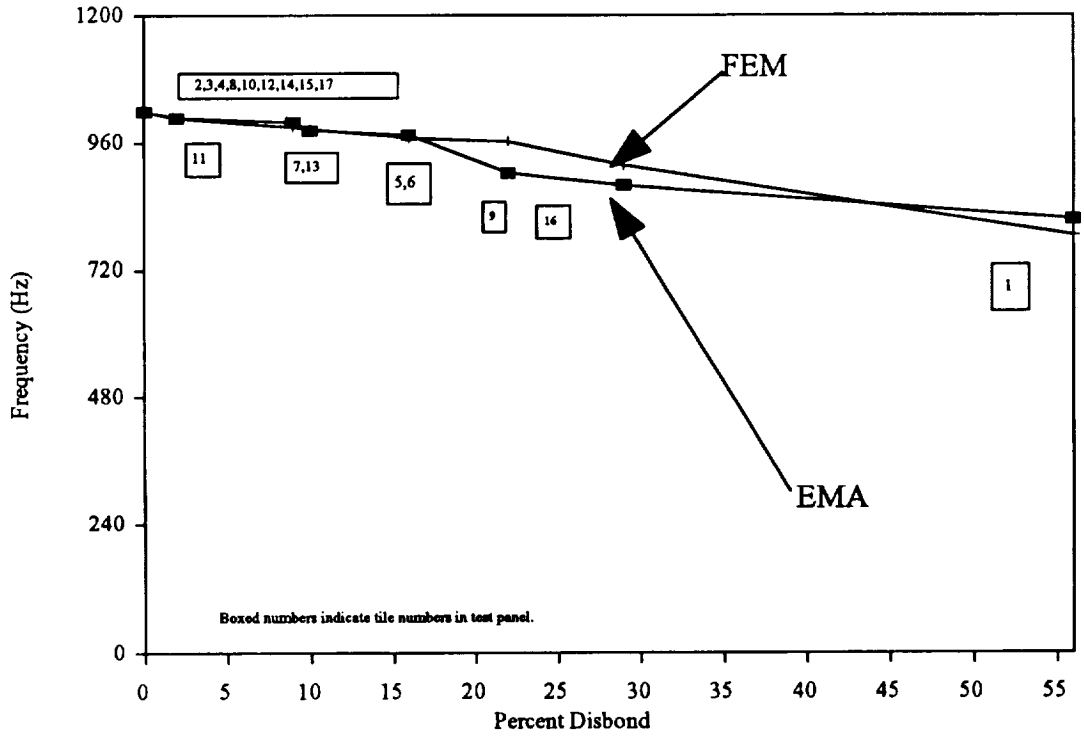

Figure 4.5-1 NATURAL FREQUENCY AS A FUNCTION OF DISBOND

4.6 EFFECT OF SPEAKER ATTACHMENTS

In the modal testing of tiles, two even three piston modes were found in some cases. In order to find the reason, the FRF of the new speaker with and without box were measured and the frequencies of the air column were calculated.

The measurement was made using a narrow band random signal to drive the power amplifier. The amplified signal went though the speaker with the box, and then was picked up by a sound level meter. The signal from power amplifier and sound level meter were used as input and output for the frequency analyzer to calculate the FRF. The the frequency range was from 500 Hz to 1500 Hz, which is used typically in the modal testing of tiles. Figure 4.6-1 shows the FRF of the speaker with box, a resonant frequency of about 1120 Hz can be found.

Also the comparison was made by measuring FRF of a tile using input signal first from power amplifier and then from the sound level meter. Figure 4.6-2 shows the FRF with the input signal from power amplifier. Basically, two peaks can be found: the frequency of one is around 1020 Hz Which is the natural frequency of the tile; another is about 1120 Hz, which is the resonant frequency of the speaker with box. Figure 4.6-3 is the FRF using the signal from sound level meter as input under the same condition. From this FRF, only the natural frequency of the tile can be seen.

Although the resonant frequency of speaker with box may effect the experimental results, if this frequency is known before the test, it can be excluded in the analysis. Therefore the speaker still can be used with a box in the experiment to reduce the environmental noise.

Another test was performed to check the resonant frequency of air column. Assuming the room temperature is 20 degree (Centigrade), using sound speed C=344 m/s, for the different distance between speaker and tile L, using the formula $f = C/(2L)$, the resonant frequencies are calculated. The results are listed in the Table 4.6-1.

L(cm)	40	36	31.5	27.5	23	20.5	18	14
f (Hz)	430	478	546	626	748	839	956	1,229

Table 4.6-1 FREQUENCY AS A FUNCTION OF AIR COLUMN LENGTH

In the experiment, the resonant frequencies of air column were not found in any case.

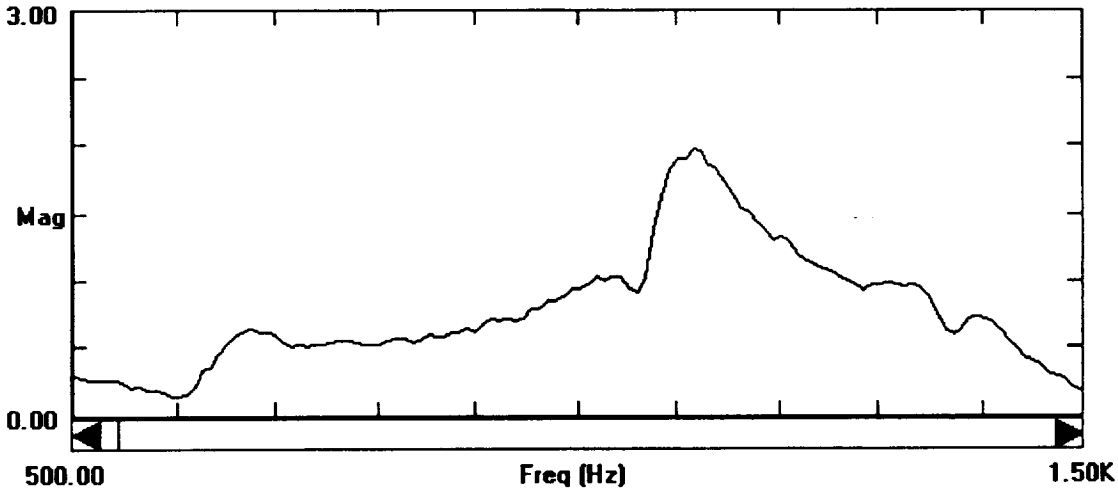

Figure 4.6-1 THE FRF OF SPEAKER WITH BOX

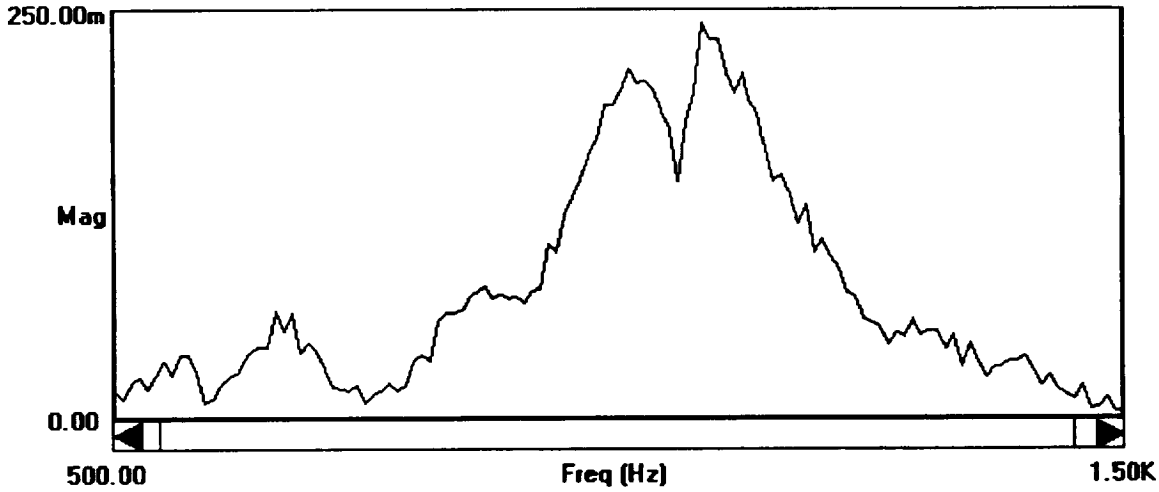

Figure 4.6-2: FRF OF THE TILE
(The input signal is from power amplifier)

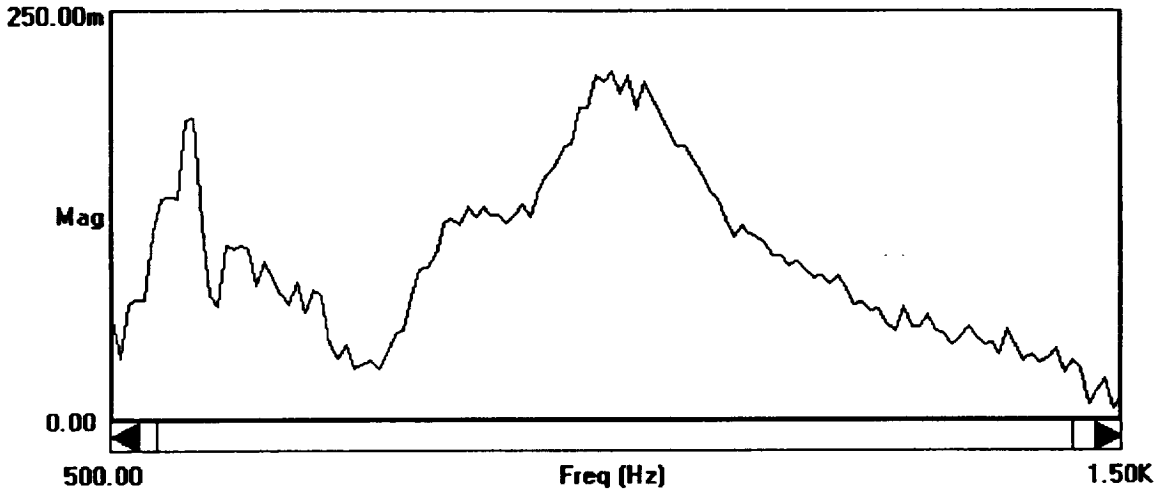

Figure 4.6-3: FRF OF THE TILE
(The input signal is from sound level meter)

4.7 ANGLE OF INCIDENCE FROM LASER SENSOR

The Laser Vibrometer measures the velocity of the test specimen along the laser beam's direction. Therefore, in measuring the out-of-plane motion of the tiles, the angle of incidence of the laser should be as close to vertical as possible. If not, corrections have to be applied to the measured velocity to get the actual out-of-plane velocity. In this test, the angle of incidence for various speaker distances was measured to determine the change in velocity due to changing angle of incidence.

The setup of the test is shown in Figure 4.7-1. Five points were labeled along one edge of the tile. When laser beam was point at one point, the physical angle between laser beam and normal direction of the tile was measured. Also the cosine of the angle was calculated as below. In this setup, the difference of COS(X) between point No.1 and No.21 (the largest error on the tile) is about 8%.

The point	No.1	No.6	No.11	No.16	No.21
The angle(degree)	52.7	51.7	50.6	49.5	48.4
COS(X)	0.61	0.62	0.64	0.65	0.66

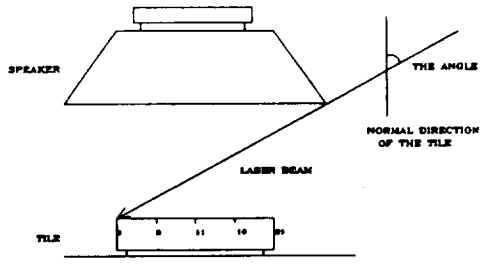

Figure 4.7-1 THE SETUP OF THE TEST

Now suppose that the distance between speaker and tile changes from 16 cm (6.25") to 32 cm (12.5"), using tile's dimension, the greatest angle between laser beam and the normal direction of the tile (when point No.1 is measured) is calculated and listed for some distance in the table below. This calculation can be used as reference of the best experimental setup.

Distance (cm)	16	20	24	28	32
Angle (degree)	52.7	46.4	41.2	36.9	33.3

4.8 STIFFENING OF TEN TILE TEST PANEL AND TESTING

Experimental Modal analysis was also performed on the 10tile panel, which was supplied by NASA. The natural frequencies were measured and mode shape were constructed for each tile. The natural frequencies for each tile are shown in Table 4.8-1.

TILE	#1	#2	#3	#4	#5
FREQ.(Hz)	1,020	1,060	1,040	1,040	1,010
TILE	#6	#7	#8	#9	#10
FREQ.(Hz)	968	1,030	1,020	1,000	1,020

Table 4.8-1 NATURAL FREQUENCY OF THE PISTON MODE
(Before the modification of the panel)

Because some aluminum bar are mounted behind the panel, in most area of the panel, the aluminum skin cannot be clamped on the table. This may introduce the local structure modes of the panel to the tile, thus change the dynamic characteristics of the tiles.

To get rid of the structure modes, the panel was modified after enough tests had been done on the original one. The area that cannot clamped on the table is filled with woodbar with 2"x4" in cross section to make the panel really rigid. Modal testing was performed after the modification, the results are shown in Table 4.8-2. Basically the results do not vary very much for the tiles before and after the tile was modified.

TILE	#1	#2	#3	#4	#5
FREQ.(Hz)	992	1,032	1,010	994	892
TILE	#6	#7	#8	#9	#10
FREQ.(Hz)	1,000	1,010	1,010	788	1,000

Table 4.8-2 NATURAL FREQUENCY OF THE PISTON MODE
(After the modification of the panel)

4.9 BAND PASS FILTER TESTING

The principle of the VPI laser sensor used in the measurement is based on a Michelson interferometer in which a laser beam is divided into reference and signal beam. The signal beam is directed onto a vibrating test surface and back-reflected light is re-combined with the internal reference beam. In the measurement of tiles, because the reflection is not very good on tile's surface, a long distance range lens have to be used although the measurement is performed in a short distance range. Even in this way, much noise comes into the signal and coherence function is poor in the FRF measurement because the focus of the laser beam is critical. To improve the testing results, a filter (KH 3700) is utilized to cut off the noise before the signal is acquired by the frequency analyzer.

The frequency response of the filter was tested. Figure 4.9-1 through Figure 4.9-3 show the FRF of the filter used as low pass , high pass and band pass one. In each case, the magnitude decrease about 3 dB at the cut off frequency.

The focus tolerance of the laser beam is improved significantly by utilize the filter. The level of focus must be over 80% indicated by the LED bargraph to get a acceptable signal without using the filter. However, the signal is satisfied at about 60% of focus level after the filter is used and therefore much less time is used for the measurement of one tile.

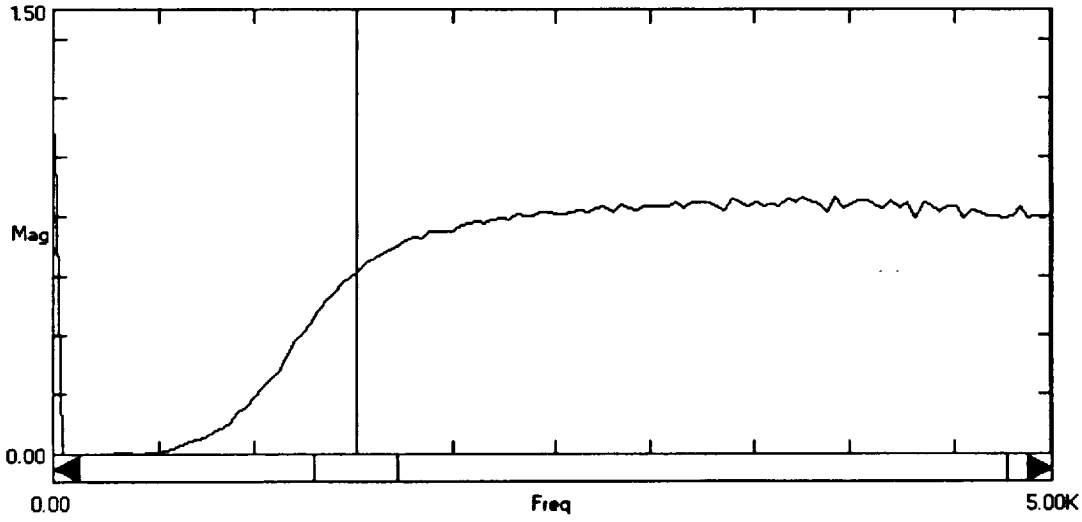

Figure 4.9-1 THE FRF OF THE BAND PASS FILTER
(Used as a high pass filter with cut off freq. of 1500 Hz)

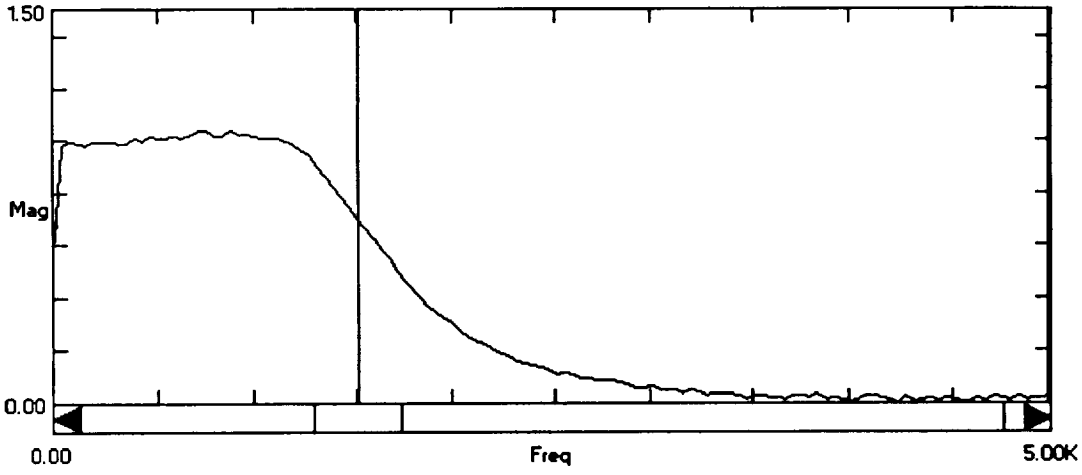

Figure 4.9-2: THE FRF OF THE BAND PASS FILTER
(Used as a low pass filter with cut off freq. of 1500 Hz)

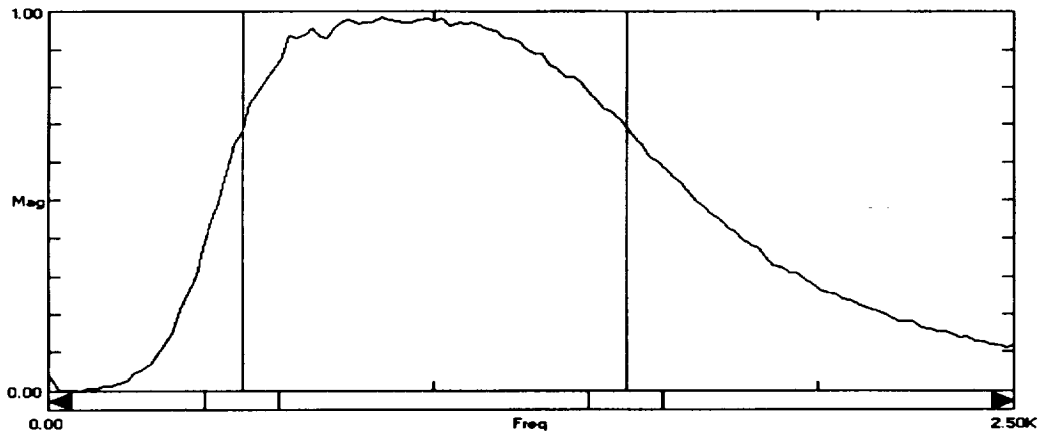

Figure 4.9-3 THE FRF OF THE BAND PASS FILTER
(Used as band pass filter with a bandwidth from 500 Hz to 1500 Hz)

4.10 MEASURE RESPONSE OF ADJACENT TILES

In the experiment of tiles on 17-tile panel, the tiles are excited and measured one after another. Although the size of the speaker is almost the sane as that of the tile, and the speaker is just put above one tile only, the adjacent tile may be excited and has some motion too. This motion may interfere the motion of the tile being measured through filler bar or the panel structure. As the results, the extra modes or the noise comes into the results.

An experiment was done to investigate the motion of a tile when the adjacent tile is being excited. Tile No.4 - No.7 on 17-tile panel are the tiles on the first row, adjacent one after another. The motion of tile No.4 is measured when the tile No.4, No.5, No.6 and No.7 are excited respectively. The Figure 4.10-1 through 4.10-4 show the FRFs of tile No.4 in each case.

The results show that when the tile No.5 (adjacent to the tile No.4) is excited, the magnitude of motion of tile No.4 is over half of that when tile No.4 itself is excited. However, when the excitation goes farther (on the tile No.6 and tile No.7), only a small motion is excited.

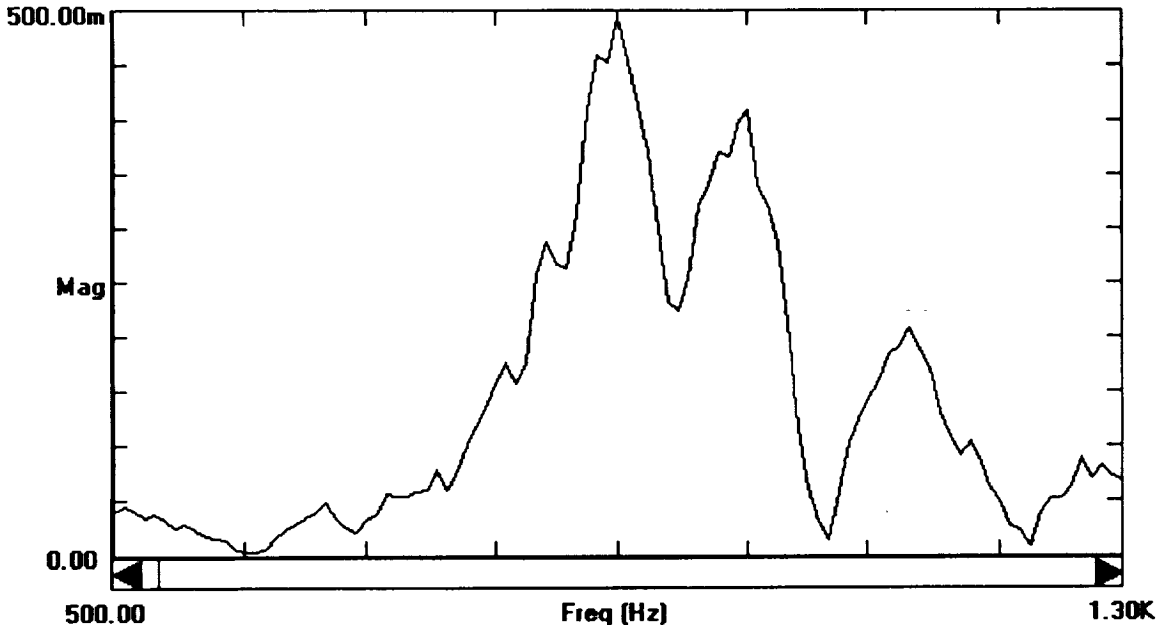

Figure 4.10-1 FRF OF THE TILE No.4 (Tile No.4 is excited)

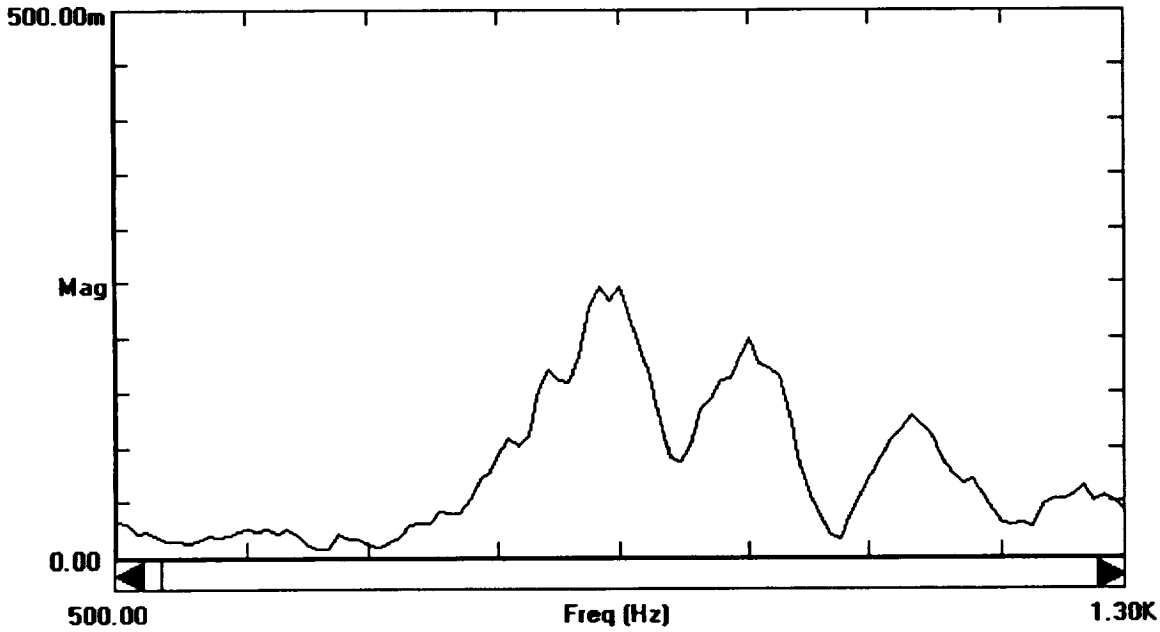

Figure 4.10-2 FRF OF THE TILE No.4 (Tile No.5 is excited)

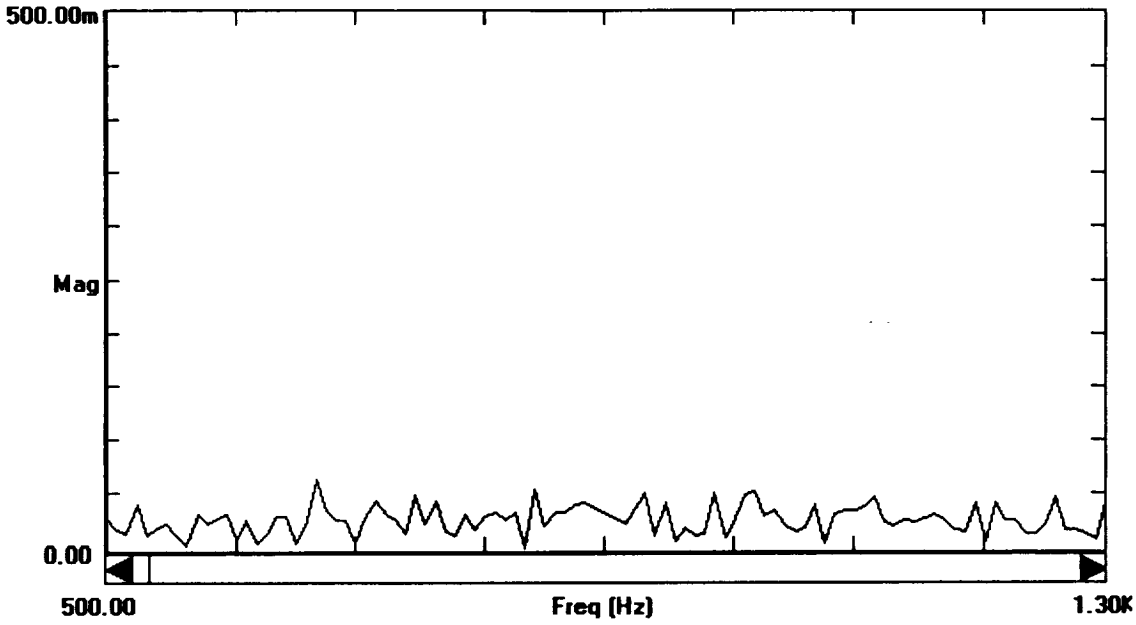

Figure 4.10-3 FRF OF THE TILE No.4 (Tile No.7 is excited)

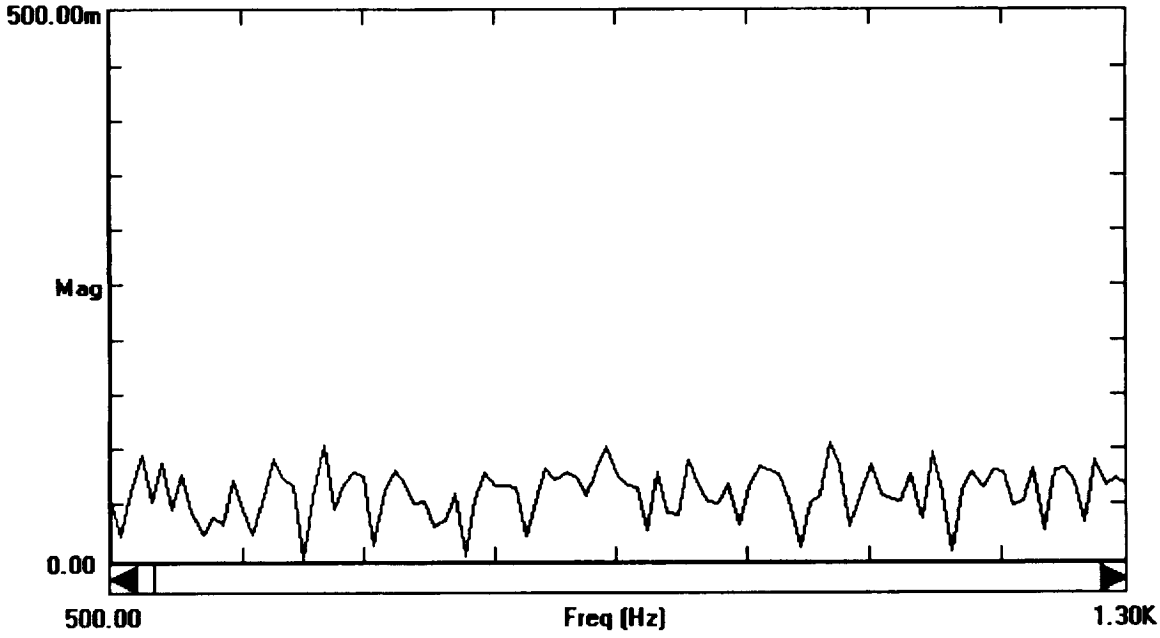

Figure 4.10-4 FRF OF THE TILE No.4 (Tile No.6 is excited)

4.11 DISTANCE BETWEEN SPEAKER AND TILES

Using acoustic energy to excite a tile, a speaker is set above the tile to make a uniform excitation on it's surface. Therefore the laser beam, which is used to pick up the vibration signal of the tile, is not perpendicular to the tile's surface because the speaker blocks the beam. The closer the speaker to the tile, the easier to excite the tile. But on the other hand, the farther away the laser beam from the normal direction of the tile's surface. To investigate how to make a compromise between the two, a test was done as follows.

Use speaker to excite the tile No.4 of 10-tile panel. The distance between the speaker and the tile changed from 16 cm to 32 cm. The FRF were taken and shown for different cases from Figures 4.11-1 to 4.11-4, and the coherence function was inspected for every FRF. The results show that when the distance is less than 20 cm, the measurement is pretty good for both the FRF and coherence function. For the distance around 25 cm, the resonant peak can be well recognized on FRF, but coherence function degrade. For the distance around 30 cm, the coherence function is very low.

Therefore the recommendation is that the distance between speaker and tiles should be less than 25 cm. The closer the speaker, the better the measurement as long as the angle between laser beam and normal direction of tile is not more than 45 degree.

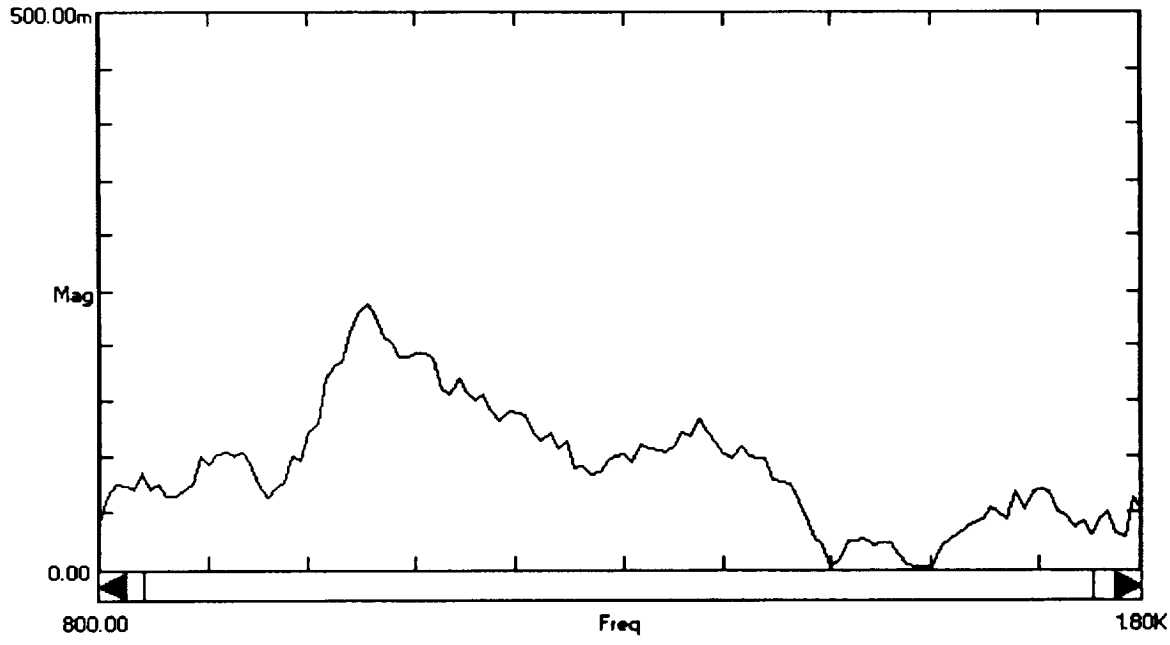

Figure 4.11-1 FRF OF THE TILE No.4 (the distance: 32 cm)

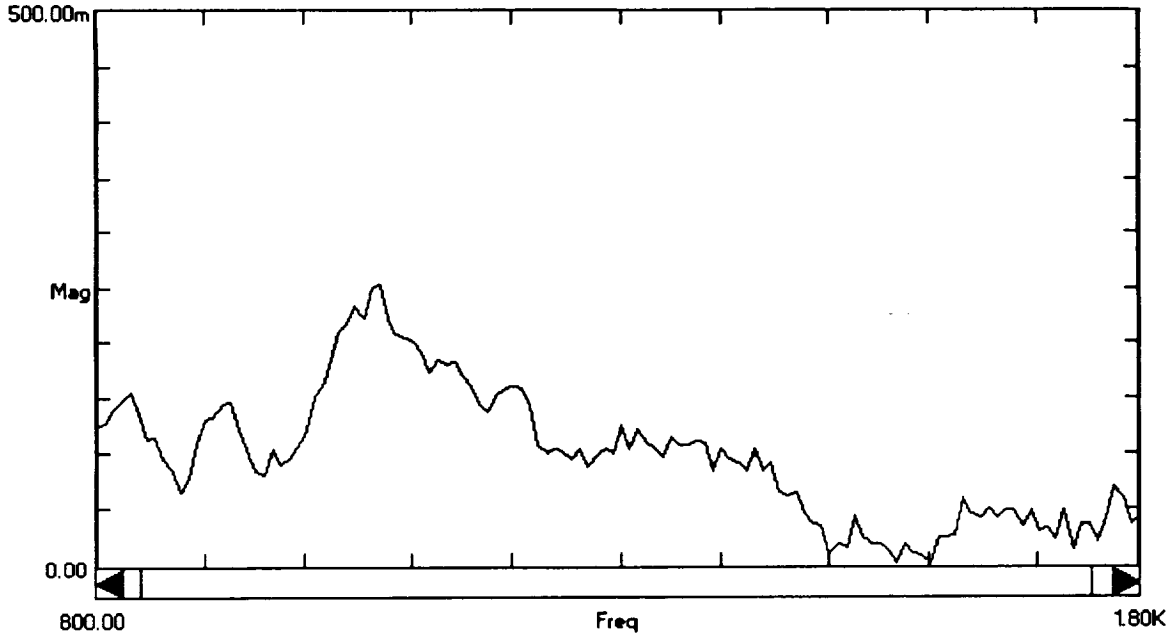

Figure 4.11-2 FRF OF THE TILE No.4 (the distance: 23 cm)

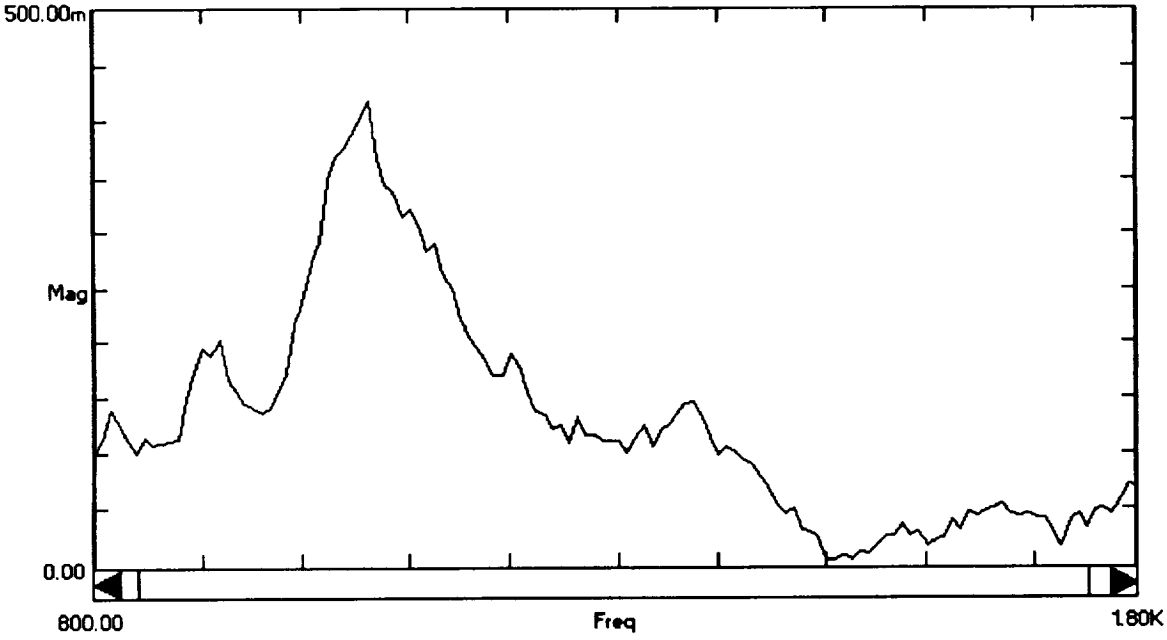

Figure 4.11-3 FRF OF THE TILE No.4 (the distance: 18 cm)

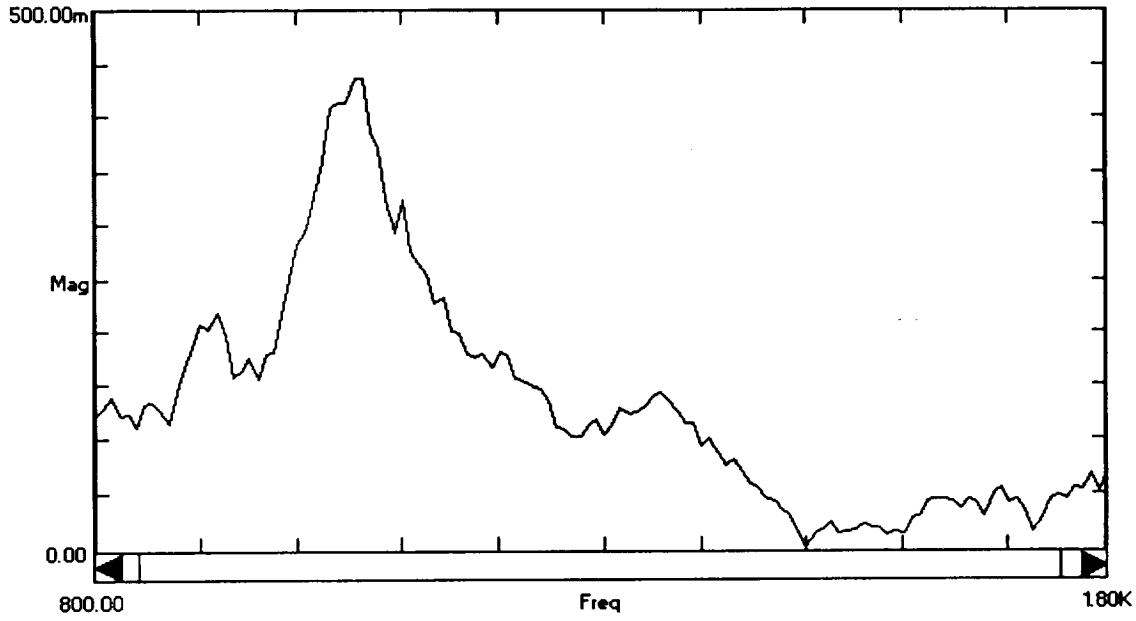

Figure 4.11-4 FRF OF THE TILE No.4 (the distance: 16 cm)

4.12 MEASUREMENT OF IN-PLANE AND OUT-OF-PLANE MOTION

In the measurement of tiles, what we are interested is the out-of -plane motion only. However, when this motion is induced by acoustic energy , the in-plane motion may be too. this may more or less introduce measuring error because the laser beam is not perpendicular to the tile's surface.

To investigate the magnitude of in plane motion of a tile while the out-of-plane motion is induced, a test was done as described below.

The setup of the test: Use a speaker to excite the tile, the in-plane motion and out-of-plane motion were measured with VPI laser sensor. For the in-plane motion, the angle between laser beam and horizontal level was 4 degree; for the out-of-plane motion, this angle was 45 degree. The signal was acquired by frequency analyzer and FRF was calculated. Figure 4.12-1 shows the FRF of out-of-plane motion and Figure 4.12-2 is that of in- plane motion.

The results: From the two figures shown here, the magnitude of the in-plane motion is less than one half of that of the out-of-plane motion. If the measuring angle is considered, the magnitude of the in-plane motion is about 1/3 - 1/4 of the out-of-plane motion.

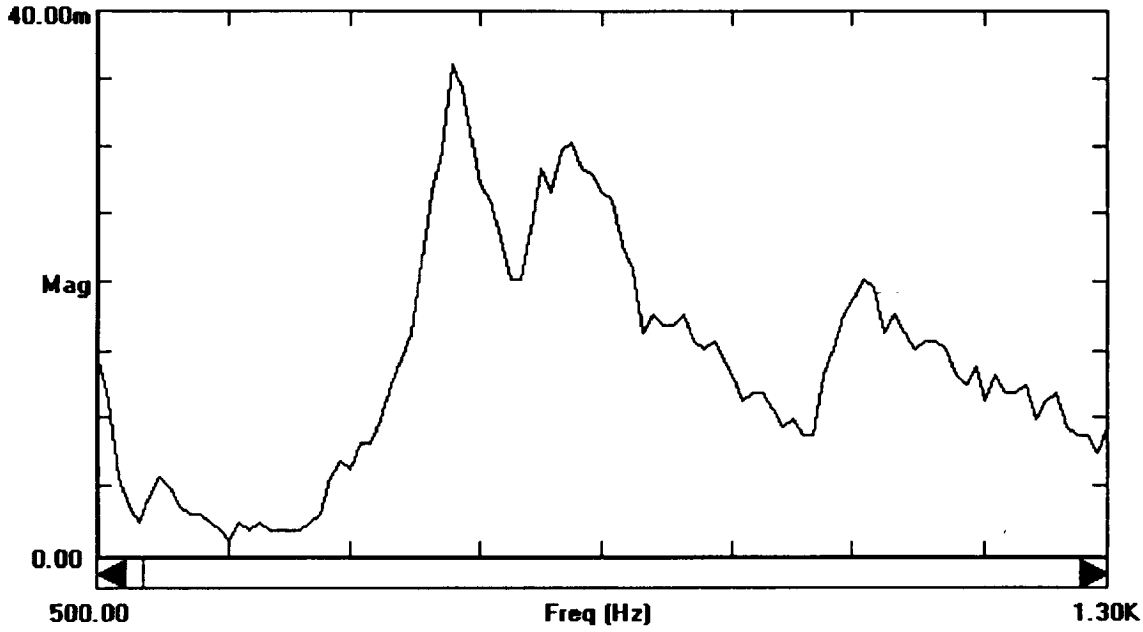

Figure 4.12-1 FRF OF THE OUT-OF-PLANE MOTION

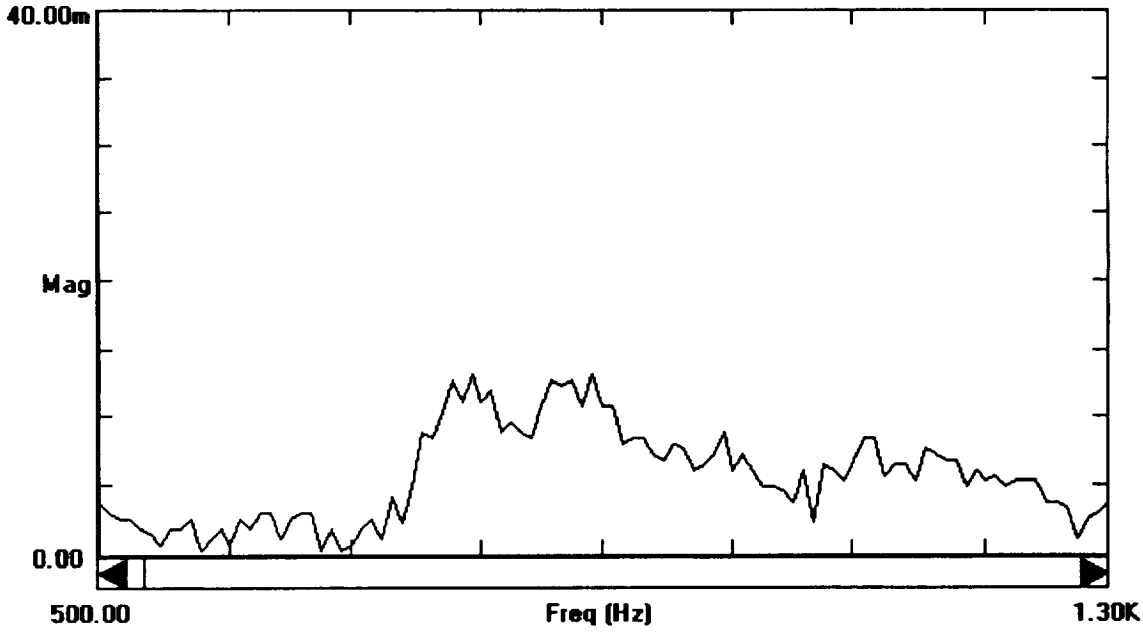

Figure 4.12-2 FRF OF THE IN-PLANE MOTION

5 NDE OF COMPOSITE MATERIALS

5.1 INTRODUCTION

Composite materials for aerospace applications feautre complex design configurations, nonuniform geometry and inhomogenous multi-layered structures. The main advantages of these materials are the high specific strength, stiffness and corrosion resistance. The increasing requirements for assuring the integrity of these composites, thus call for an intelligent selection and development of appropriate damage evaluation techniques, right through the initial phases of design.

This research addresses the application of the state of the art NDE techniques like acoustic emission (AE) and vibration pattern imaging (VPI) in monitoring the progressive damage in Graphite/Epoxy composites. Initial strength studies of these composites is also investigated by finite element analysis (FEA), right through the preliminary phases of design.

The various facets and complexities of laminate modeling and subsequent finite element analysis of Graphite/Epoxy structures have been considered. The orthotropic properties of the ply and the laminate material properties have been computed from the individual properties of Graphite fiber and Epoxy matrix. Different ply stacking sequences and their performance characteristics have been investigated for an optimum layout configuration, even before the laminate is applied to the finite element model. Ultimately, the optimum layout is assigned to the finite element model and analyzed under static loading conditions. The ply stresses, ply strains, inter-laminar shear stresses and ply failure indices are computed for the structure.

AE monitoring of Graphite/Epoxy composites have been successful in identifying the holes and cavities in the structure, where the regions are active and prone to failure. Optimum values for gain and threshold for a satisfactory performance of the AE technique have been identified by sensitivity analysis. Furthermore, the AE monitoring of the fatigue behavior of these composites have been successful in identifying and quantifying the delaminations in the structure, which has been reported as one of the most significant causes for failure.

Simultaneous NDE studies of these composites have also been conducted by vibration pattern imaging. The Finite Element estimate of the natural frequencies of the laminated Graphite/Epoxy structure have been determined and correlated with the experimentally determined frequencies. The decrease in the natural frequencies of the delaminated structures is the first and foremost indication of any local damages in the structure, which may be accounted due to the decrease in the stiffness of the structure. The structure is subjected to band limited random noise in the vicinity of the natural frequencies of the structure. The vibrating structure is scanned using a laser

Vibrometer and the vibration image is recorded. These vibration images show the presence of delaminations in the structure.

The results obtained by these NDE techniques have been compared and they have been found to be in close agreement with each other, thus demonstrating its potential application to Non Destructive Evaluation. Further, the applicability of these techniques in identifying the advanced damage states has to be investigated.

5.2 VIBRATION PATTERN IMAGING OF GRAPHITE/EPOXY COMPOSITES

A feasibility study on the use of vibration pattern imaging as a tool for nondestructive evaluation of laminated Gr/Ep composites which were previously modeled using finite elements and monitored by acoustic emission is conducted.
The experimental setup for flaw identification is as shown in Figure 5.2-1. The Gr/Ep laminate is clamped at both the ends and is excited by a speaker which derives its input energy from a signal generator, through a powerful amplifier. The vibrating structure is scanned using a laser vibrometer. The output from the laser vibrometer is processed by the software RAPIDSCAN Which provides a measure of the velocity amplitude of the structure.

The eigenvalue finite element analysis of these laminated composites is carried out to identify the resonant frequencies of the structure. The resonant frequencies of the vibrating structure are also determined experimentally. The structure is excited using a sine wave and Lassajous figures are used for determining the resonant frequencies. It has been observed that the resonant frequencies of the delaminated structures are lesser than those of the laminated ones. Once the resonant frequencies are determined, the structure is excited in narrow band about a frequency which is in the vicinity of the resonant frequency of the vibrating structure. The structure is scanned with the laser beam emanating from the Laser Vibrometer. The output from the vibrometer is processed by the software RAPIDSCAN, which gives the vibration images of the structure. These vibration images depict the presence of delaminations, if any, in the structure.

Thus, it can be concluded that the decrease in the resonant frequencies of the vibrating structure is the first and foremost indication of any physical damage in the structure. Also, the vibration technique has been found to be sensitive to physical flawing like delaminations, thus making the technique attractive for composite applications.

The vibration images obtained from the laminated and the delaminated models are included. It can be seen from the images that the laminated model has a more uniform velocity amplitude over the structure as in Figure 5.2-2, whereas the delaminated structure has higher velocity amplitudes at the delaminated portions of the structure, which is seen in Figure 5.2-3.

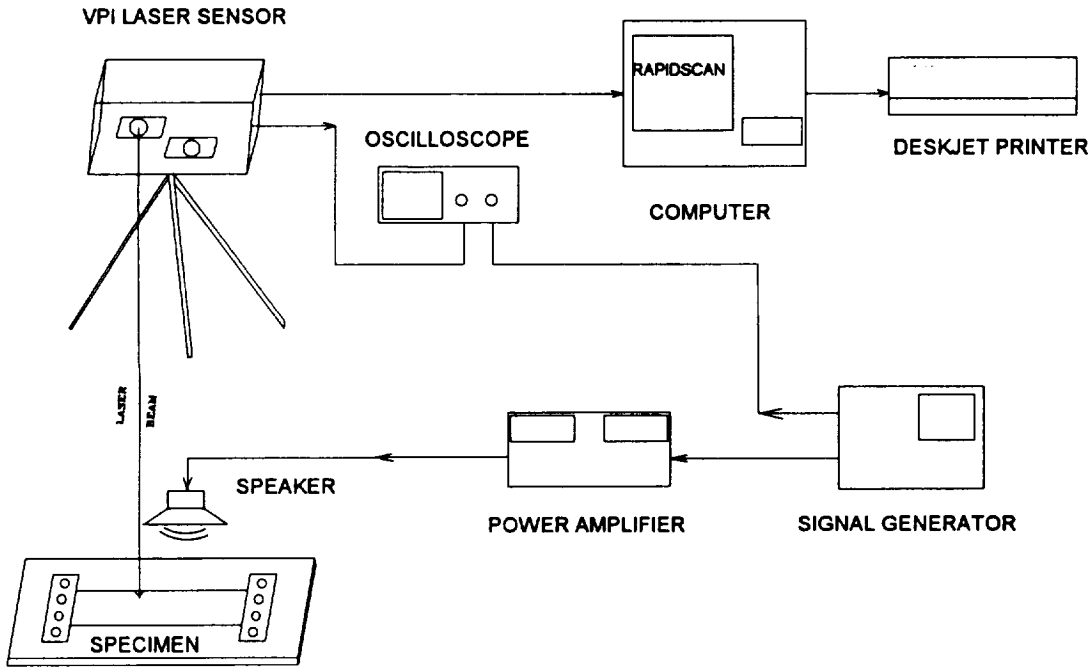

Figure 5.2-1 EXPERIMENTAL SETUP FOR FLAW IDENTIFICATION IN LAMINATED COMPOSITES.

RESONANT FREQUENCY = 508 HZ.

C F = 510 HZ. B W = 316 HZ

Figure 5.2-2 VIBRATION IMAGE OF LAMINATED

GR/EP COMPOSITE

RESONANT FREQUENCY = 500 HZ

C F = 515 HZ. B W = 316 HZ.

Figure 5.2-3 VIBRATION IMAGE OF DELAMINATED

GR/EP COMPOSITE

The results obtained from vibration pattern imaging have been compared with those obtained from acoustic emission. It is seen that the AE activity was the maximum and also most intense at the place where the delaminations have been identified in the vibration pattern images, thus demonstrating the potential application of these techniques to effective and reliable nondestructive evaluation.

5.3 ACOUSTIC EMISSION TESTING

Acoustic emission(AE) refers to the class of phenomena where transient elastic waves are generated by the rapid release of energy from localized sources from within a material. There is a wide variety of known to be responsible for AE generation, ranging from dislocation motion to crack propagation. The advantages of AE as an efficient nondestructive evaluation(NDE) technique are many, the most important one being its ability to effectively cover a wide area in a relatively short amount of time as compared with other NDE techniques. A fixed array of transducers can be used to monitor the performance of the structure in service, in real-time over long periods of time. This capability makes AE attractive for the NDE of large composite aircraft structures. This work discusses the AE monitoring of Graphite/Epoxy laminated composites under static and fatigue loading conditions to monitor the progression of damage.

The following terms are frequently used and monitored in the AE testing described in this research:

Event : A local material change giving rise to Acoustic Emission.

Count : Number of times an AE signal crosses the specified threshold.

Amplitude : Peak value of an AE signal from an event.

Energy : Amount of strain energy released by the material when subjected to loading.

Hits : Pulses which have been reflected many times within the materials being monitored before reaching the sensors.

Duration : Length of time measured from when the AE signal crosses the specified threshold to the last time it crosses the same threshold.

The AE instrumentation involved in testing includes the software LOCAN-AT by the Physical Acoustics Corporation for data storage, analysis and display, its associated hardware like LOCAN-AT computer, monitor, keyboard and printer, piezoelectric sensors and pre-amplifiers. Plumber's goop was used as the couplant between the sensors and the specimen.

Initial AE testing involved the calibration of the instrumentation and the sensors. Aluminium (Al) plate was used as the specimen and pencil lead break was used as the simulated source of emission. The source of emission was located effectively by using the linear location and triangular planar location techniques which employed two and three sensors respectively. The position of the source is calculated from the difference in arrival times between hits on the various channels used for the test.

Notched Al specimen were also monitored by AE under increasing tensile and fatigue loading conditions on the Instron loading machine. Linear source location technique was used in the tests. It was observed that AE activity which was present during the initial loading was not observed upon reloading of the specimen, until the previous maximum load was reached. This is popularly known as the Kaiser Effect. The gathered AE data was analyzed and displayed in different plots. It could be seen that most of the events occurred in the specimen, around the notch, thus displaying the active sources of emission in the structure. The specimen was loaded to failure both in tension and fatigue. It could be seen that the AE parameters like energy, amplitude and events increased at about 75% of the failure load and then increased drastically at failure. These results encouraged the application of AE techniques to NDE of composite structures.

The laminated sheet of Graphite/Epoxy composite was cut into several specimen of equal width and length, each being about 1 inch wide and 8 inches long. A diamond grinding wheel was used for this purpose. The laminated sheet was mounted on a glass plate with a double sided insulation tape. The glass plate was held firmly on a magnetic chuck gripping device. The grinding wheel was traversed along the length of the specimen, without touching it. This was done to ensure that the specimen was in perfect alignment with the path traced by the grinding wheel. Continuous flow of the coolant was maintained on the specimen. The specimen had a very good surface finish.

The Graphite/Epoxy laminate was monitored by AE under tensile loading conditions on the Instron machine, using different values of gain and threshold. From the results obtained and further investigation into AE data analysis, it was seen that the AE results were sensitive to the values of threshold, gain and system timing parameters. Hence, the optimum values of these parameters have to be determined for an effective functioning of the AE system. Thus, sensitivity analysis threshold and gain was conducted in the composite laminates.

Sensitivity in AE monitoring refers to the ability of the system to detect small signals in the structure. In part, this is determined by sensor sensitivity and spacing; and in part, it is determined by the controls set on the main equipment. The governing control is the threshold, an operator-set voltage level against which the amplified AE signals are compared. When the AE signal exceeds this voltage threshold, a hit is recognized and the signal measurement circuitry comes into play. Gain also plays an important role in determining the sensitivity of the system. The sum of gain and threshold is an

extremely important value for the effective functioning of the system. The Gr/Ep specimen were loaded on the Instron testing machine to 600 lb.. AE was monitored in the specimen, at this load for about 5 min.. The test involved four different specimen, which almost had the same dimensions.

Initially, the value of gain was fixed at 25 dB. The threshold was set at 35 dB in the first specimen and AE was monitored. The important test parameters like cumulative hits, counts and energy were recorded during the test. Similarly, the other specimen were set at threshold values of 40, 45, and 50 dB respectively, at the same value of gain. Also, the specimen was unloaded to zero, and then reloaded again to the same load to see if there was any activity in the specimen. The absence of any activity during this reloading period justified the presence of Kaiser effect in the specimen, assuming that the specimen was not damaged. On the other hand, the presence of any activity would prove that the values of gain and threshold were not right. It can be seen from Table 5.3-1 that the Kaiser effect was seen at a threshold value of 50 dB.

Now, the threshold value was fixed at 50 dB and the Gain was varied from 15 dB to 25 dB in the specimen and the tests were repeated. A gain of 25 dB was decided to be the optimum value. The test results are as shown in Table 5.3-2.

Table 5.3-1 THRESHOLD SENSITIVITY AT GAIN = 25 dB.

TEST	THRESHOLD	HITS	COUNTS	ENERGY
1	35	2,839	82,306	46,914
2	40	2,335	67,379	28,151
3	45	1,797	19,173	17,069
4	50	643	2,960	5,812

The sum of gain and threshold should be maintained between 55 dB and 88 dB for the effective functioning of the AE system.

Table 5.3-2 GAIN SENSITIVITY AT THRESHOLD = 50 dB.

TEST	GAIN	HITS	COUNTS	ENERGY
1	15	2,662	19,802	19,830
2	20	1,289	6,813	7,313
3	25	258	1,847	3,529

AE monitoring for detection of holes under fatigue loading was conducted in these composites. Two sensors were coupled to the specimen and the Linear Source Location technique was used. It was noticed that the hole which was in between the two sensors was detected and not the other one. The sensor was then removed and then placed very close to the other hole, which was then detected by the AE signals. This concludes that only the region of activity in between the sensors can be detected.

The laminates were further subjected to fatigue loading from 200 lb. to 600 lb. at a loading rate of 0.2 in/min. It can be seen from Figure 5.3-1 that channel 1 recorded more number of events, indicating the active regions in the structure. After a few cycles of loading, it was seen from Figure 5.3-2 that the maximum number of events was occurring at a place in between the holes in the specimen. The amplitude of the events occurring at this place were also relatively higher and were in the range of 60-70 db, as seen in Figure 5.3-3. Also, the duration of a few recorded hits were about 400 microseconds as seen in Figure 5.3-4. Visual inspection confirmed the presence of delaminations in the composite. Thus, long duration events are valued indicators of delaminations in composite materials. The amplitude of these events were also significantly higher, thus identifying crack initiation in the structure that ultimately led to delaminations. Thus, AE is an effective NDE technique in providing incipient warning of failure in Graphite/Epoxy laminates. The detected delaminations by Acoustic Emission were further investigated using Vibration Pattern Imaging for the correlation of results.

5.4 FINITE ELEMENT MODELING FOR GRAPHITE/EPOXY LAMINATES.

Crack initiation in composite laminates coincides with the first cracking of the weakest ply, which is termed as the first ply failure(FPF). This is followed by delaminations and fiber breakage, thus leading to ultimate failure. Hence, it has become extremely important to identify the material properties of the plies in the laminate that would provide an overall satisfactory performance of the structure under consideration. This part of the research addresses the various facets of laminate modeling and subsequent finite element analysis of laminated multilayered graphite/epoxy composites. The FE

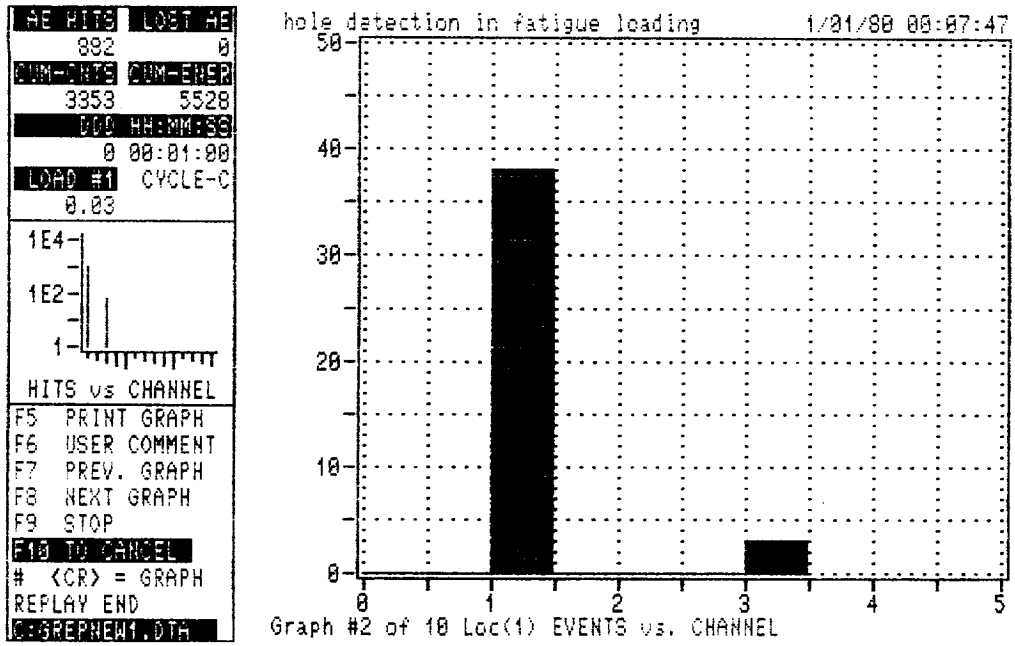

Figure 5.3-1 PLOT OF EVENTS VS. CHANNELS.

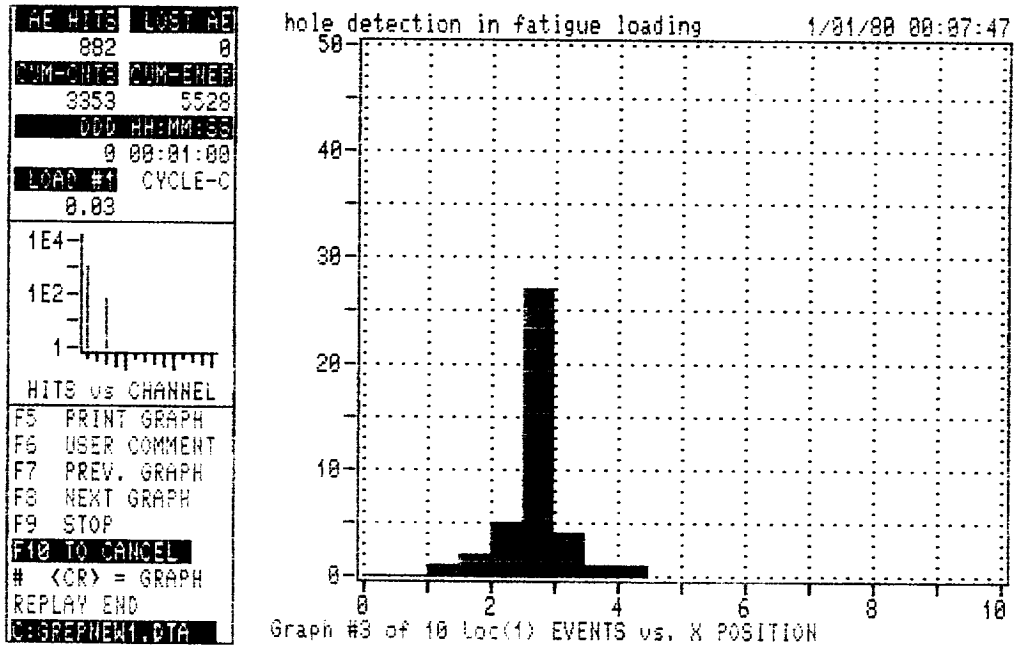

Figure 5.3-2 PLOT OF EVENTS VS. LOCATION IN THE STRUCTURE.

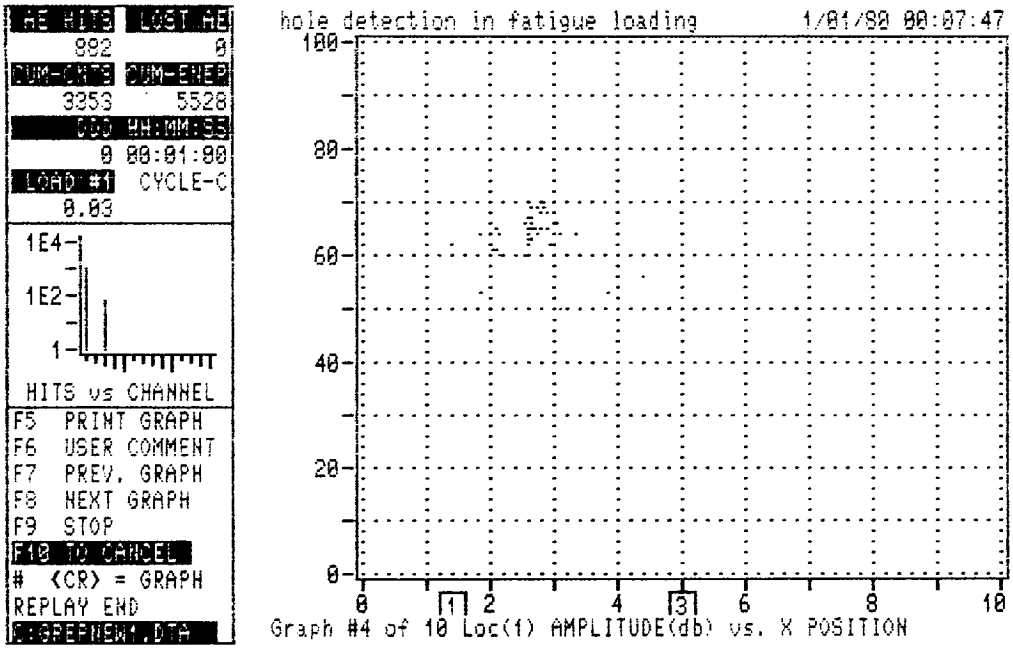

Figure 5.3-3 PLOT OF AMPLITUDE VS. LOCATION IN THE STRUCTURE.

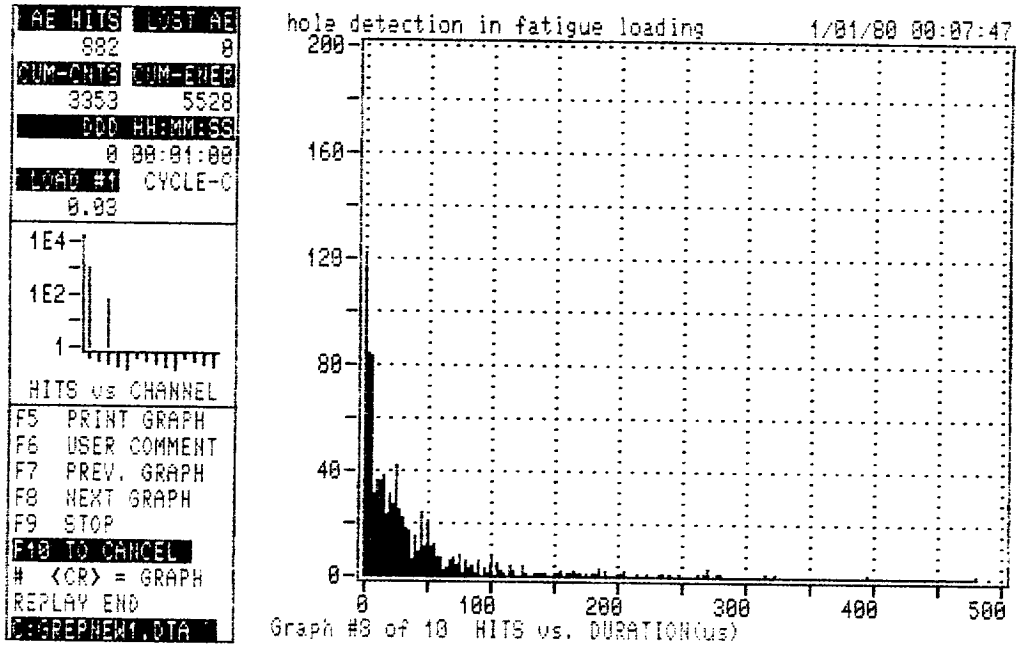

Figure 5.3-4 PLOT OF EVENTS VS. DURATION.

program IDEAS (Integrated Design Engineering Analysis Software) [23] is used in this analysis.

A typical laminate is made up of a series of plies stacked on each other in an orderly fashion. They may be of varying thicknesses or materials and generally have varying orientations. The laminates considered for this study are made up of 16 plies, with the configuration (45,90,-45,90,45,90,-45,90) and is symmetric in nature. The laminate is 0.085 inches thick and all the plies in the laminate are 0.005312 inches thick. The material properties for each ply in the laminate is computed. The plies are then stacked on each other and built into a laminate. The laminate material properties are computed and an initial loads analysis can be performed to study the strength properties of these laminates, even before they are applied to the finite element model. The various steps involved in laminate modeling and subsequent FE analysis can be shown in Figure 5.4-1.

To begin with, the individual isotropic properties of the epoxy matrix and graphite fiber are defined as shown in Table 5.4-1.

Material	Epoxy	Graphite
Type	Isotropic	Isotropic
Young's Modulus, E psi	8 E+06	23 E+08
Poisson's Ratio	0.35	0.2
Density lb/in^3	0.04	0.07
Shear Modulus psi	10E+3	10E+4

Table 5.4-1 INDIVIDUAL PROPERTIES OF EPOXY AND GRAPHITE.

Fiber volume and matrix volume fractions are specified to be 0.6 and 0.4 respectively. The mechanics of materials approach is selected for computing the properties of the ply. This approach produces equations that are among the most widely used and accepted equations in aerospace industry. In this approach, the value of E parallel to the fibers is determined by assuming that the stress acting on the lamina is distributed between the fibers and the matrix as a weighted average. The stress distribution depends on the moduli and volume fractions of both the matrix and the fiber. The computed properties of the graphite/epoxy ply are tabulated in Table 5.4-2.

The sensitivity of the values of the moduli and the allowable strengths of the ply are investigated with respect to varying matrix and fiber fractions. It was seen that the value of the allowable stress in tension in the y direction did not change with the varying fractions. The moduli of the ply material increased with increasing fiber fractions as shown in Figure 5.4-2.

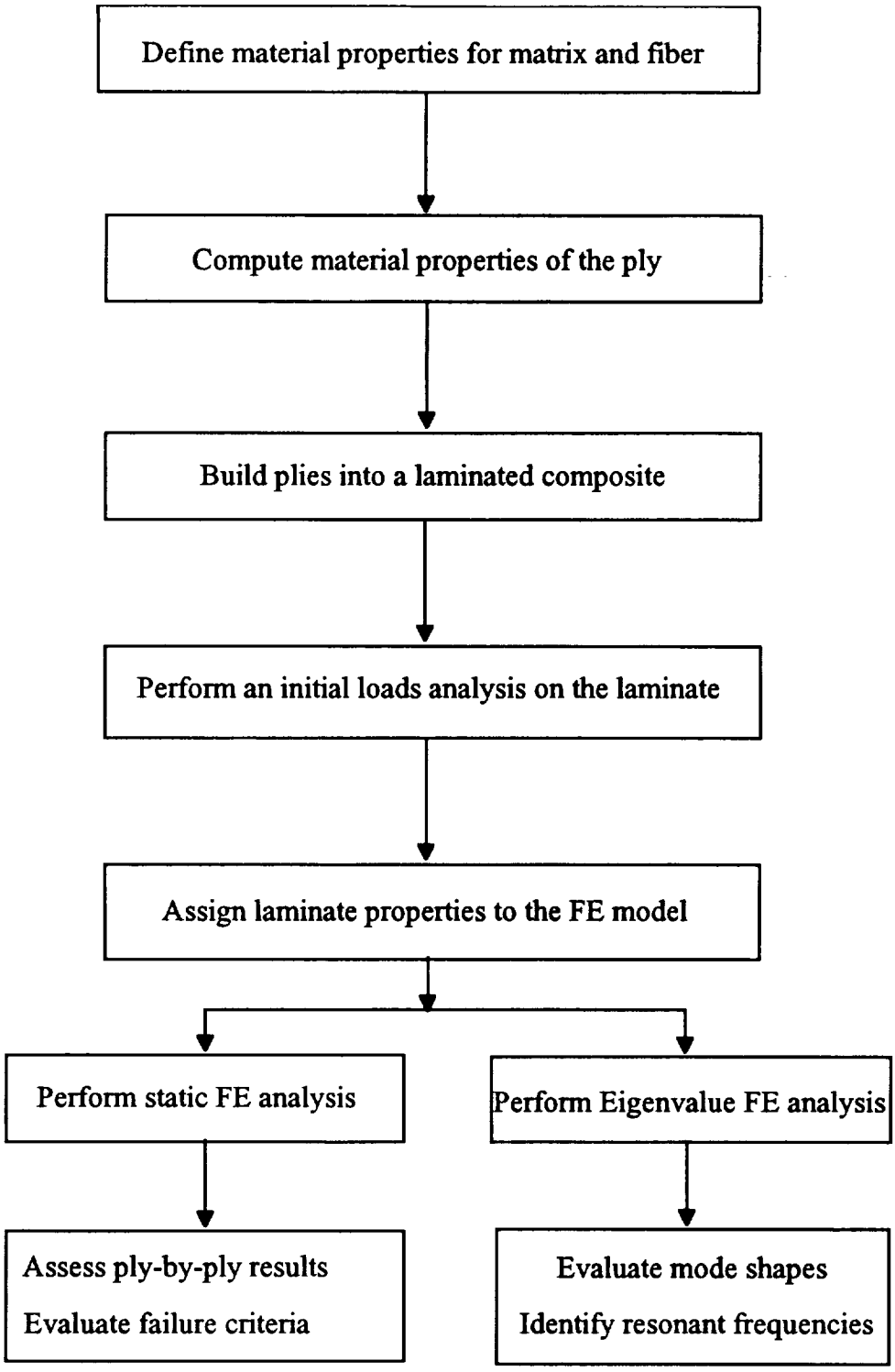

Figure 5.4-1 LAMINATE MODELING STEPS

The allowable stresses in tension and compression in the x direction also increased with the increase in fiber volume fraction but the allowable stress in compression in the y direction and the allowable inplane shear stress decreased as shown in Figure 5.4-3.

Material property	value
Young's modulus in x, Ex	13.83 E+08 psi
Young's modulus in y, Ey	19.89 E+06 psi
Young's modulus in z, Ez	19.89 E+06 psi
Poisson's ratio, xy	0.26
Mass density	0.05 lb/in^3
Shear modulus, xy	24630.54 psi
shear modulus, yz	521513.9 psi
shear modulus, xz	24630.54 psi
Allowable stress in x in tension	63145.9 psi
Allowable stress in x in compression	15750 psi
Allowable stress in y in tension	3291 psi
Allowable stress in y in compression	19531 psi
Allowable inplane shear stress	9765 psi

Table 5.4-2 COMPUTED PROPERTIES OF EPOXY/GRAPHITE.

Once the ply properties are computed, the laminate layup is defined to be a symmetric stacking sequence of plies. The thickness and orientation angle for each ply is defined. After the laminate is created, finite element computes and stores the constitutive matrix describes the material properties of the composite. These matrices relate the elemental stress resultants to elemental midplane strains and curvatures. The laminate and its associated material properties are as shown in Figure 5.4-4. In this figure, [A] relates mid-plane strains to membrane forces, [B] is the coupluing between bending and membrane action, [D] relates curvatures to bending moments and [S] represents the components of transverse shear.

A laminated composite consists of layers of highly anisotropic material whose properties depend on the orientation of each individual layer. It is very expensive to perform static tests for all possible stacking sequences and hence strength theories prove very effective. The maximum strain criterion is chosen as the failure theory for this analysis. According to this theory, a ply is assumed failed if one or more of the applied strain values exceeds the maximum allowable strain in that direction. The plots of ply failure envelopes are valuable in both stress and strain spaces for predicting the FPF of the laminate. Four different plies can be chosen for one envelope plot. Failure indices in each ply can be plotted on these failure envelopes. A failure index is a measure of how close a laminate is to first ply failure. Failure indices assume a value of

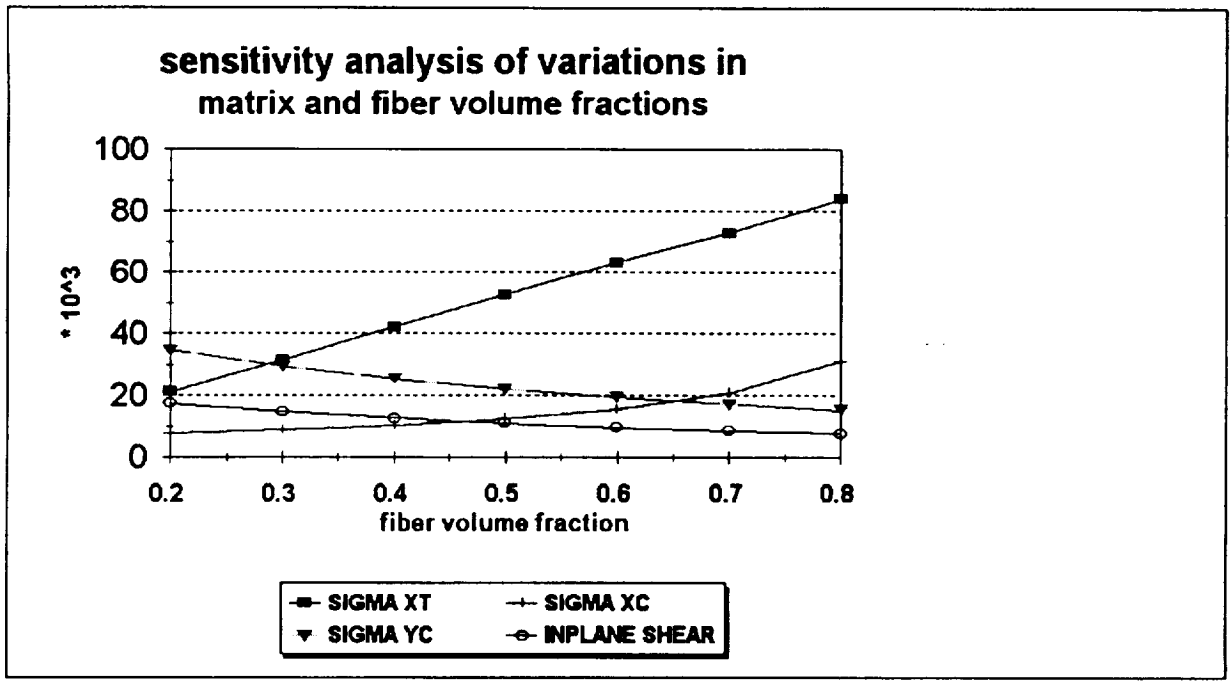

Figure 5.4-2 VARIATION OF PLY MODULI WITH CHANGES IN FIBER VOLUME FRACTION.

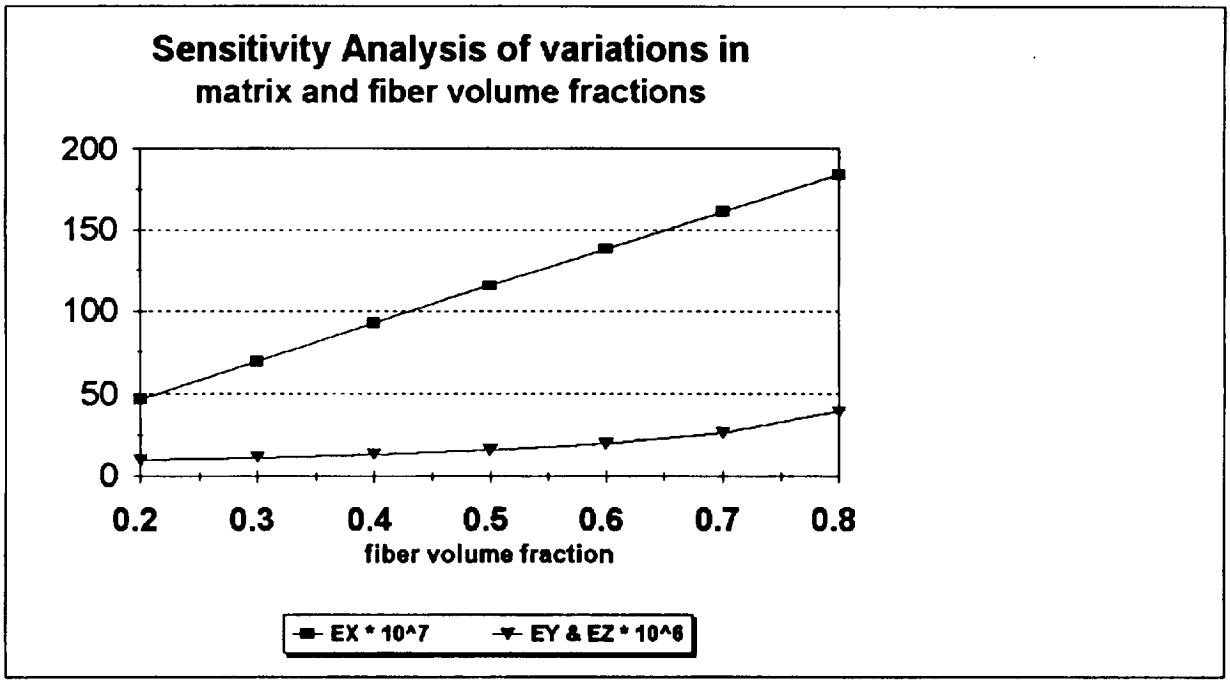

Figure 5.4-3 VARIATION OF ALLOWABLE STRESSES IN THE PLY WITH CHANGES IN FIBER VOLUME FRACTION.

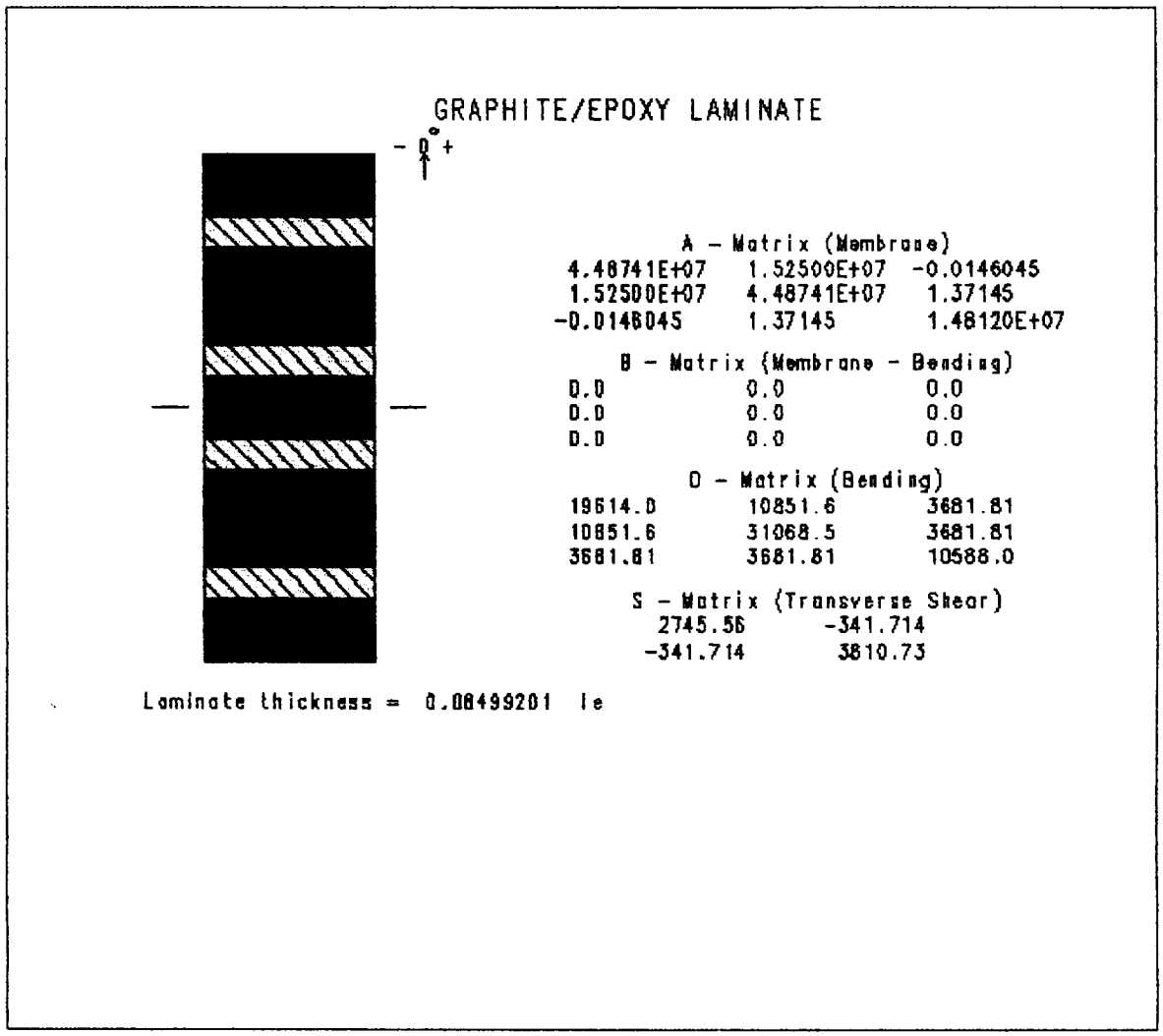

Figure 5.4-4 DOUBLE SYMMETRIC EPOXY/GRAPHITE LAMINATE.

one on the periphery of the failure surface. If the failure index is less than unity, the lamina stress occurs inside the periphery of the failure surface and is safe and the lamina fails otherwise. The failure envelopes for the 4 different plies of the laminate is plotted as shown in Figure 5.4-5. The laminate is tested under in-plane and transversely applied loads. The in-plane and the transverse shear stress and strain variations through the thickness of the laminate are to identify the probable high stresses in the laminate. Figure 5.4-6 shows the in-plane ply stress profile in the laminate.

The laminate is then assigned to the finite element model and the analysis is carried out under the specified loading conditions. All the elements of the finite element model are modified to refer to the material property table that resulted from the definition of the laminate. The material orientation has to be defined for all the elements of the laminated model. The model is solved for strains and displacements under static loading conditions. The laminated model is loaded along the direction of the fibers in the material. The ply stresses, strains, ply failure indices and bonding failure indices are then computed for computed for each and every ply of the laminate, thus identifying the critical sections of the laminated model. Ply stress and failure idex for ply no.1 of the model is plotted in Figure 5.4-7.

It was seen that the failure index is the highest for the 90 degree ply and will fail the first. Subsequent failures in the other plies is also determined and plotted as shown in Figure 5.4-8. These results are in good agreement with the initial ply failure envelopes plotted for the laminate. Similar results were obtained by using the Tsai-Wu criterion instead of the Maximum strain criterion.

It can be seen that that the ply failure indices in the plies with the same orientation angle is not exactly the same, thus justifying the importance of the position of the ply in the stacking sequence of the laminate.

5.5 FUTURE RESEARCH

The potential for modeling delaminations in composites has to be investigated by either using gap elements or reducing the values of laminate material properties and studying its effects on the behavior of the laminated finite element models. The changes in strain energies of the delaminated models can be of relative importance in correlating them with observed changes in damping ratios obtained from the experimentally determined frequency response curves of these laminated composites. This would provide a quantitative measure of the nature of delaminations and its subsequent influence on the integrity of the structure.

The combined techniques of acoustic emission and vibration pattern imaging have proved to be effective in identifying damage development in laminated composites. The applicability of these techniques in an advanced damage state has to be determined.

Also, different AE parameters can be studied, which would provide a better understanding of the failure processes in the structure under consideration.

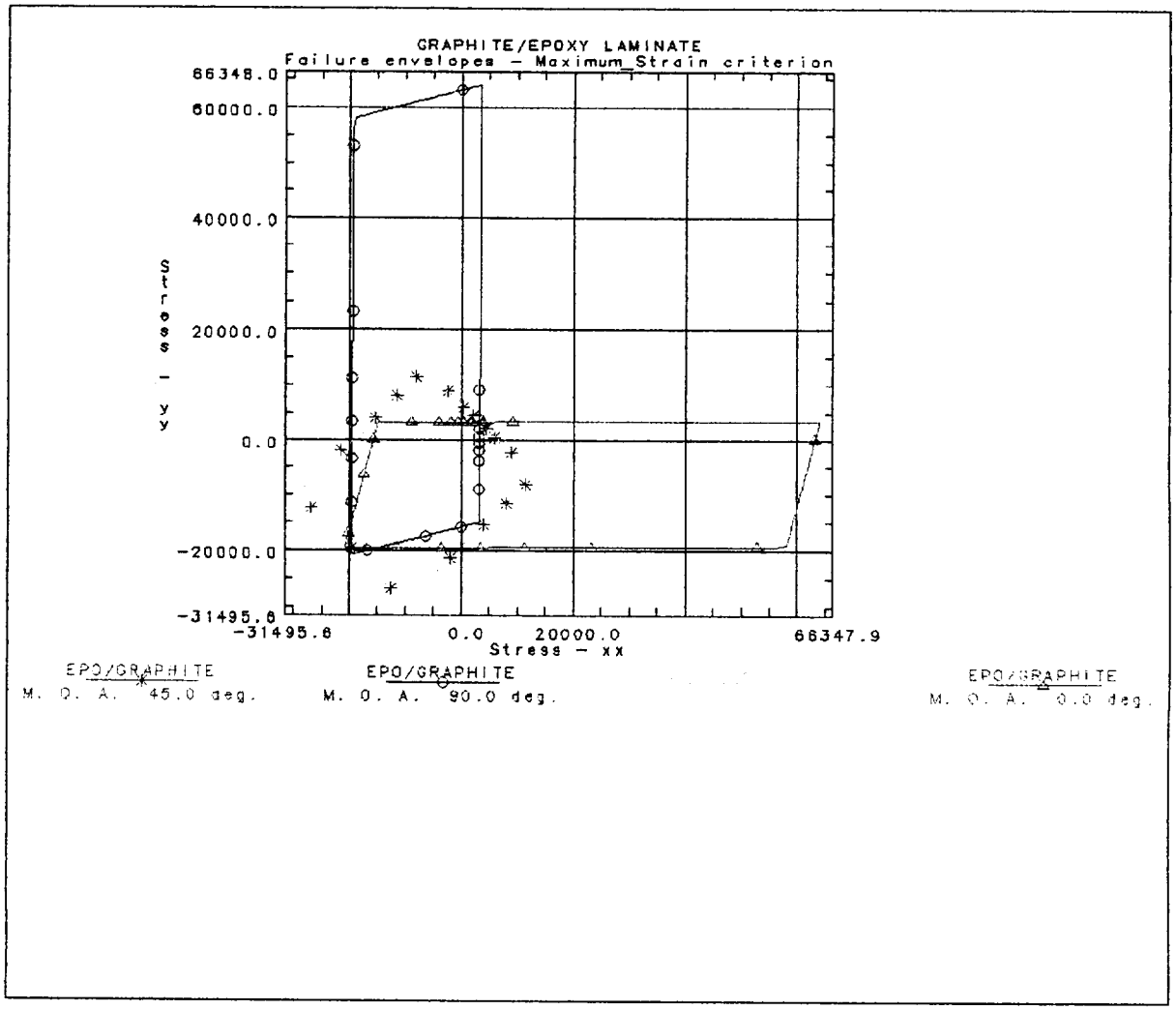

Figure 5.4-5 FAILURE ENVELOPES IN STRESS SPACE.

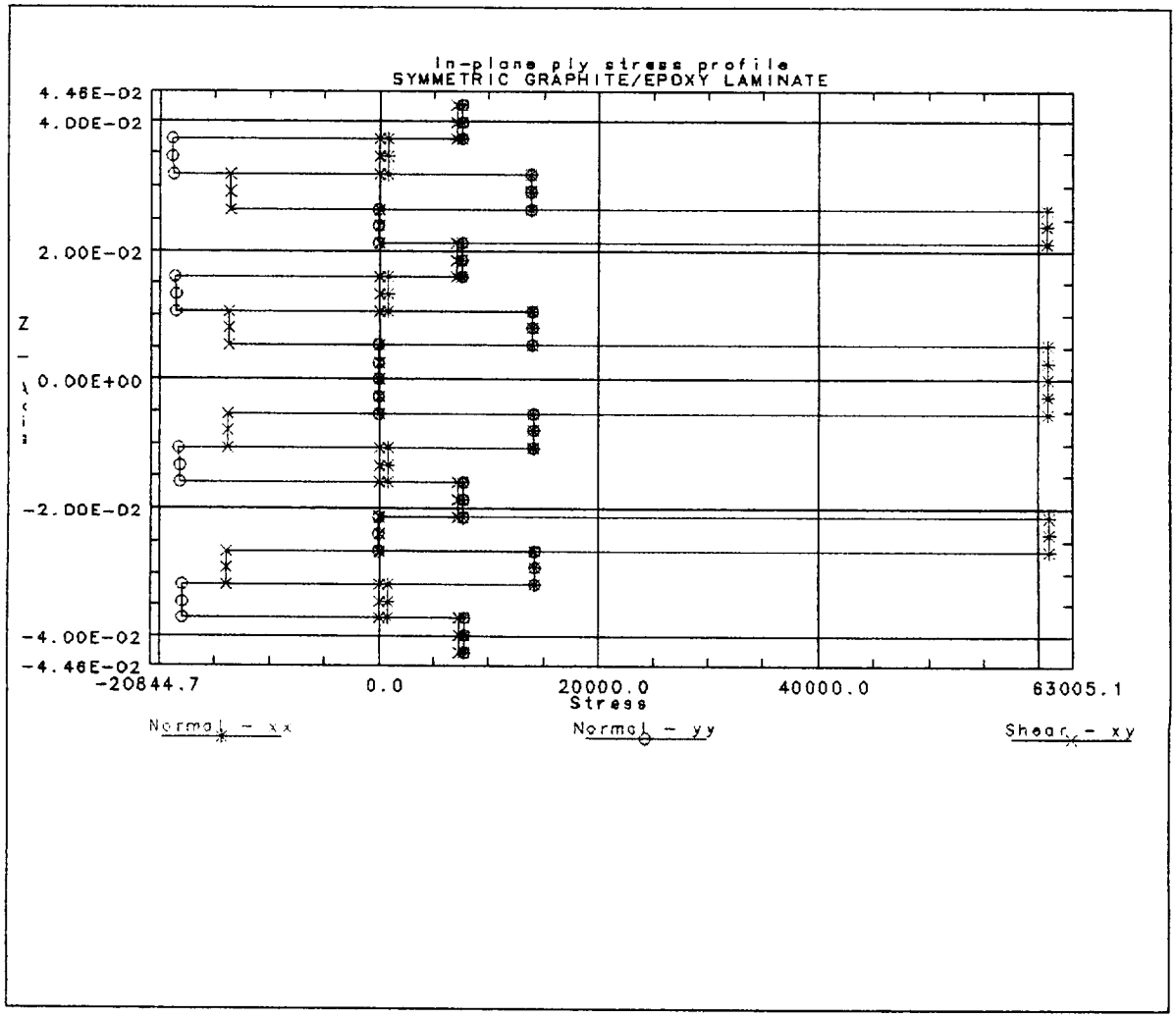

Figure 5.4-6 STRESS PROFILE IN THE LAMINATE.

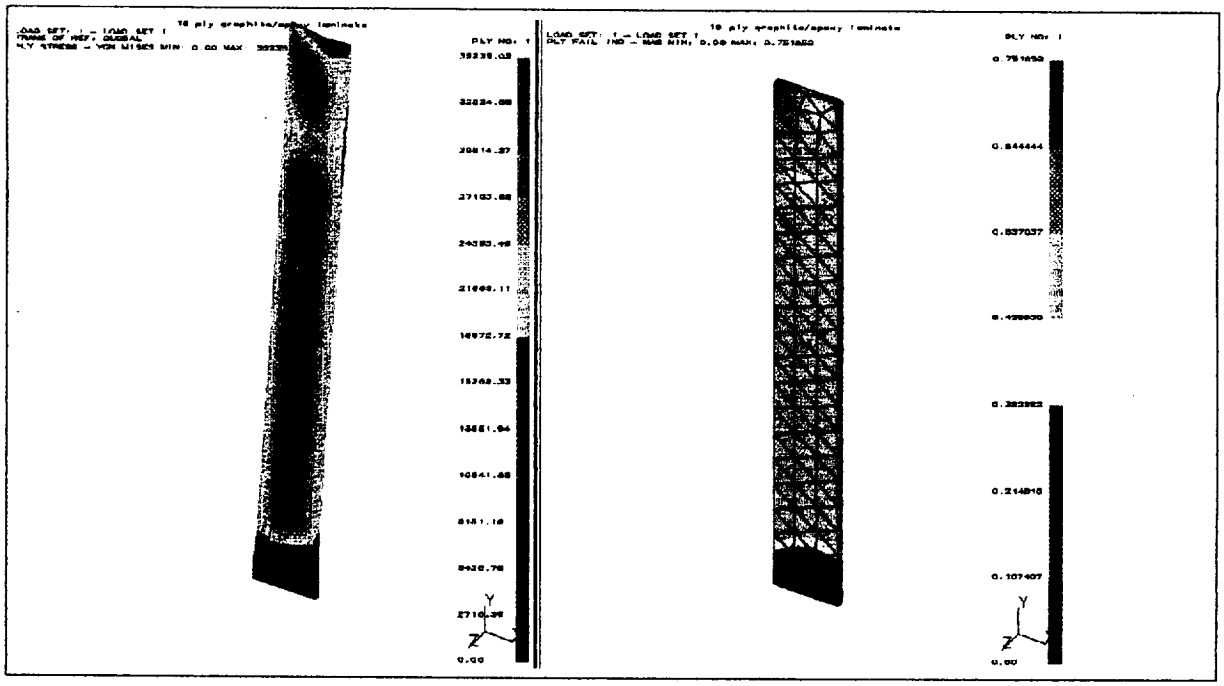

Figure 5.4-7 PLY STRESS AND PLY FAILURE INDEX IN PLY NO.1 IN THE LAMINATED MODEL.

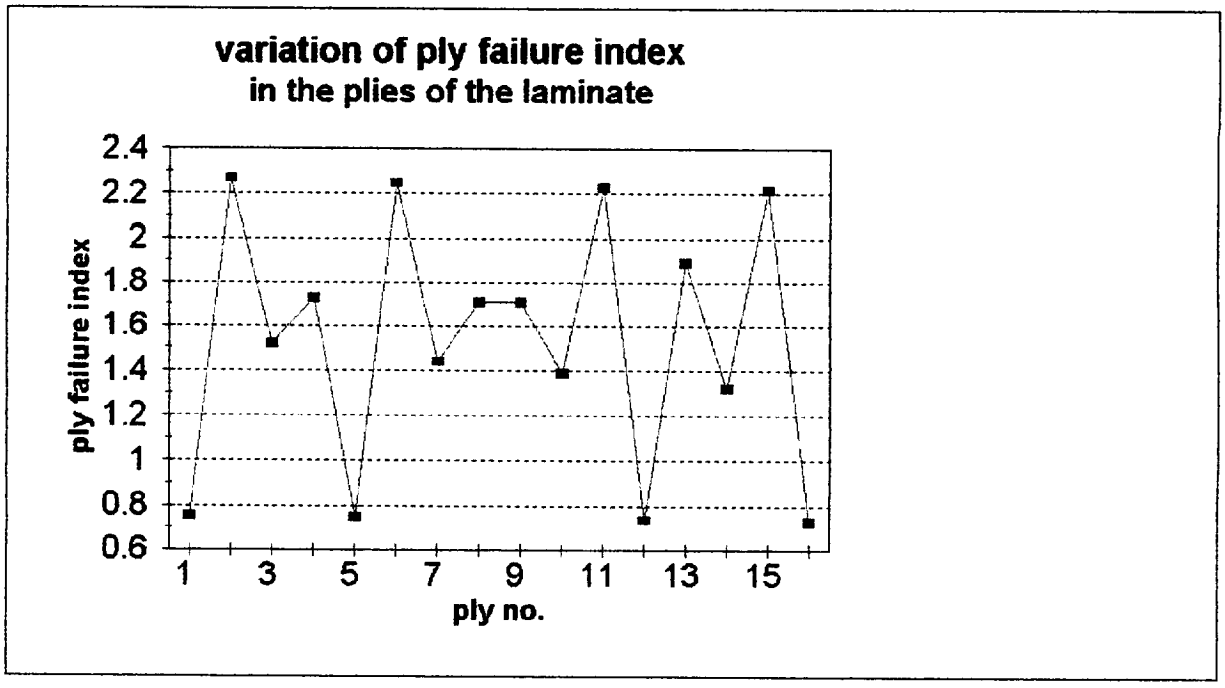

Figure 5.4-8 PLY FAILURE INDEX PROFILE IN THE LAMINATED MODEL.

6 CONCLUSIONS AND RECOMMENDATIONS

The report described a novel application of the finite element and laser-based modal measurements to evaluate the bond condition of the thermal protection system (TPS) tiles of the Space Shuttle orbiter. The results demonstrated the excellent correlation between the mathematical simulation and testing. It also demonstrated that modal testing, when integrated with finite element, can successfully be used as a reliable and quick tool for tile bond verification. The significance of this research is that it could lead to developing a user-friendly, self-contained, nondestructive, and non-contact system for tiles testing.

Several accomplishments were achieved:

- finite element models were developed for tiles bonded to both clamped and deformable integrated skin-stringer orbiter mid-fuselage.

- frequency response survey was performed using a laser rapidscan system. Results quickly identified disbonded tiles.

- testing of the 17-tile panel showed excellent agreement between the mathematical simulation and experimental results.

- laser vibration imaging and acoustic emission techniques proved to be valuable NDE tools for detecting delamination in composite materials.

Future work will include:

- developing finite element models for fuzz bond conditions and test panels provided by NASA.

- developing an inverse method for "nearly" real time assessment of size and location of disbond.

- conducting laser-based vibration testing on controlled test panels.

- validating the technique by testing tiles on the Space Shuttle orbiter.

- correlating test data and establishing baseline.

- transferring developed technology to NASA/KSC.

7 BIBLIOGRAPHY

[1] Banas, R. P., Gzowski, E. R., and Larsen, W.T., "Processing Aspects of the Space Shuttle Orbiter's Ceramic Reusable Surface Insulation," Proc. 7th Annual Conf. on Composites and Adv. Ceramic Mat., Amer. Ceramic Soc., pp. 591-612.

[2] Moslehy, F.A., Davies, T.W., and Davis, R.M., "Finite Element Modeling and Vibration Measurement Applied to the Space Shuttle TPS Tiles Bond Verification," Proceedings of the 1991 Joint Army-Navy-NASA-Air Force (JANNAF) Nondestructive Evaluation Meeting, KSC, FL, pp. 51-60, May 14-16, 1991.

[3] Moslehy, F.A., Davis, R.M., Davies, T.W., and Mueller, S.A., "Bond Assessment of Space Shuttle Tiles Using the Finite Element Method and Frequency Response Measurement ," Proceedings of the 1993 Joint Army-Navy-NASA-Air Force (JANNAF) Nondestructive Evaluation Meeting, LLNL, Livermore, CA, pp. 135-147, April 26-26, 1993.

[4] Moslehy, F.A., Mueller, S.A., and Davis, R.M., "Application of Laser-Based Methods and Finite Element Analysis to Bond Verification of Space Shuttle Tiles," SPIE Vol. 2066, Industrial Optical Sensing and Metrology, pp. 26-35, 1993.

[5] Moslehy, F.A., "Nondestructive Analysis and Development ," Final Report, NASA/KSC, August 1993.

[6] Mueller, S.A., and Moslehy, F.A., "An Inverse Solution for Bond Assessment of Space Shuttle TPS Tiles," In preparation.

[7] Adams, R.D., Cawley, P., Pye, C.J., and Stone, B.J., "A Vibration Technique for Non-destructively assessing the Integrity of structures," J. Mech. Engng Sci. Vol 20, pp. 93-100, 1978.

[8] Stubbs, N., "A General Theory of Non-Destructive Damage Detection in Structures", Proc 2nd International Symposium on Structural Control, Univ of Waterloo, p 694-713, July 1985.

[9] Springer, W.T., Lawrence, K.L., and Lawley, T.J., "Damage Assessment Based on the Structural Frequency-Response Function," Exper. Mech. Vol 28, pp. 34-37, 1988.

[10] Hearn, G., and Testa, R.B., "Modal Analysis for Damage Detection in Structures," Journal of Structural Engineering, Volume 117, pp. 3042-3063, October 1991.

[11] Chen, J., and Garba, J.A., "On-Orbit Damage Assessment for Large Space Structures," AIAA Journal, Vol 26, No. 9, pp. 1119-1126, 1988.

[12] Stubbs, N., and Osegueda, R., "Global Damage Detection in Solids - Experimental Verification", Int. J. Analy. and Exper. Modal Analy., Vol. 5, No.2, pp. 81-97, 1990.

[13] Davis, R.M., Moslehy, F.A., And Clarke, M.M., "Nondestructive Evaluation of Shuttle Columbia Tiles," Proceedings of the 29th Space Congress, pp. 2.1-2.9, April 1992.

[14] Korb, L.J., and Clancy, H.M., "Shuttle Orbiter Thermal Protection System: A Material and Structural Overview," paper No. STS 81-0219 presented at the 26th National Symposium Society for the Advancement of Materials and Process Engineering, April 1981.

[15] Goldstein, H.E., Leiser, D.B., and Katvala, V.W., "Reaction Cured Glass and Glass Coatings," U.S. Pat. 4,093,771, June 1978.

[16] LI-900: Lockheed's All-Silica Insulation Material, A Product of Space-Age Technology, Lockheed Missiles & Space Company, Inc., January 1987.

[17] LI-2200: A 22-PCF, All-Silica Insulation Material, Another Product of Space-Age Technology, Lockheed Missiles & Space Company, Inc., January 1987.

[18] FRCI-12: Fibrous Refractory Composite Insulation Material, Another Product of Space-Age Technology, Lockheed Missiles & Space Company, Inc., January 1987.

[19] Materials Properties Manual Volume 3: Thermal Protection System Materials Data, Rockwell International, August 1988.

[20] _____ , "NISA II User's Manual, Version 91.0," Engineering Mechanics Research Corporation, Troy, MI, April 1990.

[21] Zweben C., Hahn T., and Chou T., *Delaware Composites Design Encyclopedia Vol. 1 - Mechanical Behavior and Properties of Composite Materials,* Technomic Publishing Co. Inc., Lancaster, Pennsylvania, 1989.

[22] LOCAN-AT Manual, *Physical Acoustics Corporation,* Princeton, New Jersey, 1988.

[23] IDEAS Manual, *Structural Dynamics Research Corporation*, Ohio, 1989.

[24] VPI Rapidscan Manual, *Ometron Limited,* London, England, 1992.